Synthesis and Analysis of Poly(methacrylic acid-co-benzyl methacrylate) Copolymers for Stable Aqueous Pigment Dispersions

Amy Walsh

A thesis submitted to the University of Sheffield in partial fulfilment of the requirements for the degree of Doctor of Philosophy

June 2014

Author's Declaration

The work described in this thesis was carried out at the Department of Chemistry at the University of Sheffield between October 2010 and June 2014. It is the original work of the author, unless otherwise acknowledged within the text, and it has not been submitted previously for a degree at this or any other University. The views expressed in this thesis are entirely those of the author and not those of the University of Sheffield.

Amy Walsh

June 2014

Abstract

The content of this thesis is concerned with the stabilisation of pigment particles in water using poly(methacrylic acid-co-benzyl methacrylate), p(MAA-co-BzMA) copolymers. The p(MAA-co-BzMA) copolymers were synthesised by free-radical polymerisation in dipropylene glycol under either batch or semi batch conditions. Using the linear analysis methods of Finemann and Ross and Kelen-Tudos, reactivity ratios were obtained for batch produced p(MAA-co-BzMA) and showed that the microstructure of the copolymer was mostly random but with longer blocks of MAA interdispersed throughout the chain. Raman spectroscopy was used to measure the kinetics of the batch polymerisation of p(MAA-co-BzMA) by following the change of intensity of the C=C peak at 1640 cm^{-1}. Attachment of the fluorophore Acenaphylene allowed TRAMS measurements to monitor the rotation of p(MAA-co-BzMA) copolymers with MAA contents of 36, 45 and 64 mol %. The copolymers were examined as a function of pH and they all appeared to undergo a conformational transition at approximately pH 7, from a coiled structure below pH 7, to a more open chain above pH 7. Incorporation of MAA units at 45 and 64 mol % caused the copolymer chain to expand resulting in a more open structure between pH 8 to 12. This was due to the presence of more deprotanated MAA groups pushing the chain apart.

Stable aqueous dispersions of carbon black, yellow, cyan and magenta pigment particles were produced using p(MAA_{39}-co-$BzMA_{61}$) as a polymeric dispersant. The data from the depletion method was used to create an adsorption isotherm for the adsorption of p(MAA_{39}-co-$BzMA_{61}$) onto carbon black. The adsorption isotherm showed that monolayer coverage was achieved at 13 wt % loading of p(MAA_{39}-co-$BzMA_{61}$) onto pigment. IR, DLS, analytical centrifugation and rheology were used to further characterise the carbon black dispersions as a function of wt % loading of copolymer. Using analytical centrifugation a comparison between the adsorption of the diblock and the random dispersant p(MAA_{39}-co-$BzMA_{61}$) on carbon black was made. The diblock used was p(MAA_{143}-b-$BzMA_{300}$) and this was synthesised by RAFT alcoholic dispersion polymerisation.

SANS measurements were utilised to characterise neutralised aqueous solutions of p(MAA-co-BzMA) copolymers with the content of MAA being varied between 39 and 79 mol % to determine the radius of gyration using Guinier analysis. In addition, SANS was used to analyse aqueous carbon black dispersions stabilised with p(MAA_{39}-co-$BzMA_{61}$) with the loading of p(MAA_{39}-co-$BzMA_{61}$) on pigment varying from 6 to 50 wt %. Measurements carried out on the aqueous carbon black dispersions were performed in either 100 % D_2O to contrast-match carbon black or 27/73 volume % D_2O/H_2O to contrast-match p(MAA_{39}-co-$BzMA_{61}$). SANS data for contrast-matched p(MAA_{39}-co-$BzMA_{61}$) dispersions allowed the surface fractal and mass fractal dimensions of the dispersions to be determined and this data was supported by SAXS which also displayed the same scattering curves. SANS data obtained from the contrast-matched carbon black dispersions was fitted to a combined model of a Gaussian coil and mass fractal model and yielded parameters to characterise the dispersions. SANS was also used to explore the effect of using different milling techniques and different temperatures on the carbon black dispersions.

Acknowledgements

First and foremost, I would like to thank my supervisor Professor Patrick Fairclough for his advice and guidance throughout my PhD. Patrick has equipped me with a number of very useful transferrable skills for which I am truly grateful. I would also like to thank Dr Linda Swanson for sharing her fluorescence knowledge with me.

Thank you to Richard Williams and Thomas Paul at Fujifilm for their interest and contributions to this PhD.

There have been many people who have worked in office D49 over the past three years, all of which have been a pleasure to work with. Babs, you made the office a fun place to work and it would have been boring without you! Chris H, you certainly made the office an interesting place to be, we never knew what your next parcel would be! Thank you to the recent arrivals in the office, Ben P, Ben C and Rory, for being fun people to share an office with. Massive thanks to Susi for her company on long scattering trips and for being a great friend. Thanks also to Tom, Lewis, Sarah, Obed, Gary, Ads, Pierre and Josh.

A big thank you to Prykey, Sasha, Christine and Andy. P for always taking time out of their busy schedules to answer any questions I had. I would also like to thank Steven Parnell for carrying out SANS measurements for me in America.

To the fluorescence people (Tom Swift and Fateh) our in depth and informative discussions on fluorescence proved very useful in helping shape chapter three of this thesis. Thank you to Dave Growney for helping me with the lumisizer and our chats about adsorption isotherms and carbon black!

There are a number of key people who keep the chemistry department running and I would like to extend my gratitude to you all. Special thanks to Sue Bradshaw for running my ^{13}C NMRs, Pete and Nick from stores and Mel Hannah for GPC advice. I would also like to thank Chris Hill and Svet for help with TEM.

To the girls: Milly, Lara, Nish, Vicky, Zoe and Georgia. Thank you for all the brilliant nights out and our sophisticated nights in consuming cheese and wine. I'm glad we became friends, if it wasn't for you guys I would have probably gone mad during my PhD.

I owe a big thank you to my boyfriend John. Thank you for your support, help and patience for the past three years. I couldn't have done it without you.

To my Mum, thank you for being you and always providing love and support in everything I do. This thesis is dedicated to you and Dad.

Abbreviations and Symbols

^{1}H NMR	proton nuclear magnetic resonance
^{13}C NMR	carbon nuclear magnetic resonance
ACE	Acenaphthylene
AIBN	2-2’-azobisisobutyronitrile
BzMA	benzyl methacrylate
CPDB	2-cyanoprop-2-yldithiobenzoate
CTA	chain transfer agent
DLS	dynamic light scattering
D_m	mass fractal dimension
DP	degree of polymerisation
DPG	dipropylene glycol
D_s	surface fractal dimension
FT-IR	fourier transform infra-red
GPC	gel permeation chromatography
M_w	weight-average molecular weight
M_n	monomer-average molecular weight
RAFT	reversible-addition fragmentation chain transfer
R_g	radius of gyration
SANS	small-angle neutron scattering
SAXS	small-angle x-ray scattering
TEM	transmission electron microscope
TGA	thermal gravimetric analysis
TRAMS	time-resolved anisotropy measurements
Trigonox 21s	tert-butyl peroxy-2-ethylhexanoate
τ_c	correlation time

Contents

CHAPTER I

INTRODUCTION

1.1 The Ink-jet Industry

Since the 1970s the printing industry has seen the advancement of a new type of printing device, the ink-jet printer.[1] Ink-jet printing is a non-impact, computer driven technique whereby a digital image is created by propelling droplets of ink onto paper. The type of ink used in inkjet technology can either be dye-based[2] or pigment-based.[3] Dye-based inks (whereby the colourants are soluble within the ink) were used in the first ink-jet printers. These easily formulated dye-based inks and their ability to produce glossy, highly coloured images offered the ink-jet printer many advantages over the dot matrix printer.[4] However, the ink-jet printer could not match the print quality and optical density that a laser printer offered. Dye-based inks also suffered the major drawback of poor light and water resistance making the ink-jet printed material inadequate for outdoor use. The advancement of ink-jet printers began with the introduction of pigment-based inks. Pigment-based inks (whereby the colourants are dispersed within a continuous phase) were able to match the print quality of the laser printer and were more durable for outdoor use. Today pigment-based inks continue to displace dyes in the printing industry, enabling ink-jet printers to become commonplace in both homes and offices.

1.2 Colloidal Dispersions

Pigmented ink-jet inks are colloidal dispersions whereby insoluble pigment particles, in the size range of 50-200 nm, are distributed uniformly throughout a continuous phase. Colloid stability is important in the printing industry and other manufacturing industries including pharmaceuticals, paints and adhesives.[5] Without this stability, particles would aggregate together and phase-separate, causing dispersions to become useless (see Figure 1.1).

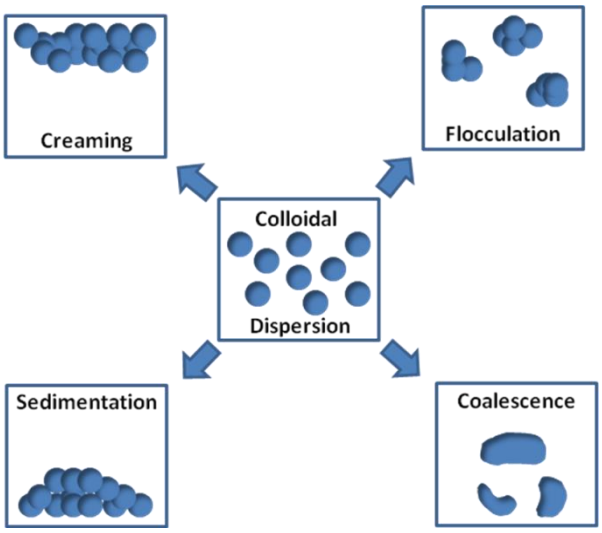

Figure 1.1 *Schematic representation of a colloidal dispersion and the different ways in which the stable dispersion can become destabilised.*

In order to generate a stabilised colloid dispersion a repulsive interaction needs to be applied which outweighs the attractive van der Waals forces between particles. This can be achieved by electrostatic, steric or electrosteric interactions.

1.2.1 Electrostatic Stabilisation

A description of electrostatic stabilisation is based upon the model developed by Derjaguin, Landau,[6] Verwey and Overbeek[7] (DLVO). DLVO theory is based on the assumption that there are only two forces acting on the dispersed particles: Van der Waals and electrostatic forces. The electrostatic force is generated by the formation of an electrical double layer, created through the diffusion of ions at the charged particle

surface. Figure 1.2 shows the potential energy curve according to DLVO theory for two particles approaching each other at distance, d. For a stable colloid dispersion, V_{max} needs to be higher than kT, where kT is the thermal energy of the dispersed particles.

A disadvantage of electrostatic stabilisation is its inability to stabilise high particle concentrations. High concentrations force particles to be at a distance from each other where the van der Waals forces become significant and the dispersion flocculates. Electrostatic dispersions also suffer from other disadvantages such as sensitivity to pH, salt[8] and freeze-thaw cycling.[9]

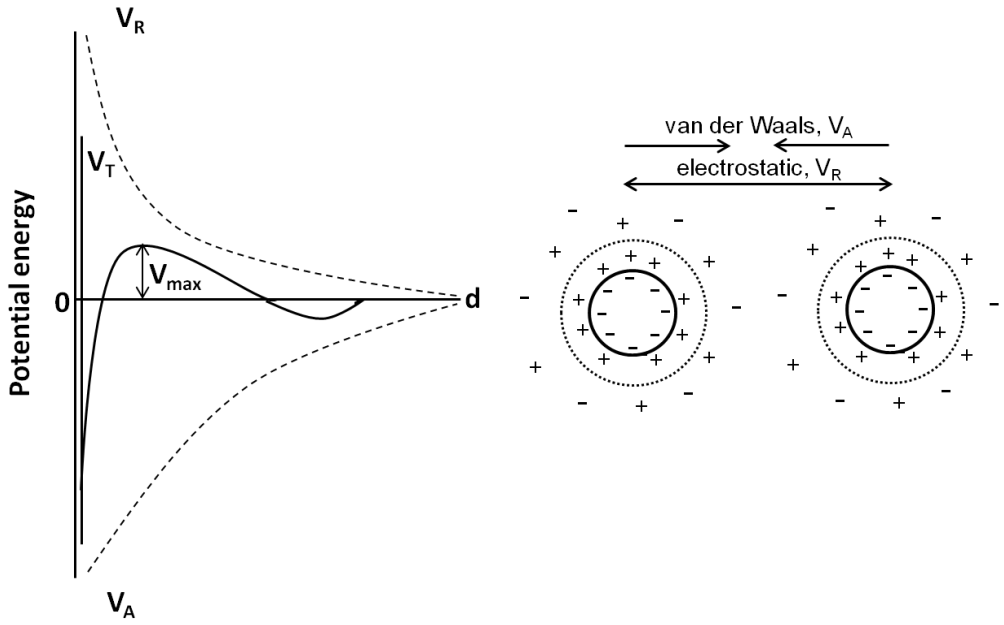

Figure 1.2. *Left: variation of potential energy with particle separation according to DLVO theory. V_R is the repulsive energy due to the electrical double layer, V_A is the attractive energy caused by van der Waals forces, V_T is the total energy and d is the particle separation. Right: Electrostatic stabilisation mechanism for negatively charged particles. Figure adapted from reference 10.*

1.2.2 Steric Stabilisation

The mechanism for steric stabilisation was proposed by Clayfield and Lumb,[11] and Vincent[12] and Napper[13]. Steric stabilisation can be achieved through adsorption[14] or grafting[15] of polymers onto the surface of colloidal particles. Stabilisation is driven by two factors: entropy and enthalpy. If two polymer-coated particles approach each other, the chains interpenetrate and become compressed; this leads to an unfavourable loss of configurational entropy and an increase in free energy of the system. The enthalpic term arises from the polymer layer interacting more favourably with solvent molecules than

other polymer segments. The interpenetration of polymer chains also results in an increase in osmotic pressure leading to repulsion between particles. The potential energy diagram for steric stabilisation is shown in Figure 1.3.

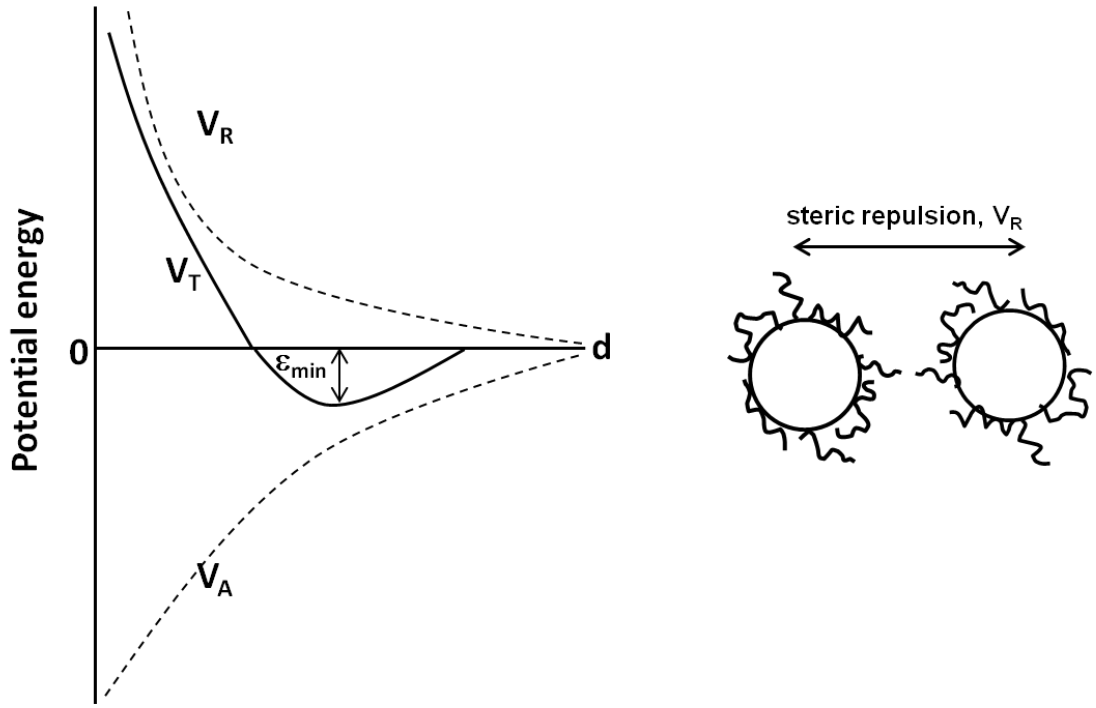

Figure 1.3. *Variation of potential energy with particle separation for steric stabilisation. V_R is the repulsive energy due to the polymer layer, V_A is the attractive energy arising from van der Waals forces, V_T is the total energy and d is the particle separation.*

The effectiveness of steric stabilisation is dependent on the amount of polymer adsorbed and the thickness of the adsorbed layer.[16,17] Adsorbed layers with greater thickness prevent colloid particles getting close enough to experience attractive van der Waals attractions. A sterically-stabilised colloidal dispersion does not become affected by a change in pH or high salt concentrations, a property that is advantageous for many applications such as corrosion-resistant coatings.[18]

1.2.3 Electrosteric Stabilisation

Electrosteric stabilisation benefits from the properties of both electrostatic and steric stabilisation, making it a very effective means for stabilising colloid particles. The potential energy diagram for electrosteric stabilisation is shown in Figure 1.4. This

diagram shows that, at long particle distances, the electrical double layer stabilises the particles, but at shorter distances steric stabilisation comes into play, preventing aggregation of particles. Electrosteric stabilisation is used to stabilise the ink-jet pigment particles that were used in the research described by this thesis.

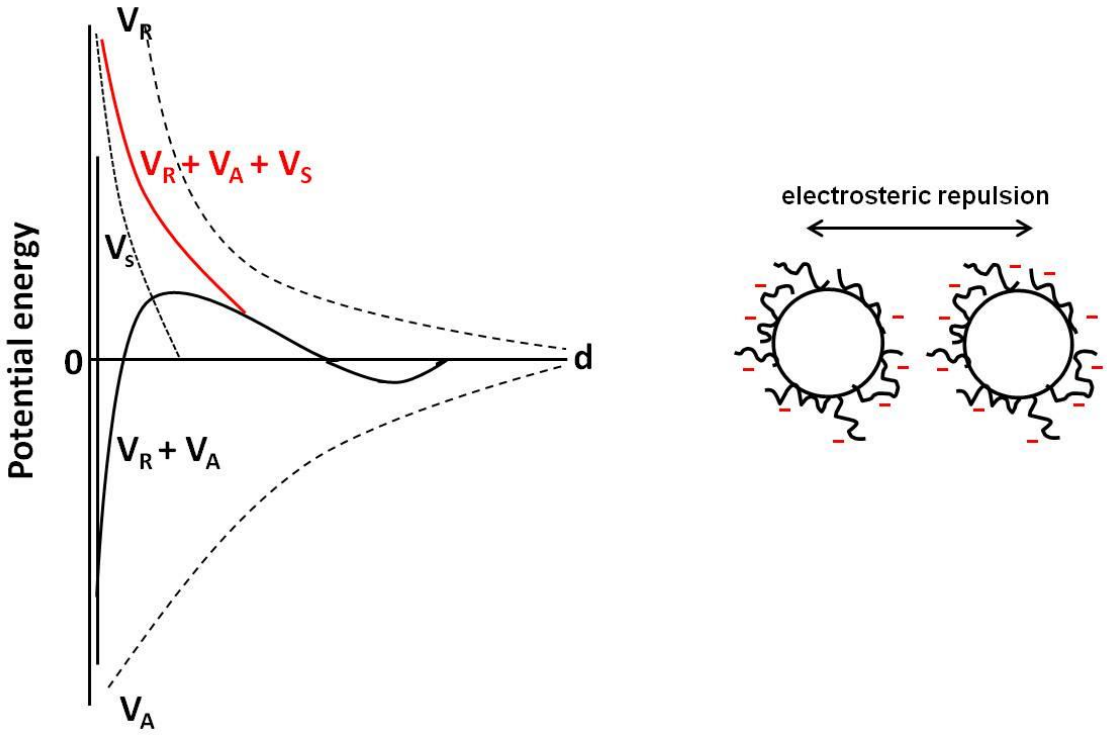

Figure 1.4. *Potential energy curve and schematic representation showing the variation of potential energy with particle separation for electrosteric stabilisation. V_R is the repulsive energy due to electrostatic repulsion, V_s is the repulsive energy due to the polymer layer, V_A is the attractive energy because of van der Waals force and d is the particle separation.*

Electrosteric stabilisation is commonly achieved by creating a structured copolymer such as a diblock copolymer that consists of hydrophobic segments that can adsorb onto the pigment surface and a hydrophilic polyelectrolyte segment that will extend out into the continuous phase to provide electrosteric stabilisation.[19] Instead of using structured polymers, the majority of ink-jet printing applications use random copolymers as dispersants, as this offers an easier and cheaper copolymer synthesis.

1.3 Polymer Adsorption

Adsorption is an increase in concentration of a solute at an interface. Adsorption occurs when the difference in free energy between polymer-solvent interactions and polymer-interface interactions is negative. If this is not the case then depletion occurs. Two types of adsorption can take place: chemisorption (when the polymer chemically bonds to the interface) and physisorption (when the polymer interacts with the surface through physical interactions such as hydrogen bonding or van der Waals forces).

The conformation of polymeric dispersants on the solid-liquid surface is important when considering their overall ability to stabilise colloid dispersions. The conformation of a polymer chain adsorbed at a colloidal solid-liquid interface can be described in terms of loops, trains, tails and bridges[20] (see Figure 1.5). Trains are sections with all polymer segments in contact with the interface. Loops connect trains and have no contact with the surface and tails are the non-adsorbed chain ends. The conformation at which the polymer adsorbs at the solid-liquid interface depends upon the interaction energies between the polymer, liquid and particles. Under certain conditions, polymer chains can adsorb onto two or more particles, causing bridging flocculation to occur.

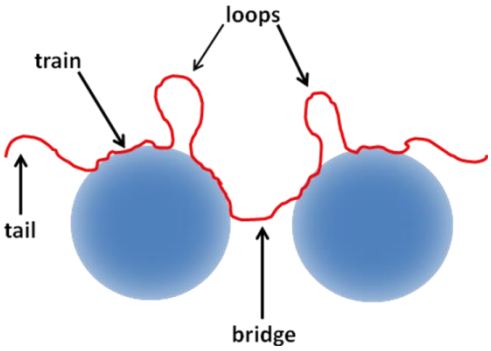

Figure 1.5. *Schematic showing possible conformations of a polymer chain adsorbed onto the surface of two particles.*

To characterise polymer adsorption at the solid/liquid interface three parameters are commonly determined:[21] (i) the amount of polymer adsorbed, (ii) the fraction of segments in direct contact with the solid surface and (iii) the volume fraction profile.

1.3.1 Adsorption Isotherms

The amount of polymer adsorbed onto an interface is commonly shown as an adsorption isotherm. An adsorption isotherm is a plot of the adsorbed amount, Γ against the equilibrium polymer concentration, C_{eq}. An adsorption isotherm for a monodisperse polymer is shown in Figure 1.6. The horizontal line is referred to as the 'plateau' and indicates that the surface is completely saturated.

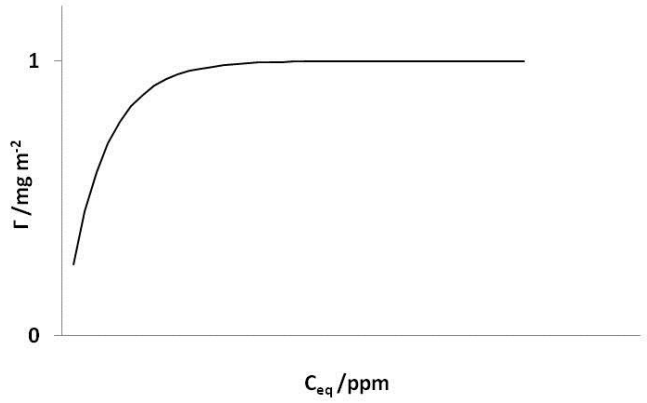

Figure 1.6. *Typical adsorption isotherm for a monodisperse polymer.*

Adsorption isotherms are commonly obtained using the indirect method, which involves measuring the difference in polymer dispersant concentration in the continuous phase before and after adsorption. If the polymer dispersant contains specific functional groups, then spectroscopic techniques such as UV[22] or IR[23] can be used to determine the change in polymer concentration. The point at which the isotherm reaches its plateau can depend on parameters such as molecular weight[24], composition and solvency.[25] Generally, as molecular weight increases the plateau value increases up to a limit where increasing molecular weight no longer has an effect on the plateau. Solvency can be altered by increasing temperature[17] or adding salt.[25] The effect of solvency with temperature was studied for the adsorption of poly(vinyl alcohol) (M_w = 65100 g mol^{-1}) on 200 nm diameter latex particles in water. As the temperature was increased from 5 to 50°C, the solvency of poly(vinyl alcohol) reduced due to a breakdown of hydrogen bonds. The reduction of solvency resulted in an increased amount of adsorbed polymer and therefore a higher plateau value. [17]

1.3.2 Bound Fraction

The bound fraction, p, gives an indication of how strongly adsorbed the polymer chains are at the interface. The bound fraction also gives insight into the conformation of the polymer. A high bound fraction indicates that the polymer chain consists of many train segments whilst a low value of p indicates that the polymer forms loops, tails and bridges. IR spectroscopy has commonly been used to calculate p.[26] If a shift in frequency occurs upon adsorption then it is possible to determine whether the polymer segments are in a bound or un-bound environment.

1.3.3 Volume Fraction Profile

The volume fraction distribution φ(z) is given by the number of segments in the direction perpendicular to the surface (conventionally the z-direction) (see Figure 1.7). The profile describes how the polymer layer is arranged at an interface. This gives an estimate of the surface area per unit volume of substrate, the hydrodynamic thickness, δ_h, of the adsorbed layer and a measure of how much polymer is present within the layer.[27] The hydrodynamic thickness is a particularly useful parameter as it indicates how effectively the adsorbed layer is stabilising the colloid particles.

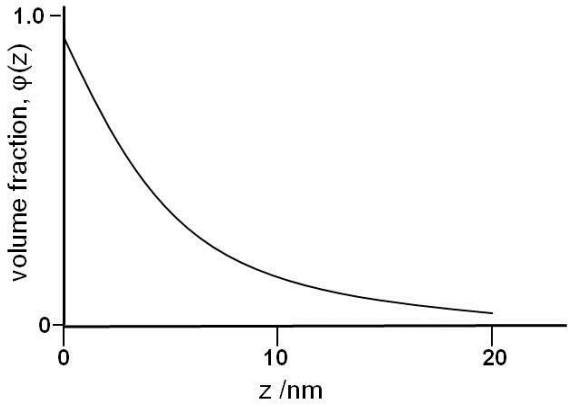

Figure 1.7. *Typical example of a volume fraction profile.*

To date, small-angle neutron scattering is the most accurate experimental method for obtaining a volume fraction profile.[28] This will be discussed further in section 1.7.2.

1.3.4 Adsorption of Random and Diblock Copolymer Dispersants

Random copolymers, whereby two or more monomer units are arranged randomly along the polymer chain, have structural properties that are intermediate compared to their corresponding homopolymers. Random copolymers used as polymeric dispersants are typically made up of two monomer types. The first has an affinity with the interface and adsorbs or 'anchors' onto the surface. The other monomer does not have an affinity for the surface and sticks out from the surface to provide steric or electrosteric stabilisation (depending on its structure).

Depending on the polydispersity and sequence distribution of the random copolymer, various adsorption scenarios can occur. Figure 1.8a) shows the adsorption of chains with the same length but different compositions. Chains that contain more of the anchor block will preferentially adsorb. In Figure 1.8b) the situation is more complex, with chains of differing lengths and composition. In this scenario there are two competing effects: (i) long chains adsorb more favourably over short chains[29,30] and (ii) chains with longer segments of anchor blocks preferentially adsorb over chains with short anchoring blocks. In this case, competing effect (ii) dominates adsorption. This leads to small chains preferentially adhering to the surface over long chains if the small chains contain large anchoring sections. Figure 1.8c) depicts what would happen if the copolymer is 'blocky', whereby the anchor units are not distributed evenly throughout the chain but are instead grouped together. This leads to chains with longer anchor blocks adsorbing at the interface. Figure 1.8d) displays self-association of copolymers at the interface that can occasionally occur if the copolymer concentration is high and the copolymer is in a poor solvent for the adsorbing block.

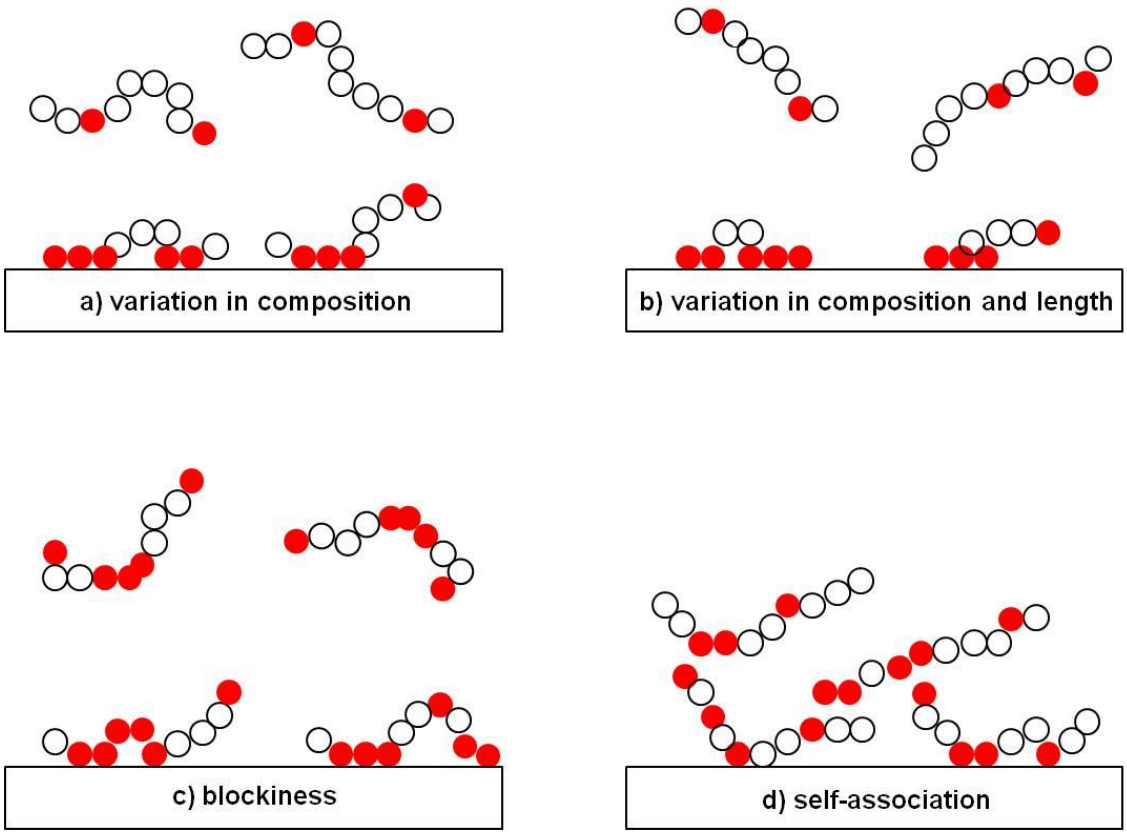

Figure 1.8. *Schematic showing possible scenarios for the adsorption of random copolymers with a) the same length but different composition, b) different composition and length, c) block-like character and d) poorly soluble segments leading to self association. Figure adapted from reference 31.*

The use of random copolymers to produce stable pigment dispersions, for utilisation in the ink-jet industry, has been studied by Yoon and Choi[32] who synthesised random copolymer dispersants by free-radical polymerisation in alcohol using two or three monomers. The polar monomer was methacrylic acid (which was made water-soluble by treatment with potassium hydroxide) and the non-polar monomer was either (i) methyl methacrylate, (ii) butyl methacrylate (iii) benzyl methacrylate or (iv) styrene (see Figure 1.9).

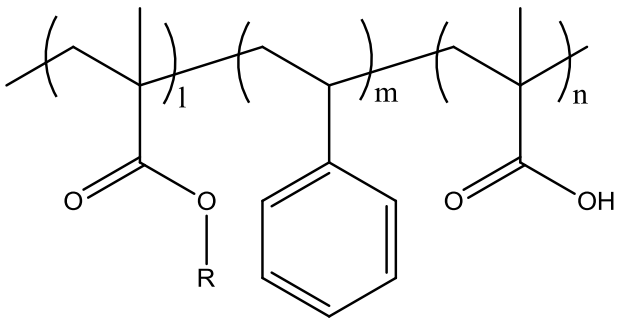

R = (i) CH_3
(ii) $(CH_2)_3CH_3$
(iii) CH_2Ph

Figure 1.9. *Schematic representation of the chemical structure of random copolymers used for dispersing pigment particles.*[32]

Diblock copolymers consist of blocks of monomer units. Block copolymer dispersants typically contain an 'anchor' block which adheres to the interface and a 'buoy' block which extends out from the surface.

Spinelli used controlled free-radical polymerisation to create acrylic diblock polymers to operate as pigment dispersants.[33] The hydrophobic block consisted of either a homopolymer or copolymer of methacrylate monomers while the hydrophilic block consisted of neutralised acid- or amine- containing copolymers that extended out in an aqueous dispersion to provide electrosteric stabilisation.

Using random copolymers as dispersants is more practical and more cost-effective as they are synthesised by simple free-radical polymerisation. However block copolymers offer more dispersion stability since they are able to bind more efficiently onto particles[32] (see Figure 1.10). Diblocks offer thicker layers and can adsorb more strongly onto the particle surface.

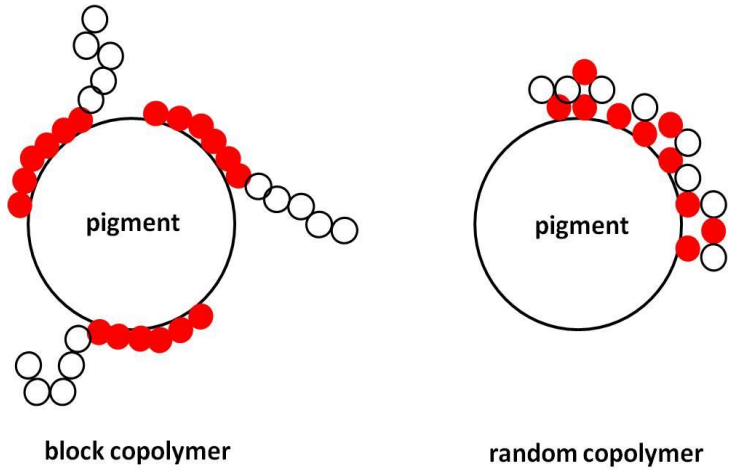

Figure 1.10. *Schematic representation showing the difference between the adsorption of a block and random copolymer on a pigment particle surface. The random copolymer binds with more difficulty due to the irregularity between the hydrophobic and hydrophilic parts. Figure adapted from reference 32.*

The difference in dispersion performance between block and random copolymers was demonstrated by Chang and co-workers.[34] The group used block copolymers of polystyrene and poly(acrylic acid) p(St-b-AA) with varying molecular weights to stabilise pigment particles used in ink-jet inks. P(St-b-AA) was made by first synthesising a block copolymer of polystyrene and poly(tert-butyl acrylate) p(St-b-tBA) by atom transfer radical polymerisation (ATRP), then selectively hydrolysing the ptBA block with trifluoroacetic acid to generate the hydrophilic PAA block.

P(St-b-AA) and p(St-ran-AA) random copolymers were both used to make pigment dispersions. The random and diblock versions both had the same styrene/acrylic acid molar ratio of 1.5/1.0 Pigment dispersions were made with the same pigment/dispersant mass ratio of 1.0/0.5. The stability of the dispersions was studied by monitoring the change in size of these pigment particles when varying amounts of monomers (styrene and acrylic acid) were added to the dispersion (see Figure 1.11). The monomers were introduced to induce flocculation of the stable pigment dispersion. Addition of monomers induced flocculation because it increased the tendency of the polymeric dispersant to become fully dissolved in the solvent.

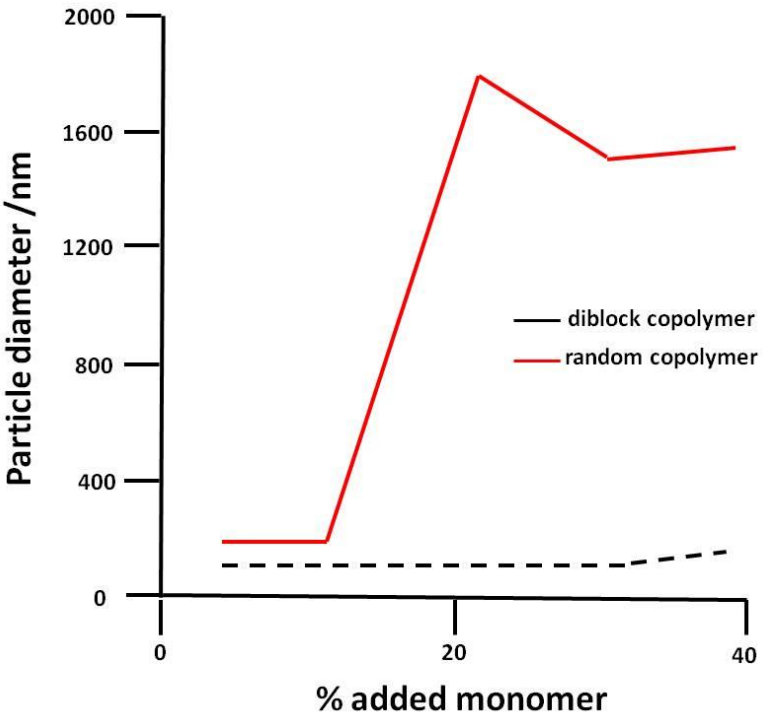

Figure 1.11. *Change in diameter of pigment particles stabilised with a block copolymer p(St-b-AA) or random copolymer p(St-ran-AA) with increasing addition of St and AA monomers. The random and block copolymer both have the same styrene/acrylic acid molar ratio of 1.5/1.0. Figure adapted from reference 34.*

When the diblock was used as a pigment dispersant, the size increased by ~40 nm after addition of 40 % monomer. However, dispersions where the random copolymer had been used as the dispersant increased in size even at 20 % monomer content. This result was attributed to the hydrophobic styrene block of the block copolymer being able to anchor more efficiently onto the pigment surface compared to the random distribution of styrene units in the random copolymer.

Auschra et al.[35] investigated how changing the block length of a polymeric dispersant affected pigment dispersant performance. The polymeric dispersant used was poly(n-butyl acrylate-b-(2-dimethylamino)ethyl acrylate), p(BA-b-DMAEA) and the solvent was a volume ratio of xylene/butanol/1-methoxy-2-propanol (70/15/15). The pDMAEA block was able to absorb onto the pigment particles whilst the pBA provided steric stabilisation. Red pigment particles were used and either had a surface area of 15 m^2/g or 94 m^2/g. For the pigment particles with a specific surface area of 15 m^2/g optimum performance was achieved when the pigment adsorbing pDMAEA block had a DP above 20. It was also observed that the DP of the pBA block could be lowered to 53 and still adequately disperse these pigment particles. For pigment particles with a specific

surface area of 94 m^2/g, optimum performance was achieved when the pBA steric stabiliser block had a DP larger than 100 and the pDMAEA had a DP below 20. The higher specific surface area of these pigment particles required a higher density of adsorbed copolymer at the pigment surface to be stabilised. This could only be achieved when the anchor pDMAEA block was relatively short, allowing more of the chains to adsorb and pack onto the pigment surface. This explanation is illustrated in Figure 1.12. The highest amount of adsorbed block copolymers occurs when the adsorbing block is 10-20 % of the total chain length.[31]

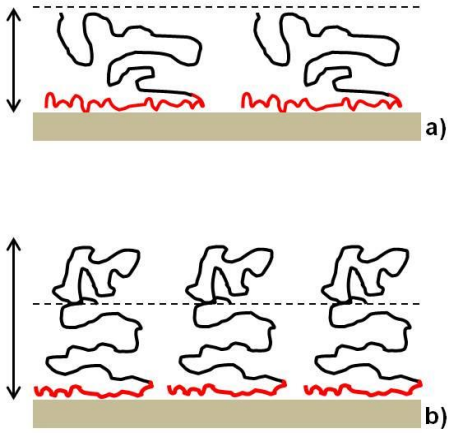

***Figure 1.12**. Schematic representation of different adsorption scenarios for block copolymers: a)adsorption of a long pigment anchor block; b) adsorption of a short anchor block allowing a higher surface coverage and forcing the steric stabiliser block to stick out further and stabilise more effectively. Figure adapted from reference 35.*

For a number of years, polymer adsorption has been the subject of both experimental and theoretical studies.[21,36] The focus of this PhD will be the investigation of the adsorption of polymers at the solid-liquid interface using various of experimental techniques. The techniques and their application in this research will be described in sections 1.4 to 1.9.

1.4 Rheology

The term rheology was coined by Bingham in the 1920s[37] and is defined as the science of deformation and flow. Rheology is very sensitive to small changes in a material's structure, making it useful for characterising the conformation of polymers.

Viscosity is the most sought-after rheological quantity and can differ depending on whether the liquid is Newtonian or non-Newtonian. Viscosity, η is defined as the ratio of shear stress to shear rate, σ/γ. The most common effect associated with non-Newtonian fluids is shear-thinning behaviour, whereby viscosity decreases as it is exposed to higher shear rates. An example of shear-thinning behaviour can be seen with paint which, when applied to a surface, will decrease in viscosity allowing easier application. On the other hand, some non-Newtonian materials such as corn flour in water can exhibit the opposite effect, called shear-thickening. A Newtonian fluid, e.g. water, would show neither of these effects and would remain at the same viscosity within a range of shear rates (at a sufficiently high shear rate, all liquids become non-Newtonian). It has been estimated that water would be required to be sheared at an unfeasible 10^{12} s^{-1} in order to observe non-Newtonian behaviour.[38] All of these effects are shown in Figure 1.13.

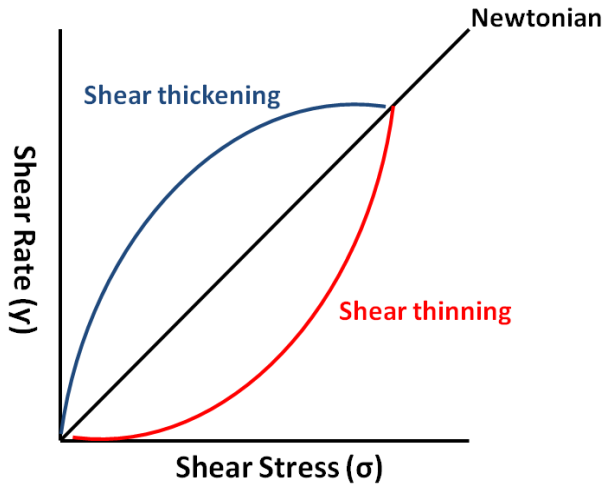

Figure 1.13. *Schematic illustration to show the different behaviours of liquids under shear.*

The Otsubo group has frequently utilised rheology to study the conformation of adsorbed polymers onto different surfaces. One particular focus was on the occurrence of polymer bridging between particles and its effect on the rheological behaviour of colloidal dispersions.[39]

The rheological behaviour of a silica suspension in an aqueous solution of associating polymer was investigated by Otsubo et al.[40] This paper described the effect of hydrophobically-modified ethoxylated urethane (HEUR) with a molecular weight of approximately 25,000 g mol^{-1} in the presence of aqueous silica suspensions with a mean

diameter of 1.3 μm. The main findings of this paper are illustrated in Figure 1.14. When the HEUR was added to the silica suspensions at low concentrations, flocculation was induced by an irreversible bridging mechanism, and the suspension became shear-thinning (Figure 1.14a). The suspensions containing HEUR slightly above full silica coverage displayed Newtonian behaviour due to the weak associating interaction between the polymer chain-ends breaking and reforming via Brownian motion (see Figure 1.14b). Suspensions with a large excess of HEUR showed Newtonian flow and high stability against sedimentation. This was due to an association network between the hydrophobic ends of the HEUR being created in the solution (see Figure 1.14c).

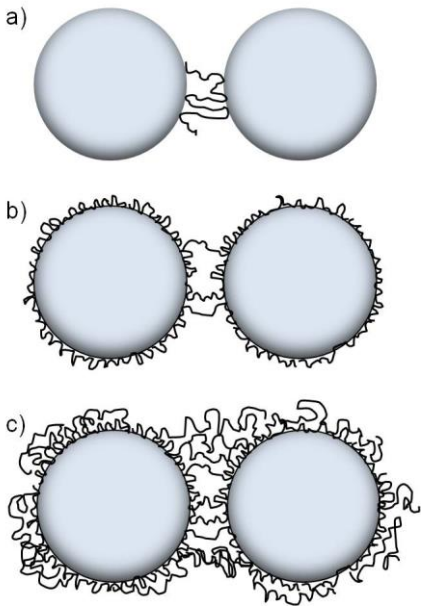

Figure 1.14. *Conformation models of bridging flocculation induced by associating polymer; a) irreversible bridging at low polymer concentrations; b) weak reversible bridging slightly above the saturation coverage; c) stabilised particles in the associating network of polymer. Figure adapted from reference 40.*

1.5 Fluorescence Spectroscopy

Luminescence is the emission of light from the electronically excited state of a substance.[41] Depending on the nature of the excited state, luminescence can be divided into two categories: fluorescence and phosphorescence. The difference between the two emissions can be described by a Jablonski diagram (see Figure 1.15). Fluorescence occurs via emission of light from the singlet state, while phosphorescence occurs through emission from the triplet state at a longer wavelength.[42]

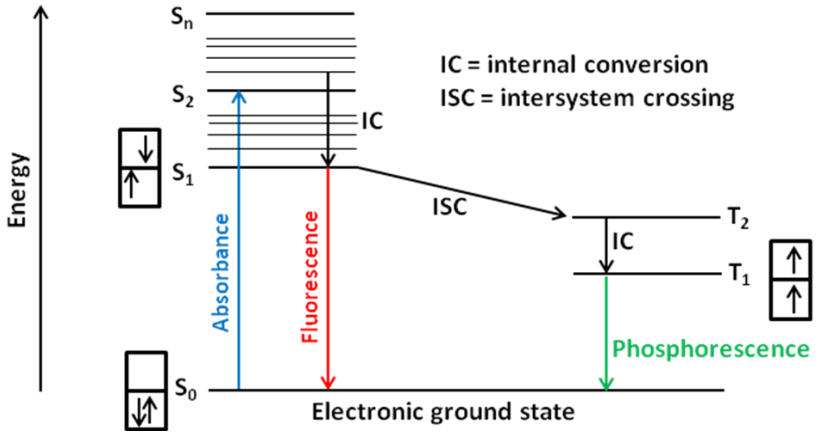

Figure 1.15. *Jablonski diagram illustrating the electronic states of a molecule and the transitions between them. Adapted from reference 41.*

Fluorescence techniques have long since been employed to investigate the dynamics of a chemical species at a molecular level. By attaching a fluorescent label (fluorophore) to a polymer chain, it is possible to observe the chain dynamics by looking at the properties of the fluorophore (intensity, lifetime, anisotropy). Examples of fluorophores that have been used to probe polymer conformation include acenaphthylene (ACE)[43], 9-anthrylmethyl methacrylate (AMMA)[44], 1-vinylnaphthalene (1-VN)[45] and pyrene[46,47,48] (Figure 1.16). One advantage of using fluorescence is its sensitivity. Only a trace amount of fluorophore is needed to monitor molecular processes, which prevents the fluorophore perturbing the system under investigation.

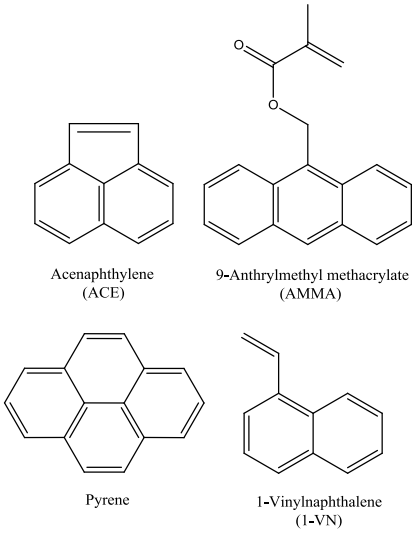

Figure 1.16. *Examples of fluorophore labels used to probe a polymer's molecular structure. ACE, AMMA and 1-VN can be covalently bound to polymers and pyrene becomes solubilised inside the polymer.*

1.5.1 Time-Resolved Anisotropy Measurements

Time-resolved anisotropy measurements (TRAMS) allow the motion of fluorophores to be observed during the lifetime of its excited state.[49] TRAMS data reports the orientation of the fluorophore, which in turn reflects the motion of the polymer chain to which it is attached. TRAMS has been found to be particularly useful for monitoring biological systems. Some of the biological processes examined with TRAMS include protein-protein interactions[49], enzyme flexibility[50] and lipid bilayers.[51] The rotation of macromolecules can depend on various factors such as size, shape and the solvent.[52]

The first step in TRAMS is to use vertically-polarised light to excite only the fluorophores that are vertically aligned. This is called photoselection and results in a degree of anisotropy, r, to be created in an otherwise isotropic solution. Once excited, the molecule may rotate during the lifetime of the excited state (typically ~10^{-9} s) leading to a decay in anisotropy (see Figure 1.17).

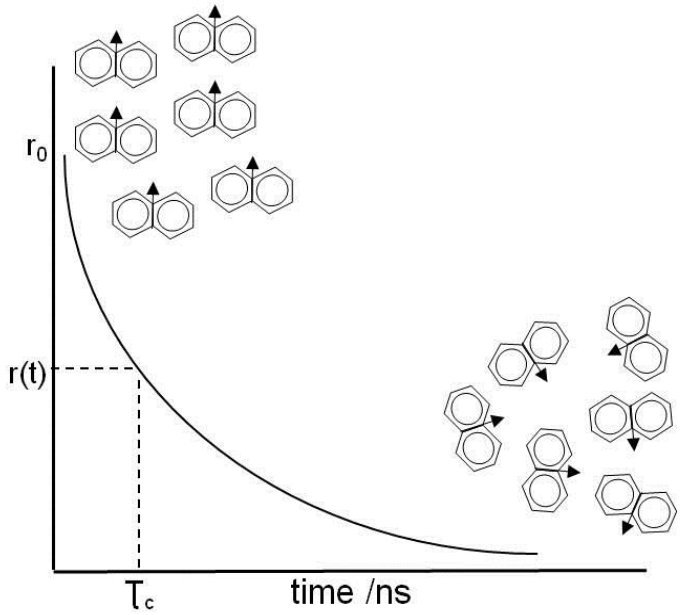

Figure 1.17. *Decay of anisotropy of vertically-excited fluorophores over time.*

The anisotropy, r, is derived by measuring the intensities of the vertically, I_{VV} and horizontally, I_{VH} polarized components of the fluorescence emission (see equation 1.1).

$$r = \frac{I_{VV} - I_{VH}}{I_{VV} + 2I_{VH}}$$ **Equation 1.1**

The decay of anisotropy can be treated mathematically using equation 1.2 to produce a correlation time, τ_c, which is characteristic of the molecular motion of the fluorophore. τ_c is the time taken for r to fall to 1/e of its initial value, r_0, see Figure 1.17.

$$r(t) = r_0 \exp(-\frac{t}{\tau_c})$$ **Equation 1.2**

Equation 1.2 is a single exponential decay model which provides a good fit to data when all excited fluorophores are in the same environment. A poor fit to the data indicates that the fluorophores are in more than one environment, requiring a more complicated decay model containing more than one τ_c.

1.5.2 Un-Adsorbed Polymer Conformation

TRAMS has been extensively used to investigate the conformation of polymers in solution. These include the conformation of poly(methacrylic acid) (PMAA) in water,[53] which has had either ACE or 1-VN fluorophores attached to its backbone. In basic aqueous media the fluorescence anisotropy could be described using a single exponential model of r(t) and had a τ_c of 5 ns. Below pH 4, at least two exponential terms were required for an adequate description of r(t) and a larger τ_c of ~23 ns was observed (see Figure 1.18).

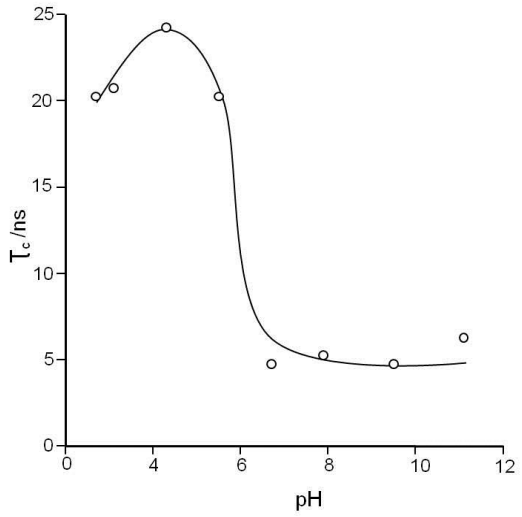

Figure 1.18. *pH dependence of τ_c for ACE-labelled PMAA. Figure adapted from reference 53.*

The larger τ_c observed below pH 4 indicated that the ACE label had more restricted motion, leading to the assumption that the polymer had become more coiled. The coiling was due to the COO- groups becoming protonated below pH 4, making the chains insoluble in water and hence minimising their contact with water. The requirement of two exponential terms below pH 4 showed that the label existed in two environments, as shown by Figure 1.19. The 'pearl necklace' model has been suggested for the presence of label in two domains. The pearl necklace model assumes there are collapsed regions of polymer joined together with water-swollen segments.[54] Above pH 4, electrostatic repulsion leads to PMAA to extend into a more open structure.

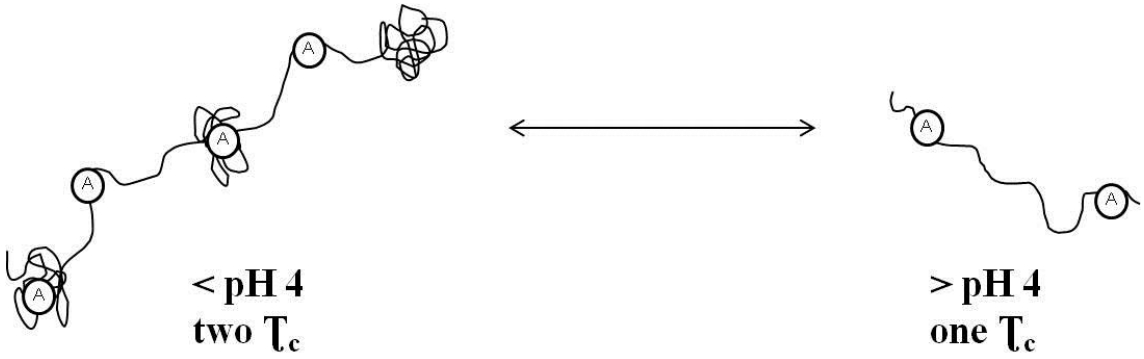

Figure 1.19. *Schematic showing the two possible conformations of PMAA above and below pH 4. Below pH 4, the ACE label exists in two environments (pearl necklace conformation) leading to the correlation time, τ_c to be resolved into two values. Above pH 4 the carboxylic acid groups become deprotonated, leading to PMAA to be pushed out into a more open conformation.*

The effect of substituents being attached to the polymer backbone was studied by comparing the correlation time of PMAA with poly(acrylic acid) (PAA) in dilute methanolic solution.[55] It was shown that PMAA had an average correlation time of 4.2 ns while PAA had a shorter average correlation time of 1.3 ns. The longer correlation time was attributed to the methyl group attached to the PMAA backbone, causing steric hindrance.

1.5.3 Adsorbed Polymer Conformation

TRAMS is a useful technique for studying the adsorption of molecules at interfaces as adsorption is associated with restricted mobility. The adsorption of a rhodamine B

(RhB) labelled polyelectrolyte adsorbed onto 18 nm diameter LUDOX silica in water was investigated by TRAMS.[56] The polyelectrolyte was a copolymer of diallyldimethyl ammonium chloride and N-(3-aminopropyl)methylacrylamide hydrochloride p(DADMAC-APMAA).

Figure 1.20 shows that, upon adsorption, the rate of decay of anisotropy, r(t), was longer in the presence of silica. Two correlation times of 2.8 ns and 685 ns were obtained from the fitting of anisotropy decay in Figure 1.20b. It was suggested that these two correlation times could arise from the polyelectrolyte adopting a loop and chain conformation on the silica. The RhB label attached in a loop should have more mobility and therefore a shorter correlation time of 2.8 ns. The higher correlation time of 685 ns should correspond to RhB label attached to bound train segments on the silica surface. The adsorption of poly(dimethylacrylamide) at the silica/water interface was also studied and was found to exist in a 'flat' conformation as trains on the silica.[57]

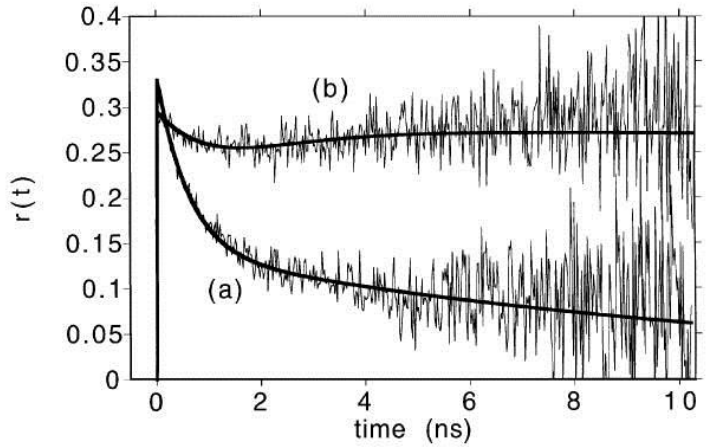

Figure 1.20. *TRAMS decay curves for aqueous solutions of RhB-labelled p(DADMAC-APMAA) (0.02 wt %) in a) the absence and b) presence of 18 nm silica (0.75 wt %).*[56]

Following this study, the adsorption of anthracene-labelled polystyrene onto quartz in cyclohexane was examined.[58] Upon adsorption, rotational motion of the anthracene label was hindered, leading to the decay of anisotropy to increase from 2.6 to 4.4 ns. The small increase in correlation time led to the hypothesis that the label was located in loops, so it could still rotate freely.

1.5.4 Steady State Spectroscopy

TRAMS is often used in combination with steady-state spectroscopy to provide additional information. The conformation of fluorophore-labelled polymers adsorbed at surfaces has been studied by looking at fluorescent emission via steady-state spectroscopy. For example, Tjipangandjara and Somasundaran[59] investigated the conformation of pyrene-labelled poly(acrylic acid) adsorbed onto 0.3 μm alumina particles in water using this technique. Excimer fluorescence was used to study polymer adsorption onto the alumina particles. An excimer is a short-lived dimeric or heterodimeric molecule that is formed from two species, with at least one of these species existing in its excited state. Excimers are characterised by broad emission at longer wavelengths. In this case, the excimer was obtained when an electronically excited pyrene encountered its identical self in the ground state. Emission from pyrene excimer formation gave a broad band at around 480 nm. The coiling index (intensity of excimer-to-monomer ratio I_e/I_m) for adsorbed pyrene-labelled PAA at the alumina-liquid interface was studied as a function of pH (see Figure 1.21). A high coiling index indicated that pyrene labels were in close contact signifying that the polymer was in a coiled conformation.

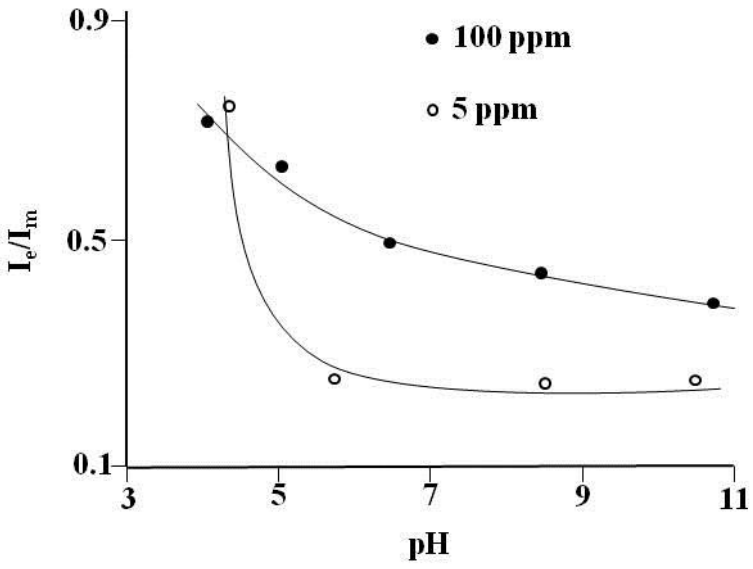

Figure 1.21. *The coiling index (excimer-to-monomer ratio, I_e/I_m) of poly(acrylic acid) at the alumina-liquid interface as a function of pH. The PAA concentration was either 5 ppm or 100 ppm. The alumina concentration was fixed at 5 wt %.*[59]

At pH 4, the adsorbed chains adopted a coiled conformation as shown by the high coiling index. Above pH 5, ionisation led to the carboxylic acid groups becoming negatively charged, leading to the chains to uncoil as shown by the reduced coiling index. The effect of polymer concentration also became significant above pH 5. At 100 ppm, the uncoiling of adsorbed polymer above pH 5 was less pronounced due to its higher concentration at the alumina surface, restricting expansion of adsorbed coils. It was shown that the polymer concentration was important if a stable dispersion was required. Above pH 6, a low polymer concentration led to flocculation of particles due to the chains being able to fully uncoil and bridge between particles. When a higher concentration was used, a stable dispersion was obtained above pH 6 due to the poly(acrylic acid) chains becoming more compact. This behaviour is illustrated in Figure 1.22.

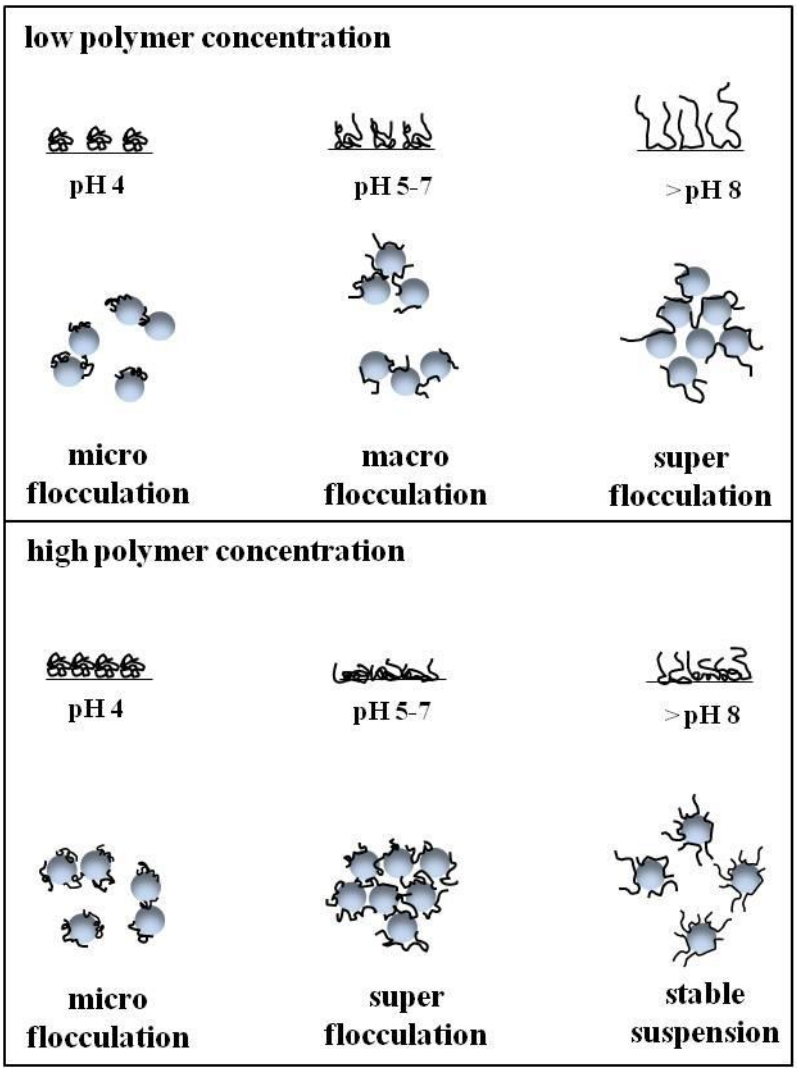

Figure 1.22. *Schematic representations of the conformation of adsorbed poly(acrylic acid) at the alumina-liquid interface at various pH and at both high and low polymer concentration. Figure adapted from reference* 59.

1.6 Small-angle scattering

Small-angle scattering (SAS) developed by Guinier in the 1930's is an extremely powerful technique which can be used to determine the average size and shape of colloidal systems.[60] The principles of scattering can vary depending on the type of particles being studied. If the probing particles are electrons then only the surface of the sample is analysed due to electrons being electrostatically repelled by the orbital electrons in the sample. X-rays are electromagnetic waves and can penetrate further into the sample but still get absorbed and scattered by the orbital electrons. Neutrons, which possess no charge, can penetrate a sample considerably further and interact with the nucleus of the atom. Depending on the source of particles and experimental set-up being used, different length scales can be investigated.

In scattering experiments, length scale is related to the scattering vector, q. q quantifies length in reciprocal space by describing the relationship between the incident, k_i, and scattered, k_s, wave vectors, as shown by Figure 1.23. The isosceles triangle in Figure 1.23 has two equal sides of length $2\pi/\lambda$ and trigonometry yields equation 1.3. By substituting the Bragg law of diffraction (equation 1.4) into equation 1.3 we obtain equation 1.5 which is a simple expression that relates q to the size, d, of the scattering particle.

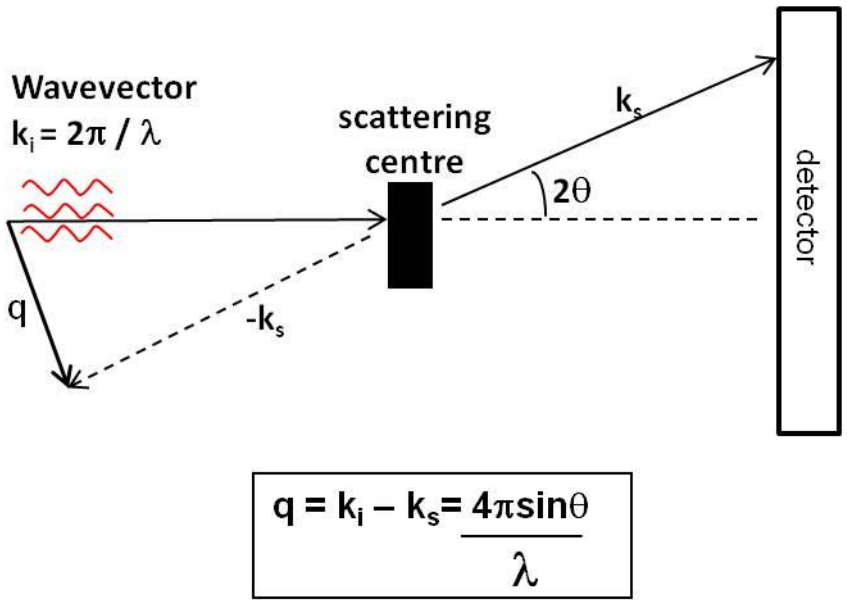

Figure 1.23. *Schematic representation showing elastic scattering of an incident beam at an angle of 2θ.*

$$q = \frac{4\pi sin\theta}{\lambda}$$ **Equation 1.3**

$$\lambda = 2dsin\theta$$ **Equation 1.4**

$$d = \frac{2\pi}{q}$$ **Equation 1.5**

Figure 1.24 shows the typical q-ranges available using various scattering techniques, the length scale will vary slightly depending on experimental conditions.

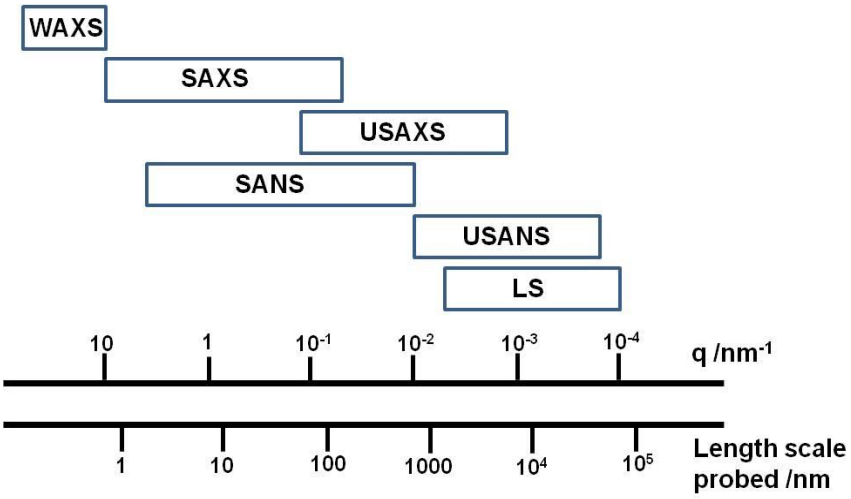

Figure 1.24. *Typical q-range and length scales probed by various scattering methods. Wide-angle scattering (WAXS), small-angle X-ray scattering (SAXS), ultra-small X-ray scattering (USAXS), small-angle neutron scattering (SANS), ultra-small neutron scattering (USANS) and light scattering (LS).*

Scattering is a very useful technique with the scattering profile containing a wealth of information on the sample under analysis. SANS and SAXS data contain information about the size and shape of the object (form factors) and also the particles interactions (structure factors). To extract valuable information out of the scattering curves, the correct model must be fitted to the data.

1.7 Small-angle neutron scattering (SANS)

Neutron scattering is a non-invasive technique used to probe the surface and perform bulk analysis of materials. Scattering can be either coherent or incoherent. The coherent scattering (whereby the phase of the scattering is conserved) reveals structural information for the sample under analysis.

1.7.1 Instrument set-up

Neutron instruments consist of a neutron source, moderator, collimator and a detector.

- **Neutron source**

Neutrons can be produced either by reactor sources or pulsed sources. Reactor sources continuously produce neutrons by nuclear fission. The Institute Laue-Langevin (I.L.L) in Grenoble, France is an example of an institute that utilises a reactor source. Pulsed sources produce neutrons by spallation through bombardment of a metal target with protons from a particle accelerator. ISIS in Rutherford, UK uses a spallation source using a uranium target. Nuclear fission sources operate in continuous mode whereby the neutrons are continuously generated, whereas spallation sources operate in time-of-flight mode whereby neutrons are produced in pulses.

- **Moderator**

Once neutrons are produced, by either a reactor or spallation source, they need to be moderated. Moderation is a process whereby the neutrons lose some kinetic energy and velocity to become 'thermal' neutrons. Thermal neutrons are needed in SANS as they provide longer wavelengths, allowing larger sizes to be probed. Moderation is achieved by passing the neutrons through a material with a low atomic number such as H_2O or D_2O in a liquid, gas or solid form. The thermal neutrons can be used in two ways: i) filtered so only neutrons with a narrow range of wavelengths exist or ii) use the broad range of wavelengths available. The filtering of neutron wavelengths creates a fixed-wavelength instrument and is used at reactor sources. The latter approach gives a fixed-geometry instrument and is used in conjunction with time-of-flight spallation sources.

- **Collimator**

Through the use of apertures coated with neutron-absorbing material, the cold neutron beam is collimated to a suitable size and shape before hitting the sample.

- **Detector**

The scattering pattern from neutrons hitting the sample is commonly displayed on a two-dimensional detector. Most detectors are created from Geiger-Muller tubes containing a detection medium such as ^{3}He. Any part of the beam that passes straight through the sample without scattering is prevented from reaching the detector using a beam-stop. This is to prevent damage to the detector through over-exposure.

1.7.2 Contrast Matching

Neutron scattering is nucleus-dependent, leading to neutron scattering lengths varying with atomic number. Neutron scattering is so sensitive that even isotopes of the same element, such as hydrogen and deuterium, can give very different scattering lengths. Contrast matched conditions arise when the scattering length density, ρ, of a solvent is matched to the scattering length density of the sample, rendering it 'invisible'. The wide availability of deuterated solvent makes manipulating the contrast-matched point easy. The most commonly used deuterated solvent is D_2O due to it being relatively cheap and abundantly available. Contrast matching is advantageous as it allows the scattering problem to be simplified. This is especially useful when studying multi-component systems, such as the conformation of polymers adsorbed onto a particle surface in solution. Through contrast matching, a three-component system can be reduced to a two-component system.

The use of SANS and contrast matching to examine the structure of adsorbed polymer layers at interfaces has extensively been employed by Cosgrove et al. who have investigated the structure of adsorbed poly(ethylene oxide) (PEO) on silica[61], polystyrene[28,62] and Laponite[63]. By using contrast matching to look only at scattering from the adsorbed polymer layer, a volume fraction profile, φ(z), could be constructed.

Despite the many advantages of using SANS to investigate the conformation of a polymer at a surface, there are also disadvantages associated with this technique. An overview of the advantages and disadvantages is given below.

Advantages

- Can probe both bulk and surface properties of matter.
- Can penetrate far into the sample due to neutrons only interacting by short-range nuclear interactions without destroying the sample.
- Good probe to investigate solid and liquid materials.
- Can use 'contrast matching' to simplify scattering patterns.

Disadvantages

- Neutrons are expensive.
- Neutron sources are associated with a low flux of neutrons.
- Scattering is weak, so relatively large amounts of sample is needed (~1 ml). This can be expensive if deuterated sample or solvent is used.

1.8 Small-angle X-ray scattering (SAXS)

Small-angle X-ray scattering (SAXS) is a very similar technique to SANS and often the two are compared in the literature.[64] SAXS probes a similar length scale to SANS so often the two scattering methods complement each other and can be used to gather more information on the probed matter. Like SANS, SAXS also enables contrast matching by using the same electron density for two materials. By altering the electron density of the solvent or sample, components can be made invisible. However, contrast matching using SAXS is not often used as changing electron density is often accompanied with changing the sample structure and environment. For this reason, SANS is the preferred technique for contrast matching experiments.

1.9 Present Work

Stored pigment dispersions experience a change in viscosity over time, in many cases a reduction. Along with a decrease in viscosity, a drop in pH is often observed. A critical physical performance parameter for inks is that their viscosity remains stable during storage. The change in viscosity cannot solely be explained by a change of the polyelectrolyte structure.

It is hypothesised that some bridging flocs could be generated during the pigment milling process. It is assumed that during storage this flocculation is not persistent and this results in an irreversible change in polymer/particle structure manifesting itself as a change in viscosity.

The objective of this research was to study the conformation of the copolymer dispersant poly(methacrylic acid-benzyl methacrylate), p(MAA-BzMA) adsorbed onto pigment particles.

In summary, the project aims are:

- The generation of model systems for electrostatically-stabilised colloidal dispersions using silica particles and weak amphiphilic polyelectrolytes as dispersants.
- Characterisation of such dispersions using scattering and fluorescent analytical techniques.
- To gather a better understanding of bridging flocculation and the polyelectrolyte structure
- To probe the stability of bridging flocs and their contribution to the dispersion viscosity

1.10 References

1. Gregory, P., *High-Technology Applications of Organic Colorants*, Plenum Press: New York, 1991, 175-205.
2. Gunther, M. S.; Sarkisian, G. M.; Xu, Y., *Inkjet printing using pigments and dye-based inks*, **2004**, US patent 6705702B2.
3. Ma, S.; Matrick, H.; Shor, A. C.; Spinelli, H. J., *Aqueous pigmented inks for ink jet printers*, **1992**, US patent 005085698.
4. Le, H. P., *Journal of Imaging Science and Technology*, **1998**, *42*, 49-62.
5. Daniels, E. S.; Sudo, E. D.; El-Aasser, M. S., *ACS Symposium Series*, **1992**, *492*, 282-288.
6. Daryaguin, B. V.; Landau, L., *Acta Physicochim*, **1941**, *14*, 633-662.
7. Verwey, E.J.; Overbeek, J.T.G., *Theory of the Stability of Colloidal Dispersions*, Elsevier, Amsterdam, 1948.
8. Einarson, M. B.; Berg, J. C., *Journal of Colloid and Interface Science*, **1993**, *155*, 165-172.
9. Ottewill, R. H.; Satgurunathan, R., *Colloid and Polymer Science*, **1995**, *273*, 379-386.
10. Napper, D. H., *Industrial and Engineering Chemistry Product Research and Development*, **1970**, *9*, 467-477.
11. Clayfield, E. J.; Lumb, E. C., *Macromolecules*, **1968**, *1*, 133-138.
12. Vincent, B., *Advances in Colloid and Interface Science*, **1974**, *4*, 193-277.
13. Napper, D. H., *Journal of Colloid Interface Science*, **1977**, *58*, 390-407.
14. Stenkamp, V. S.; Berg, J. C., *Langmuir*, **1997**, *13*, 3827-3832.
15. Zhulina, E. B.; Borisov, O. V., *Journal of Colloid and Interface Science*, **1990**, *144*, 507-520.
16. Sato, T.; Ruch, R., *Stabilization of Colloidal Dispersions by Polymer Adsorption*, Marcel Dekker, New York, 1980.
17. Napper, D. H., *Polymeric Stabilisation of Colloidal Dispersions*, Academic Press, London, 1983.
18. Urban, D.; Takamura, K., *Polymer Dispersions and Their Industrial Applications*, Wiley-VCH, Weinheim, 2002.
19. Schofield, J.D., *Handbook of Coating Additives*. Vol. 2, Marcel Dekker: New York, 1992, 71–104.

20. Scheutjens, J. M. H. M.; Fleer, G. J., *The Journal of Physical Chemistry*, **1980**, *84*, 178-190.
21. Cohen Stuart, M. A.; Cosgrove, T.; Vincent, B., *Advances in Colloid and Interface Science*, **1986**, *24*, 143-239.
22. Im, D. H.; Park, S. Y.; Hyun, S. H.; Lee, B. Y.; Kim, Y. H., *Journal of Materials Science*, **2004**, *39*, 3629-3633.
23. Thies, C., *The Journal of Physical Chemistry*, **1966**, *70*, 3783-3790.
24. Howard, G. J.; McConnell, P., *Journal of Physical Chemistry*, **1967**, *71*, 2974-2981.
25. Boomgaard, T.; King, T. A.; Tadros, T. F.; Tang, H.; Vincent, B., *Journal of Colloid and Interface Science*, **1978**, *66*, 68-76.
26. Cohen Stuart, M. A.; Fleer, G. J.; Bijsterbosch, B. H., *Journal of Colloid and Interface Science: Part B*, **1982**, *90*, 321-334.
27. King, S.; Griffiths, P.; Hone, J.; Cosgrove, T., *Macromolecular Symposia*, **2002**, *190*, 33-42.
28. Marshall, J. C.; Cosgrove, T.; Leersmakers, F.; Obey, T. M.; Driess, C. A., *Langmuir*, **2004**, 20, 4480-4488.
29. Cohen Stuart, M. A.; Scheutjens, J. M. H. M.; Fleer, G. J., *Journal of Polymer Science, Physics Edition*, **1980**, *18*, 559-573.
30. Koopal, L. K., *Journal of Colloid and Interface Science*, **1981**, *83*, 116-129.
31. Fleer, G. J.; Cohen Stuart, M. A.; Scheutjens, J. M. H. M.; Cosgrove. T.; Vincent, B., *Polymers at Interfaces*, Chapman and Hall: London, 1993.
32. Yoon, C.; Choi, J., *Society of Dyers and Colourists*, Colouration Technology, **2008**, *124*, 355-363.
33. Spinelli, H. J., *Advanced Materials*, **1998**, *10*, 1215-1218.
34. Chang, C.; Chang, S.; Shih, K.; Pan, F., *Journal of Polymer Science: Part B: Polymer Physics*, **2005**, *43*, 3337-3353.
35. Auschra, C.; Eckstein, E.; Mühlebach, A.; Zink, M.; Rime, F., *Progress in Organic Coatings*, **2002**, *45*, 83-93.
36. Kislenko, V. N.; Somasundaran, P., *Encyclopedia of Surface and Colloid Science*, 2nd edition, Taylor and Francis: Boca Raton, 2012.
37. Steffe, J. F., *Rheological Methods in Food Process Engineering*, 2nd edition, Freeman Press: East Lansing, 1996.
38. Barnes, H. A., *A Handbook of Elementary Rheology*, Cambrian Printers:

Aberystwyth, 2000.

39. Otsubo, Y., *Journal of Colloid and Interface Science*, **1999,** *215*, 99-105.
40. Saito, Y.; Ogura, F.; Otsubo, Y., *Colloid and Polymer Science,* **2008**, *286*, 1537-1544.
41. Lakowicz, J. R., *Principles of Fluorescence Spectroscopy*, 3rd edition, Springer: New York, 2006.
42. Jablonski, A., *Z Phys*, **1935**, *94*, 38-46.
43. Chee, C.K.; Rimmer, S.; Soutar, I.; Swanson, L., *Polymer*, **2001**, *42*, 5079-5087.
44. Soutar, I.; Swanson, L., *Polymer International*, **2006,** *55***,** 729–739.
45. Ebdon, J.R.; Hunt, B.J.; Lucas, D.M.; Soutar, I.; Swanson, L.; Lane, A.R., *Canadian Journal of Chemistry,* **1995**, *73*, 1982-1994.
46. Chu, D. Y.; Thomas, J. K., *Macromolecules*, **1984**, *17*, 2142-2147.
47. Olea, A. F.; Thomas, J. K., *Macromolecules*, **1989**, *22*, 1165-1169
48. Chen, T. S.; Thomas, J. K., Journal of Polymer Science: *Polymer Chemistry Edition*, **1979**, *17*, 1103-1116.
49 . Beechem, J. M.; Brand, L., *Annual Review of Biochemistry*, **1985**, *54*, 43-71.
50. Broos, J.; Visser, A. J. W. G.; Engbersen, J. F. J.; Verboom, W.; Hoek, A.; Reinhoudt, D. N., *Journal of the American Chemical Society*, **1995**, *117*, 12657-12663.
51. Stubbs, C. D.; Kinosita, K.; Munkonge, F.; Quinn, P. J.; Ikegami, A., *Biochimica et Biophysica Acta*, **1984**, *775*, 374-380.
52. Chee, C. K.; Hunt, B. J.; Rimmer, S.; Soutar, I.; Swanson, L., *Soft Matter*, **2011**, *7*, 1176-1184.
53. Soutar, I.; Swanson, L., *Macromolecules*, **1994**, *27*, 4304-4311.
54. Ghiggino, K. P.; Tan, K. L., *Polymer Photophysics: Luminescence, Energy Migration and Molecular Motion in Synthetic Polymers*, Chapman and Hall: London, 1985, 341-375.
55. Soutar, I.; Swanson, L.; Imhof, R. E.; Rumbles, G., *Macromolecules*, **1992**, *25*, 4399-4405.
56. Smith, T. A.; Irwanto, M.; Haines, D. J.; Ghiggino, K. P.; Millar, D. P., *Colloid and Polymer Science*, **1998**, *276*, 1032-1037.
57. Soutar, I.; Swanson, L.; Wallace, S. J. L.; Ghiggino, K. P.; Haines, D. J.; Smith, T. A., *Multidimensional Spectroscopy of Polymers*, American Chemical Society, 1995, 363-378.

58. Jeon, S.; Bae, S. C.; Granick, S., *Macromolecules*, **2001**, *34*, 8401-8404.
59. Tjipangandjara, K. F.; Somasundaran, P., *Colloids and Surfaces*, **1991**, *55*, 245-255.
60. Guinier, A., *Ann. Phys. Paris*, **1939**, *12*, 161-237.
61. Qiu, D.; Flood, C.; Cosgrove, T., *Langmuir*, **2008**, *24*, 2983-2986.
62. Hone, J. H. E.; Cosgrove, T.; Saphiannikova, M.; Obey, T. M.; Marshall, J. C.; Crowley, T. L., *Langmuir*, **2002**, *18*, 855-864.
63. Nelson, A.; Cosgrove, T., *Langmuir*, **2004**, *20*, 2298-2304.
64. Pethrick, R. A.; Dawkins, J. V., *Modern Techniques for Polymer Characterisation*, John Wiley and Sons: West Sussex, 1999, pp 172.

CHAPTER II

Synthesis and Characterisation of Poly(methacrylic acid-co-benzyl methacrylate) Copolymers

2.0 Introduction

The free-radical polymerisation of two or more monomers offers an extremely useful route to a range of copolymers exhibiting combined properties of the corresponding homopolymers.[1] It was Staudinger who first reported that during copolymerisation the rate at which monomer units entered the chain differed.[2] Depending on the reactivity of the monomer units, the final sequence distribution of the monomers can be alternating (-ABABAB-), block (-AAABBB-) or random (-ABBAABA-). The reactivity of monomers can be quantified by obtaining the monomer reactivity ratios, r_1 and r_2. If the reactivity ratios are known, an estimation of copolymer composition can be made as they give an indication of the preference of a monomer to either react with itself or cross-propagate with the second monomer. Over the years, monomer reactivity ratios have been determined for a vast number of copolymer systems and this work is well documented in the literature.[3] Figure 2.1 displays the different distribution of monomers that can occur for various reactivity ratios. The difference in reactivity of monomers has been found to depend on three factors: resonance stability, polarity and steric effects.[2]

Figure 2.1. *Possible copolymer structures that can occur with different reactivity ratios, r_1 and r_2. The red monomer unit corresponds to r_1 and the black monomer unit corresponds to r_2.*

Free-radical polymerisation is often employed in industry to manufacture copolymers as the method is easy, cheap and efficient. The production of copolymers in industry by free-radical polymerisation can be split into three processes: batch, semi-batch and continuous. The batch process is the simplest of the three methods, simply requiring all reactants to

be added to the vessel prior to polymerisation, and during the process no reactants are removed or added. The final structure of the copolymers synthesised under batch conditions is controlled by the reactivity of the monomers. After each batch polymerisation, the reaction vessel needs to be discharged of its contents and prepared for the next reaction. This is time-consuming and leads to poor reproducibility between batches. During polymerisation, an increase in viscosity occurs which makes it difficult to stir the mixture, resulting in a variation in temperature throughout the reaction mixture. For the aforementioned reasons, batch polymerisations are not commonly used in industry.

Semi-batch polymerisation involves gradually adding reactants to a reaction vessel that already contains a polymerising mixture. The addition of reactants is occasionally accompanied by product simultaneously being removed from the vessel. The gradual addition of monomer and simultaneous removal of product avoids the issue of increasing viscosity and overcomes the stirring problems. This technique is favoured in industry as it allows some control over polymer properties and reaction rate.

Polymerisations conducted via a continuous process involve continuous addition of reactants to the reaction vessel, while at the same time unused reactants and products are simultaneously removed. This process is an efficient method for mass production of polymer, as no time is lost extracting product and restarting the polymerisation process.

This chapter focuses on the characterisation of poly(methacrylic acid-co-benzyl methacrylate), p(MAA-BzMA) copolymers synthesised by free-radical polymerisation under semi-batch and batch conditions. Raman spectroscopy was used to follow the kinetics of the batch copolymerisation of MAA and BzMA. Reactivity ratios, r_1 and r_2 for the batch copolymersation of MAA and BzMA were obtained using the Finemann and Ross[4] and Kelen-Tudos[5] method in conjunction with ^{13}C NMR to analyse the microstructure of the copolymer through the assignment of triads.

2.1 Experimental

2.1.1 Materials

Methacrylic acid (MAA) and benzyl methacrylate (BzMA) were purchased from Aldrich. Methacrylic acid and benzyl methacrylate were passed through an inhibitor removal column to remove monomethyl ether hydroquinone before use. Dipropylene glycol, 99 % mixture of isomers (DPG), tert-butyl peroxy-2-ethylhexanoate (Trigonox 21s), methyl iodide and triethyl amine (TEA) were purchased from Aldrich and used as received. Deuterated DMSO ($(CD_3)_2SO$), tetrahydrofuran (THF), hexane and dimethylfuran (DMF) were purchased from Fisher and used as received. Ultrapure deionised water was used in all experiments.

2.1.2 Synthesis

2.1.2.1 Synthesis of Poly(methacrylic acid-co-benzyl methacrylate) p(MAA-BzMA) 36 mol % MAA : 64 mol % BzMA

- **Semi-Batch free-radical polymerisation (40 wt % solids)**

DPG (40.0 g) was placed into a three-necked reaction vessel equipped with a mechanical stirrer, under a nitrogen atmosphere and heated to 70°C. Two lines were used to feed in the remaining reactants using a peristaltic pump. The first line fed in MAA (11.47 g, 0.13 mols), BzMA (38.53 g, 0.22 mols) and DPG (20.0 g). The second line fed in Trigonox 21s (0.89 g, 4.1 mmols) and DPG (20.0 g). Feeding of all the reagents into the vessel commenced at the same time at a flow rate whereby all the reagents were added over a period of three hours. Once all of the reagents had been added, the reaction solution was stirred for another 3 h at 70°C. The resulting copolymer was purified by precipitation twice into excess water and finally into excess hexane. Between each precipitation, the copolymer was dried in a vacuum oven and re-dissolved into THF.

- **Batch free-radical polymerisation (20 wt % solids)**

MAA (2.10 g, 24.4 mmols), BzMA (7.90 g, 44.8 mmols), AIBN (0.10 g) and DPG (40.0 g) were added to a two-necked 100 ml round-bottom flask. The reaction mixture was purged with nitrogen for 1 h and placed into a pre-heated oil bath at 70°C. The reaction solution was stirred at 70°C under a nitrogen blanket for 6 h. The reaction was quenched through exposure to oxygen. The resulting copolymer was purified by precipitation twice into water and finally into hexane.

2.1.2.2 Esterification of poly(methacrylic acid-benzyl methacrylate)[6]

Prior to GPC analysis, all p(MAA-BzMA) copolymers were methylated using the following protocol. Carboxylic acid groups in the p(MAA-BzMA) copolymers were converted into methyl ester groups using a two-fold excess of methyl iodide in dimethylfuran (DMF) at 20°C in the presence of triethylamine (TEA). TEA, copolymer and DMF were placed in the flask and stirred for 15 minutes to allow the acid-base reaction to occur. After this time, methyl iodide was added, and the reaction was left to stir at room temperature for 24 h. Methylation was shown to be successful by ^{1}H NMR in $(CD_3)_2SO$ which gave a new peak at ~3.7 ppm resulting from the COOH group in MAA being converted to $COOCH_3$.

2.1.2.3 Monomer reactivity ratio (r_1 and r_2) determination for the batch copolymerisation of BzMA and MAA (20 wt % solids)

Six BzMA and MAA mixtures were investigated. Each had a constant amount of AIBN initiator (1 wt % based on monomers) and a constant amount of dipropylene glycol (DPG) solvent. Varying amounts of MAA, BzMA, DPG and AIBN were placed in a flask with a magnetic stirrer. The flask was purged with N_2 for 30 minutes, sealed and immersed into an oil bath at 70°C to start the polymerisation. After 10 minutes the polymerisation was quenched by exposure of the reaction mixture to oxygen and plunging the reaction vessel into ice cold water. Precipitation of the copolymer was carried out in methanol for copolymerisations with 55 mol % or above of BzMA in the reaction feed. Precipitation of copolymers with 73 mol % or above of MAA was precipitated into acidic water. After each precipitation, the copolymer was filtered and dried in a vacuum oven at room

temperature. Dried copolymer was weighed to calculate conversion and analysed by ^{1}H NMR in $(CD_3)_2SO$ to calculate the mol fraction of MAA and BzMA in the copolymer.

2.1.3 Characterisation

2.1.3.1 ^{1}H NMR and ^{13}C NMR Spectroscopy

All ^{1}H NMR spectra were recorded in $(CD_3)_2SO$ using a 400 MHz Bruker Avance-400 spectrometer. ^{13}C NMR spectra were recorded on a 500 MHz Bruker DRX. ^{13}C NMR was recorded on 200 mg of sample dissolved in 1 ml of $(CD_3)_2SO$ and run for 16 h to get high signal-to-noise ratios.

2.1.3.2 Gel Permeation Chromatography (GPC)

Molecular weight distributions of batch and semi-batch prepared copolymers were assessed using GPC. M_n and M_w values were determined using a THF GPC equipped with a RI detector and Polymer Laboratories PL gel 5 µm Mixed-C columns. The THF eluent contained 0.05 wt % BHT and monodisperse polystyrene standards were used for calibration. The column was set at 30ºC.

2.1.3.3 Raman Spectroscopy

Kinetic studies of the batch copolymerisation of MAA and BzMA were followed by Raman spectroscopy. Raman spectra were obtained using an Ocean Optics QE65000 spectrometer with an Ocean Optics 785 nm laser excitation source. Spectra were collected between 0-2792 cm^{-1} using a fibre optic probe with a focal length of 10 mm and 210 µm focal spot size. Spectra were obtained by holding the probe 8 mm outside the 25 cm^3 round bottom flask containing the reaction mixture. Measurements began when the reaction was placed on a heated mantle set at 70ºC. Spectra were collected over one minute (5 second integration, averaged over 10 scans). This scanning time was used as it allowed high signal-to-noise for good-quality spectra. For all spectra the 'dark signal' was subtracted (intensity signal when the laser was covered). Data were processed using

Ocean Optics software. Conversion of monomer was calculated using equation 2.1 where I_0 is the intensity of a peak at 0 minutes and I_t is the intensity of the same peak at time t.

$$\textbf{Conversion } \% = \left(\mathbf{1} - \frac{\mathbf{I_t}}{\mathbf{I_0}}\right) \times \mathbf{100} \qquad \textbf{Equation 2.1}$$

2.2 Results and Discussion

2.2.1 Synthesis

Poly(methacrylic acid-co-benzyl methacrylate), p(MAA-co-BzMA), was prepared by free-radical copolymerisation in dipropylene glycol (DPG) at 70°C (see Figure 2.2). DPG is commonly used in industry due to its low toxicity and high boiling point of 230°C.[7] It has the molecular formula of $C_6H_{14}O_3$ and exists as a mixture of three isomers (see Figure 2.3).

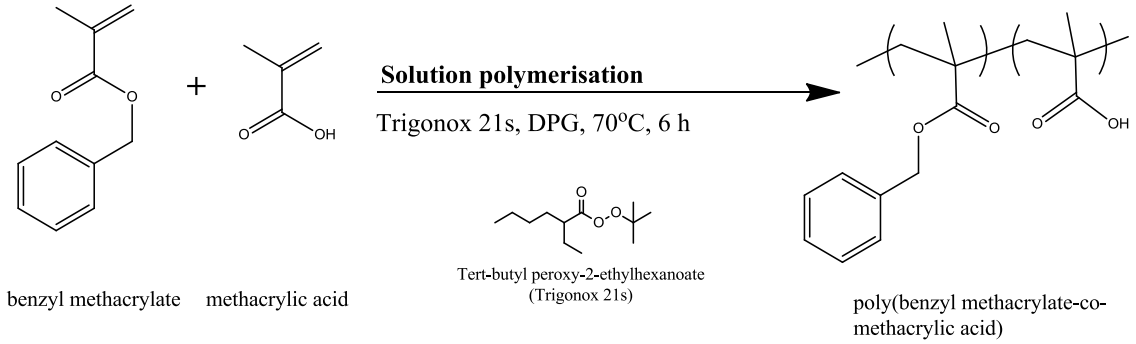

Figure 2.2. *Schematic representation of the synthesis of poly(benzyl methacrylate-co-methacrylic acid) p(BzMA-co-MAA) by free-radical polymerisation in DPG at 70°C.*

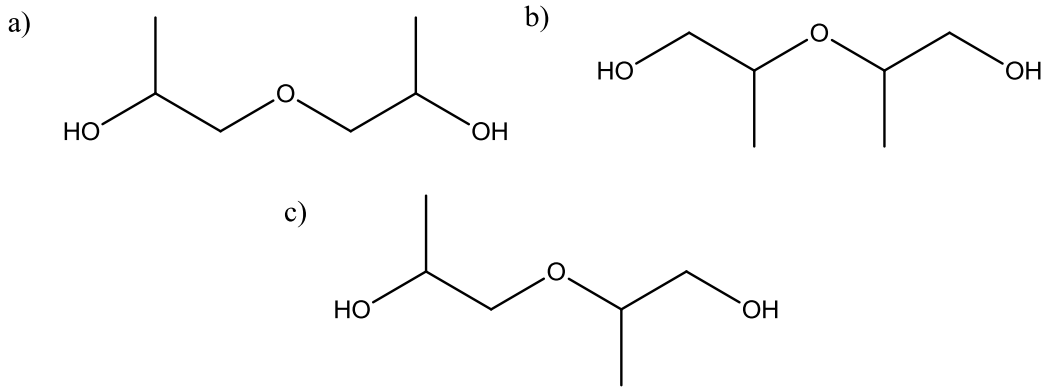

Figure 2.3. *Three isomers of dipropylene glycol (DPG).*

The p(MAA-co-BzMA) copolymer was synthesised under two conditions: semi-batch and batch. Semi-batch conditions were achieved by feeding monomers (MAA and BzMA) and Trigonox 21s initiator into a reaction vessel containing DPG via two separate

lines (see experimental section 2.1.2 for more details). Table 2.1 shows data obtained for the two p(MAA-co-BzMA) copolymers synthesised under semi-batch and batch conditions. For each copolymer a 64:36 mol % of BzMA:MAA was targeted. It can be seen from Table 2.1 how the actual mol % differed to the target mol %, especially in the case of the batch synthesis. In batch copolymerisations, the overall copolymer composition is highly dependent on the reactivity of the two monomers which can lead to divergences from the originally targeted composition. The ^{1}H NMR of p(MAA-co-BzMA) prepared under semi-batch conditions is shown in Figure 2.4.

Method of polymerisation	M_n[a] / g mol^{-1}	M_w / g mol^{-1}	M_w/M_n	Target mol % MAA	Actual mol % MAA[b]
Semi-batch	47800	86200	1.8	36	39
Batch	24500	37700	1.5	36	43

Table 2.1. *P(MAA-co-BzMA) copolymers synthesised under semi-batch and batch conditions by free radical polymerisation in DPG at 70°C. [a]M_n and M_w/M_n values were determined by THF GPC against PS standards. [b]Determined by ^{1}H NMR spectroscopy in* $(CD_3)_2SO$.

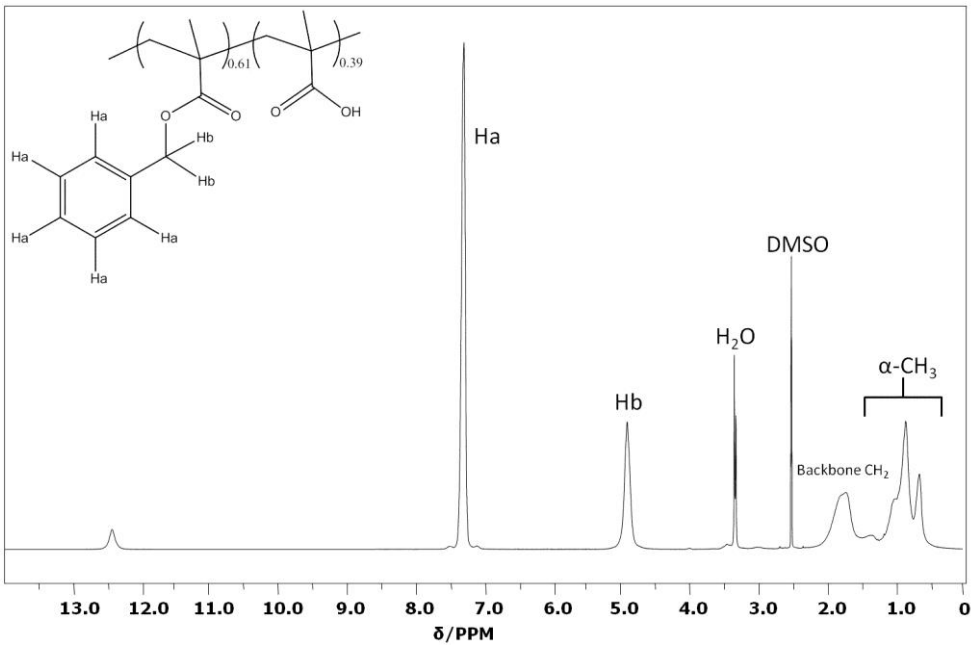

Figure 2.4. *^{1}H NMR spectrum of p(MAA-BzMA), 39 mol % MAA in $(CD_3)_2SO$ after two precipitations into water and then finally into hexane.*

2.2.2 Determination of the monomer reactivity ratios for the batch copolymerisation of methacrylic acid and benzyl methacrylate in dipropylene glycol.

In order to gain insight into the copolymer structure (and hence its performance) the sequence distribution needs to be known. If it is assumed that the copolymerisation of two monomers, M_1 and M_2, follow the terminal unit copolymerisation model, then there are only four ways in which the monomers can propagate (see Figure 2.5). The terminal unit model assumes that the propagating chain is only dependent on the radical monomer unit at the chain end and any occurring side reactions are insignificant. For each propagation reaction shown in Figure 2.5, a propagation constant, k, is given.

$$-M_1\cdot + M_1 \xrightarrow{k_{11}} -M_1M_1\cdot$$

$$-M_1\cdot + M_2 \xrightarrow{k_{12}} -M_1M_2\cdot$$

$$-M_2\cdot + M_1 \xrightarrow{k_{21}} -M_2M_1\cdot$$

$$-M_2\cdot + M_2 \xrightarrow{k_{22}} -M_2M_2\cdot$$

Figure 2.5. *The four different ways in which two monomer units can propagate if it is assumed that the terminal unit polymerisation model is valid.*

Reactivity ratios are defined in equations 2.2 and 2.3, as the ratio of the reactivity of the self-propagating reactions (k_{11} or k_{22}) to the ratio of reactivity for the cross-propagating reactions (k_{21} or k_{12}).

$$r_1 = \frac{k_{11}}{k_{12}} \qquad \textbf{Equation 2.2}$$

$$r_2 = \frac{k_{22}}{k_{21}} \qquad \textbf{Equation 2.3}$$

From the terminal model, the well-known Mayo-Lewis[8] copolymer equation was derived (see Equation 2.4), which allows the sequence distribution of a copolymer to be predicted at low conversions.

$$\frac{d[M_1]}{d[M_2]} = \frac{[M_1]\, r_1[M_1] + [M_2]}{[M_2]\, r_2[M_1] + [M_2]}$$ **Equation 2.4**

Alternatively, if the mole fraction of monomer in the feed, f, and the mole fraction of monomer in the copolymer, F, is considered then the copolymer equation can be transformed into equation 2.5, which was originally proposed by Finemann and Ross.[4]

$$F_1 = \frac{r_1 f_1^{\,2} + f_1 f_2}{r_1 f_1^{\,2} + 2 f_1 f_2 + r_2 f_2^{\,2}}$$ **Equation 2.5**

This is a convenient form of the equation because by plotting f(1-F)/F vs f^2/F a linear plot can be obtained where r_1 can be extrapolated from the slope and r_2 can be obtained from the intercept (equation 2.6). In this equation $f=m_1/m_2$ and $F=M_1/M_2$ where m is the mole fraction of monomer in the feed and M is the mole fraction of monomer in the copolymer.

$$\frac{f(1-F)}{F} = r_1\left(\frac{f^2}{F}\right) - r_2$$ **Equation 2.6**

Figure 2.6 displays a plot of f(1-F)/F versus f^2/F for the batch copolymerisation of MAA and BzMA. Reactivity ratios for the free-radical copolymerisation of MAA and BzMA in DPG at 70°C were determined by setting up six reactions at various monomer concentrations and then analysing the reaction products by ^{1}H NMR to calculate the mole fraction of MAA and BzMA in the final copolymer (see section 2.1.2.3 for more details).

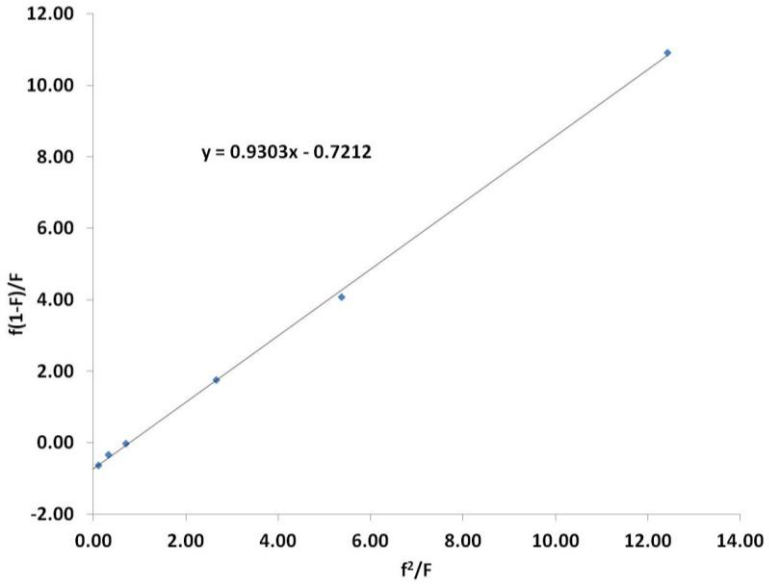

Figure 2.6. *Finemann-Ross plot for the free-radical copolymerisation of various mole fractions of MAA and BzMA at 70°C in DPG.*

The data used to produce the Finemann-Ross plot for the statistical copolymerisation of BzMA and MAA are listed in Table 2.2. The mole fraction of MAA and BzMA in the copolymer was calculated by integrating the two ester protons from the BzMA units at 4.9 ppm and comparing this integral with the polymer backbone region between 0.0-2.0 ppm (see Figure 2.4). Each copolymerisation was terminated at ten minutes to limit conversion to between 5-10 %. Conversions were kept low because equation 2.4 is only valid for the instantaneous formation of copolymer where the concentration of monomers has not changed through progression of the reaction.

Name	Conversion /%	Mole fraction of MAA in feed (m_1)	Mole fraction of BzMA in feed (m_2)	Mole fraction of MAA in copolymer (M_1)	Mole fraction of BzMA in copolymer (M_2)
AW39 a	8.5	0.12	0.88	0.15	0.85
AW39 b	9.2	0.30	0.70	0.36	0.65
AW39 c	8.8	0.45	0.55	0.49	0.51
AW39 d	7.9	0.73	0.27	0.74	0.26
AW39 e	8.0	0.84	0.16	0.83	0.17
AW39 f	9.2	0.92	0.08	0.92	0.08

Table 2.2. *Copolymerisation of MAA and BzMA at various monomer feeds in DPG using AIBN initiator (1 wt % based on monomer) at 70°C. Conversion was calculated by weighing the dried precipitated copolymer. 20 wt % solids was targeted for each copolymerisation.*

Figure 2.6 shows that a Finemann-Ross plot yielded the reactivity ratios r_1 (MAA) and r_2 (BzMA) to be 0.93 and 0.72, respectively. These values indicate that MAA has a slight tendency to preferentially react with itself as opposed to reacting with BzMA. This yields a copolymer with a random distribution containing longer sequences of MAA.

The significance of reactivity ratios is often illustrated by plotting copolymer composition against feed composition. Figure 2.7 displays a copolymer composition vs feed composition plot for MAA using data from Table 2.2. Figure 2.7 shows other reactivity ratio scenarios for comparison and illustrates how the copolymerisation of MAA and BzMA is almost completely random, which would require $r_1=r_2=1$.

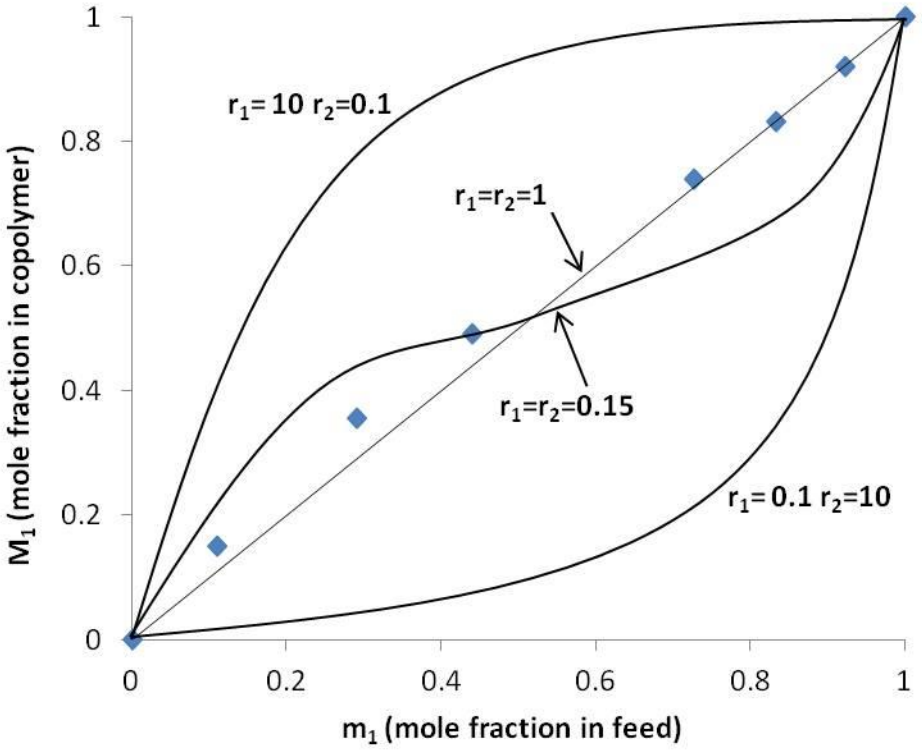

Figure 2.7. *Mole fraction of MAA in copolymer, M_1 vs the mole fraction of MAA in feed, m_1 for the free radical copolymerisations of BzMA and MAA in DPG at 70°C (♦). All reactions were terminated at ten minutes. The mole fraction of MAA in the copolymer was determined by ^1H NMR in $(CD_3)_2SO$.*

The Finemann-Ross method for estimating reactivity ratios using a linear graphical method was further refined by Kelen and Tudos.[5] The Kelen-Tudos equation is given in Equation 2.7 where r_1 and r_2 are the monomer reactivity ratios for monomers M_1 and M_2 respectively and G and H are values that have already been obtained from the Finemann-

Ross model where G=f(F-1)/F and H=f^2/F. The parameters for the six BzMA and MAA copolymerisations described in Table 2.2 are detailed in Table 2.3.

$$\eta = (r_1 + r_2 / \alpha)\, \xi - r_2 / \alpha \qquad \textbf{Equation 2.7}$$

where:

$$\left(\eta = \frac{G}{\alpha + H}, \xi = \frac{H}{\alpha + H} \; and \; \alpha = (H_{min} H_{max})^{1/2}\right)$$

Name	$f=m_1/m_2$	$F=M_1/M_2$	G=f(F-1)/F	$H=f^2/F$	η=G/a + H	ξ=H/a + H
AW39 a	0.13	0.18	-0.63	0.10	-0.45	0.19
AW39 b	0.42	0.55	-0.35	0.33	0.02	0.61
AW39 c	0.82	0.96	-0.03	0.70	0.67	1.32
AW39 d	2.73	2.81	1.76	2.65	4.21	4.99
AW39 e	5.12	4.88	4.07	5.37	8.96	10.11
AW39 f	11.95	11.50	10.91	12.42	22.06	23.40

Table 2.3. *Kelen-Tudos parameters for the copolymerisation of MAA and BzMA. m_1 = mole fraction of MAA in feed; m_2 = mole fraction of BzMA in feed, M_1 = Mole fraction of MAA in copolymer; M_2 = mole fraction of BzMA in copolymer, $\alpha = (H_{min}H_{max})^{1/2}$ = 1.13, H_{min}: lowest value of H, H_{max}: highest value of H.*

Using the data in Table 2.3 a plot of η versus ξ yields a straight line (see Figure 2.8). From the slope and intercept of the line, the monomer reactivity ratios of MAA (r_1) and BzMA (r_2) were determined to be 1.03 and 0.66, respectively. A comparison of reactivity ratios using the Finemann-Ross and Kelen-Tudos models are shown in Table 2.4.

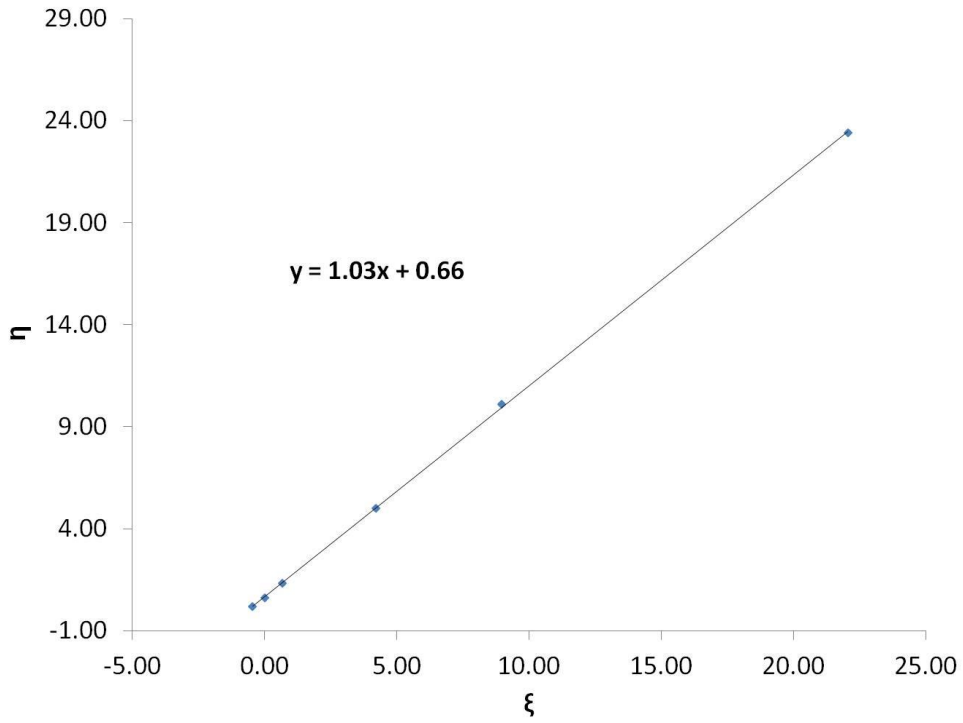

Figure 2.8. *Kelen-Tudos plot of η vs. ξ for MAA and BzMA copolymer systems prepared by free-radical polymerisation in DPG at 70°C using AIBN as initiator.*

Model	r_1 (MAA)	r_2 (BzMA)	r_1r_2
Finemann-Ross	0.93	0.72	0.67
Kelen-Tudos	1.03	0.66	0.68

Table 2.4. *Reactivity ratios for the copolymerisation of MAA and BzMA in DPG at 70°C using the Fineman-Ross and Kelen-Tudos model.*

Reactivity ratios from the Finemann-Ross and Kelen-Tudos models both indicate that that p(MAA-BzMA) copolymers are mostly random, but with longer blocks of MAA. Also displayed in Table 2.4 is the product r_1r_2, reactivity ratio data is often displayed in this manner for simplification, the closer the product r_1r_2 is to zero the more likely the chain is alternating and the closer r_1r_2 is to unity the more random the copolymer. There is no evidence in the literature estimating reactivity ratios for the copolymerisation of MAA and BzMA to act as comparison for the data collected and listed in Table 2.4. In the absence of data for a direct comparison to a copolymer of MAA and BzMA, the reactivity ratios were compared to the free-radical copolymerisation of methacrylic acid and methyl methacrylate (MMA). In the literature, r_1 and r_2 values varied widely for the

copolymerisation of MAA (0.43-1.6) and MMA (0.3-2.60) under differing reaction parameters such as solvent, temperature and different analysis models. Given this wide variation in values, a meaningful comparison could not be made.[3] Multiple studies of other copolymerisations also yielded varying reactivity ratios, which indicated r_1 and r_2 can vary due to minor modifications to the reaction environment and model.

The differences in monomer reactivity for the copolymerisation of BzMA and MAA can be explained by considering three effects: (i) polarity, (ii) resonance and (ii) steric. These three effects dictate how reactive the monomer is towards addition of a free-radical and the relative stability of the formed radical. In general, the more stable the monomer radical the lower the rate of polymerisation. To get an idea of the polarity and resonance of MAA and BzMA, the Q-e scheme from Alfrey and Price was examined.[9] The Q-e scheme attempts to compare copolymerisation tendencies by giving a measure of the reactivity of monomers. This is achieved by considering the resonance (Q) and polar (e) properties of the monomers (see Equations 2.8 and 2.9). The Q and e values and calculated reactivity ratios for MAA and BzMA are listed in Table 2.5.

$$r_1 = \frac{Q_1}{Q_2}\exp(-e_1\,(e_1 - e_2)) \qquad \textbf{Equation 2.8}$$

$$\mathrm{r_2} = \frac{\mathrm{Q_2}}{\mathrm{Q_1}}\exp(-\mathrm{e_2}\,(\mathrm{e_2} - \mathrm{e_1})) \qquad \textbf{Equation 2.9}$$

Monomer	Q	e	Reactivity ratio, r
MAA	0.98	0.62	0.94
BzMA	0.88	0.35	0.99

Table 2.5. *Q (resonance) and e (polar) values for MAA and BzMA. Values were taken from the Polymer Handbook.[3] Reactivity ratios were calculated using equation 2.8 and 2.9.*

The Q-e scheme shows that r_1 and r_2 for MAA and BzMA are 0.94 and 0.99 respectively, with the r_1r_2 product being 0.93. The r_1r_2 product is close to unity indicating the copolymerisation would result in a random copolymer due to both monomers having nearly the same tendency to react with each other. The difference in reactivity ratios between the Q-e scheme (r_1=0.94, r_2=0.99) and experimentally obtained values (r_1=1.03,

r_2=0.66) is thought to be due to two major drawbacks of the Q-e scheme: (i) steric effects are not taken into account and (ii) the assigned polar and resonance values are considered to be the same for the monomer and radical. Steric effects are particularly significant for the copolymerisation of BzMA and MAA because BzMA contains a bulky benzyl side group. It is speculated that this makes MAA more reactive towards MAA, as opposed to being more reactive towards another BzMA unit. Although the Q-e scheme has its limitations, it still offers an efficient means of gaining a quick estimate for reactivity ratios for any copolymerisation.

In this study linear analysis was the only method used to calculate reactivity ratios. The limitations of utilising linear methods to estimate reactivity ratios have been researched by Tidwell and Mortimer, who suggested non-linear least squares analysis as a more accurate approach.[10] In this study, accurate values for the reactivity ratios were not required; thus linear analysis was deemed adequate. Many other studies which have been published within the last five years continue to use linear analysis to calculate approximate reactivity ratios.[11,12,13] Regardless of the method of analysis used, it is important to remember that the final calculated reactivity ratios are only an estimation and not an accurate value, this is due to the many assumptions and simplifications which are made.

2.2.3 Determination of the sequence distribution in batch prepared p(MAA-co-BzMA) copolymers using ^{13}C NMR.

As there are many uncertainties associated with reactivity ratio calculations, it is good practise to gather data on the microstructure of polymers using spectroscopic techniques. There are three spectroscopy techniques commonly cited in the literature which are used to probe polymer structure: Fourier transform infrared spectroscopy (FTIR),[14] Raman spectroscopy[15] and NMR spectroscopy.[16] NMR spectroscopy is useful for studying the microstructure of copolymers as this technique is highly sensitive to the nucleus environment. NMR can be used to analyse the sequence distribution of p(MAA-co-BzMA) by calculating the fraction of triads along the copolymer chain. Figure 2.9 lists the 8 possible triad structures for p(MAA-co-BzMA), where A is the methacrylic acid unit and B is the benzyl methacrylate unit. In the case of AAB and BAA, these triads are

indistinguishable from NMR, so are considered to be the same as denoted by the line above.

$$\mathbf{AAA}$$

$$\mathbf{AAB} = \mathbf{BAA} = \overline{\mathbf{AAB}}$$

$$\mathbf{ABA}$$

$$\mathbf{ABB} = \mathbf{BBA} = \overline{\mathbf{ABB}}$$

$$\mathbf{BAB}$$

$$\mathbf{BBB}$$

Figure 2.9. *Figure showing the eight possible triads available in a copolymer sequence made up of monomers A (methacrylic acid) and B (benzyl methacrylate). Triads with a line above show that the forward and reverse of the triad is indistinguishable by NMR.*

The reactivity ratios obtained from the Kelen-Tudos method (r_1=1.03, r_2=0.66) were used to estimate the triad fractions using equations 2.10-2.15. $P_{A/B}$ is the probability of an A (MAA) reacting with a B (BzMA) unit and $P_{B/A}$ is vice versa. The estimated fractions are listed in Table 2.6. Once the triads were measured, the sequence order parameter, χ was estimated using equation 2.16. Figure 2.10 shows examples of copolymers that can be expected for different χ values. Table 2.6 shows that the average sequence order parameter is 1.1, indicating a random copolymer with a slight tendency towards alternating.

$$\mathbf{AAA} = (\mathbf{1} - \mathbf{P_{B/A}})^{\mathbf{2}} \qquad \textbf{Equation 2.10}$$

$$\overline{\mathbf{AAB}} = \mathbf{2}\left(\mathbf{P_{B/A}}\right)(\mathbf{1} - \mathbf{P_{B/A}}) \qquad \textbf{Equation 2.11}$$

$$\mathbf{ABA} = (\mathbf{P_{B/A}})^{\mathbf{2}} \qquad \textbf{Equation 2.12}$$

$$\mathbf{BBB} = (\mathbf{1} - \mathbf{P_{A/B}})^{\mathbf{2}} \qquad \textbf{Equation 2.13}$$

$$\overline{\mathbf{ABB}} = \mathbf{2}\left(\mathbf{P_{A/B}}\right)(\mathbf{1} - \mathbf{P_{A/B}}) \qquad \textbf{Equation 2.14}$$

$$\mathbf{BAB} = (\mathbf{P_{A/B}})^{\mathbf{2}} \qquad \textbf{Equation 2.15}$$

where:

$$\mathbf{P_{A/B} = \frac{1}{1 + r_1/f} \quad P_{B/A} = \frac{1}{1 + r_2 f}}$$

$$\mathbf{f\ (monomer\ feed\ ratio) = \frac{[MAA]}{[BzMA]}}$$

$$\boldsymbol{\chi = P_{A/B} + P_{B/A}} \qquad \textbf{Equation 2.16}$$

Mol % of MAA in feed (m_1)	Mol % of BzMA in feed (m_2)	f (m_1/m_2)	AAA	BAB	BAA	BBB	ABA	ABB	χ
0.12	0.88	0.13	0.01	0.77	0.21	0.69	0.03	0.14	1.05
0.30	0.70	0.42	0.09	0.48	0.42	0.37	0.15	0.24	1.09
0.45	0.55	0.82	0.21	0.29	0.50	0.20	0.31	0.25	1.10
0.73	0.27	2.73	0.54	0.07	0.39	0.04	0.65	0.16	1.07
0.84	0.16	5.12	0.71	0.03	0.27	0.01	0.78	0.10	1.05
0.92	0.08	11.95	0.86	0.01	0.14	0.00	0.90	0.05	1.02

Table 2.6. *Estimated triad fractions and sequence order parameters, χ for the copolymerisation of MAA and BzMA at 70°C using reactivity ratios (r_1=1.03, r_2=0.66) calculated from the Kelen-Tudos linear analysis.*

$\chi = 1$	**Random copolymer**
$\chi > 1$	**Alternating tendency**
$\chi < 1$	**Block forming tendency**
$\chi = 2$	**Alternating copolymer**
$\chi = 0$	**Block copolymer**

Figure 2.10. *Possible copolymer structures that can be obtained with different sequence order parameters χ.*

^{13}C NMR was used to directly analyse the fraction of triads in p(MAA-BzMA) copolymers. The region between 174-182 ppm in the ^{13}C NMR of p(MAA-BzMA) shown in Figure 2.11 appeared as a multiplet, indicating that the carbonyl group was sensitive to its environment. Following this, the copolymers listed in Table 2.2 and the corresponding homopolymers (MAA and BzMA) were all analysed by ^{13}C NMR and expanded over 174-182 ppm to extract triad information from the multiple peaks (Figure 2.12).

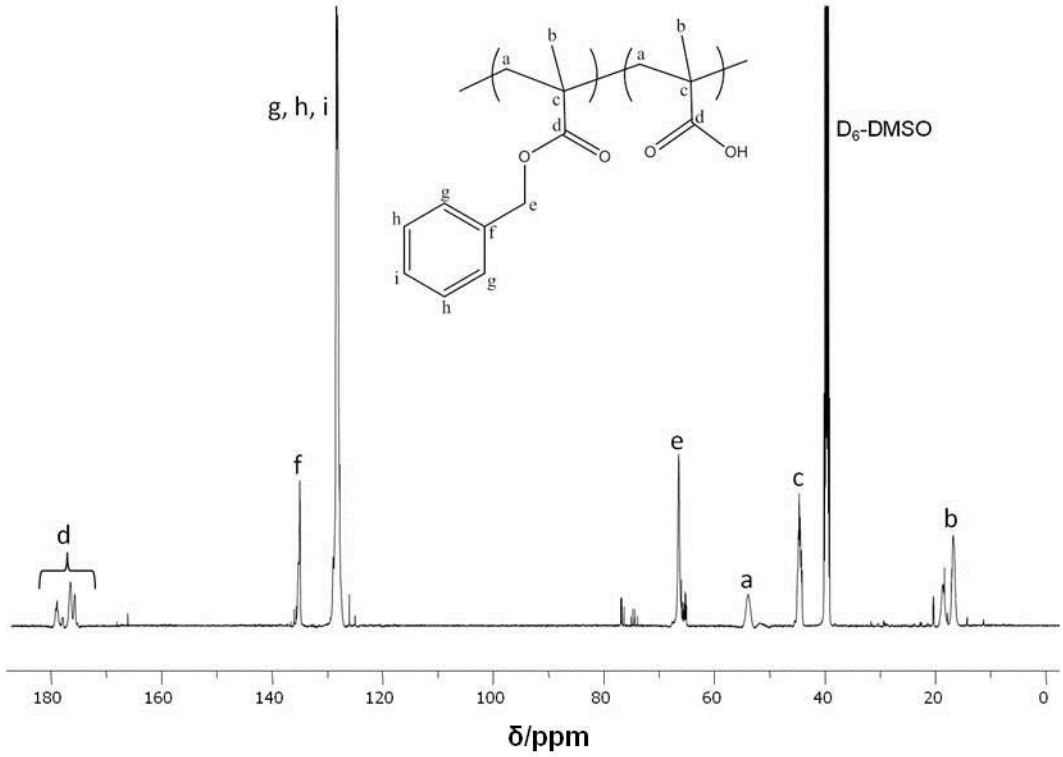

Figure 2.11. *^{13}C NMR spectra of p(MAA-co-BzMA) 39 mol % MAA in $(CD_3)_2SO$.*

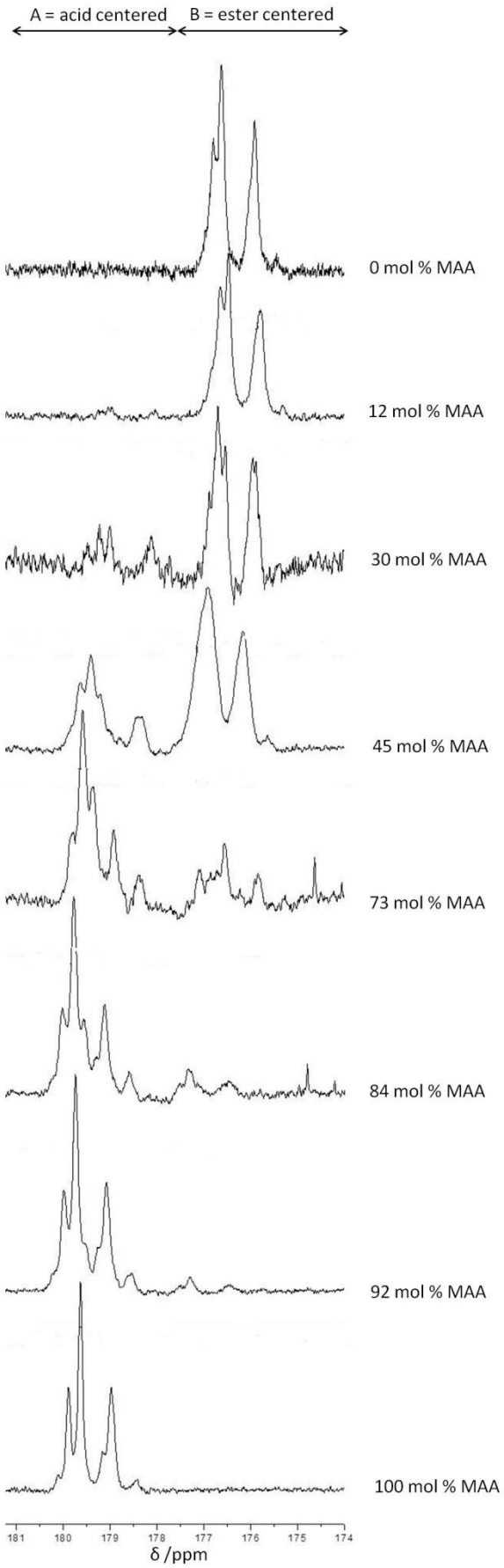

Figure 2.12. *Expanded region (174-182 ppm) of the ^{13}C NMR spectra recorded for p(MAA-co-BzMA) copolymers in $(CD_3)_2SO$.*

The ^{13}C NMR spectra of MAA and BzMA homopolymers showed that peak splitting was occurring due to tacticity, which would overlap with any peaks arising from copolymer sequence effects. As the tacticity in the p(MAA-co-BzMA) copolymers led to an overlap of any splitting occurring from triad structures, reliable structural information could not be obtained from these spectra. This problem has previously been reported by Lyeria, who described how the microstructure of poly(methacrylic acid-methyl methacrylate) copolymer was analysed by NMR.[17] Lyeria overcame the resonance overlap problem by using a computer program to generate theoretical ^{1}H and ^{13}C NMR spectra of the copolymer. Another study analysing the microstructure of poly(methacrylic acid-(dimethylamino)ethyl methacrylate) eliminated splitting from tacticity by running all ^{13}C NMR in alkaline NaOD/D_2O mixtures.[18]

2.2.4 Kinetic analysis of the batch polymerisation of MAA and BzMA in DPG using Raman spectroscopy

Often in polymerisation reactions, monomer conversion is monitored using ^{1}H NMR whereby aliquots are taken at time intervals and conversion is determined by integrating monomer peaks for comparison with polymer peaks.[19] This approach could not be used for the copolymerisation of BzMA and MAA in DPG due to DPG having a complex ^{1}H NMR spectrum that overlaps peaks from the MAA and BzMA monomers and copolymer backbone. Instead, the kinetics of BzMA and MAA in DPG was followed by Raman spectroscopy, which offered a simple, non-invasive route for obtaining spectra during polymerisation. Previously, Raman spectroscopy has successfully been used to study homopolymerisations[20] and copolymerisations[21]. The advantages of using Raman spectroscopy to follow polymerisations have been discussed in a review by Edwards et al.[22]

Prior to initiation of the polymerisation, the MAA, BzMA, AIBN and DPG mixture was analysed by Raman spectroscopy. It was observed that the band at 1660 cm^{-1} corresponding to the C=O in MAA was shifted to ~ 1700 cm^{-1} and became broader (Figure 2.13). The band at 1660 cm^{-1} was attributed to the methacrylic acid units forming cyclic dimers through intra-molecular hydrogen bonding (see Figure 2.14a). It is speculated that the shift of ~40 cm^{-1} to higher wavenumber when mixed with DPG is due to the hydroxyl groups present in DPG hydrogen bonding with the carboxylic acid groups in MAA, leading to a reduction in the number of dimer structures (see Figure 2.14b). This

observation can be compared to the shift observed for the C=O present in acetic acid.[23] When water was added to pure acetic acid the C=O peak shifted from 1665 to 1715 cm^{-1}. A shift to a higher wavenumber indicated that the hydrogen bonding had become weaker.

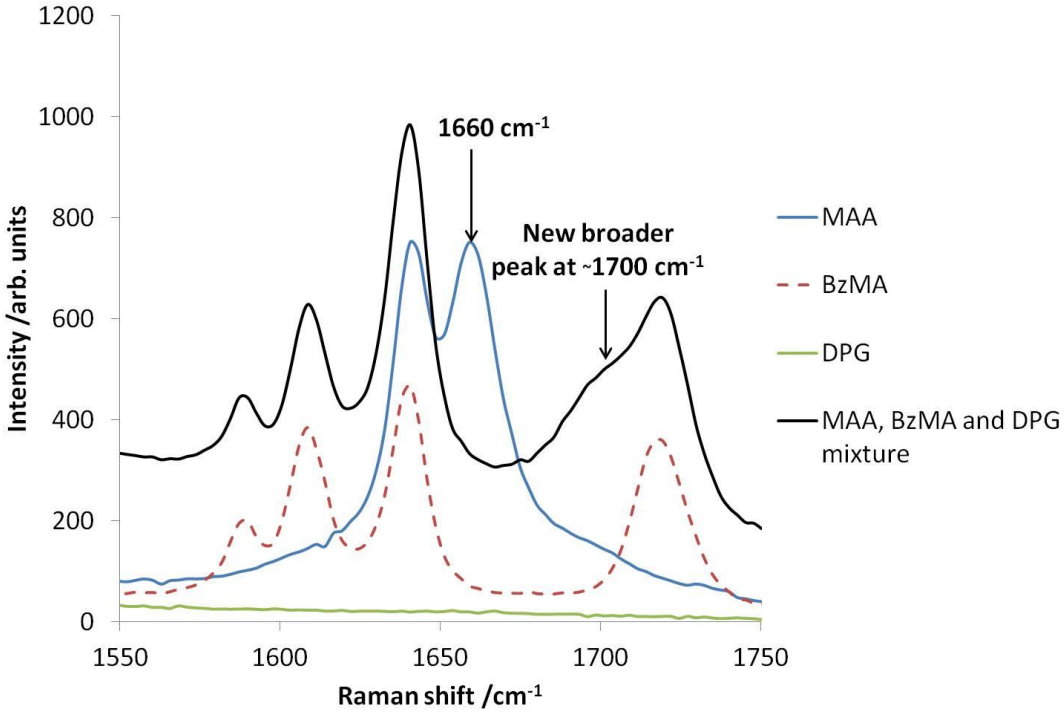

Figure 2.13. *Raman spectra of MAA, BzMA, DPG and a mixture of all three components where monomers make up 20 wt % of the overall mixture (36:64 mol % MAA:BzMA).*

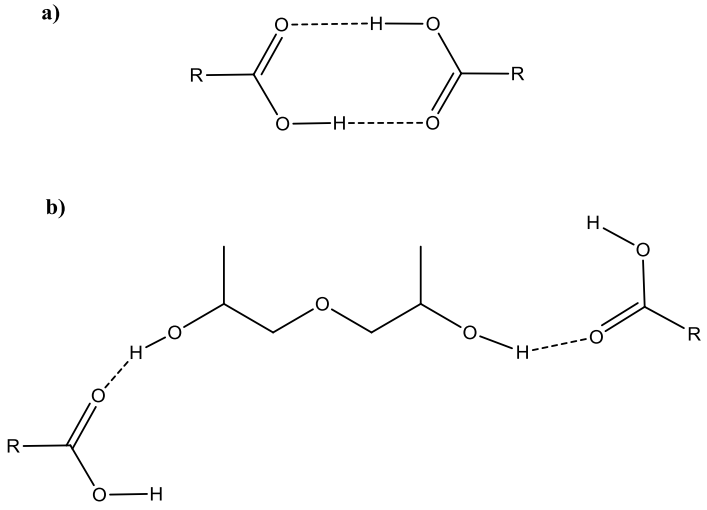

Figure 2.14. *a) Formation of cyclic dimer between two carboxylic acid groups through intramolecular hydrogen bonding and b) possible intermolecular hydrogen bonding between methacrylic acid and DPG.*

Commonly, polymerisation kinetics are observed by following the transformation of the C=C bond to a C-C bond in the monomer residues.[20,21] This method was used to follow the conversion of BzMA and MAA by examining the change in intensity from the Raman band associated with the C=C bond at 1640 cm^{-1} (see Figure 2.15). Figure 2.16 shows the structure of MAA and BzMA with the labelled Raman band used to follow kinetics.

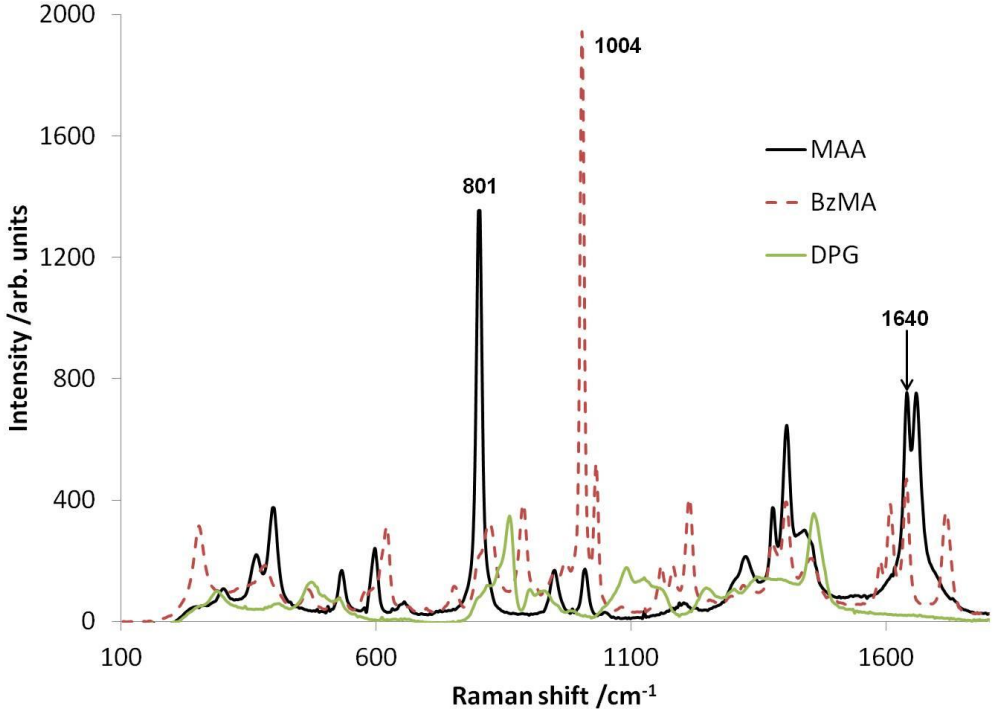

Figure 2.15. *Raman spectra of methacrylic acid (MAA), benzyl methacrylate (BzMA) and dipropylene glycol (DPG). The band at 1640 cm^{-1} represents the C=C bond and its intensity was monitored to follow the kinetics of the copolymerisation of MAA and BzMA.*

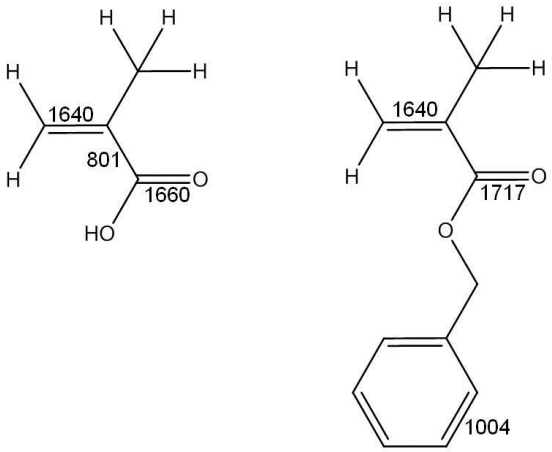

Figure 2.16. *Structures of (left) methacrylic acid (MAA) and (right) benzyl methacrylate (BzMA) with labelled band stretches that were examined by Raman spectroscopy. All numbers are quoted in cm^{-1}.*

The conversion of MAA and BzMA in DPG at 70°C was monitored by observing changes in the intensity of the C=C (1640 cm^{-1}) peak (see Figure 2.17). Conversion versus time graphs were plotted with and without the 1640 cm^{-1} shift being made relative to an internal standard peak (see Figure 2.18). The band at 1004 cm^{-1} corresponding to the C=C bond in the benzene ring on BzMA was chosen as an internal standard due to its shift not being affected during copolymerisation. Comparison of graph (a) with graph (b) in Figure 2.18 shows that the relative conversion of 1640 cm^{-1} gave a better result, as expected. Analysing kinetic data by comparing the absolute intensity of a peak to a reference peak was also used by Özpozan et al. who used the CH_3 band (2942 cm^{-1}) as a relative internal standard for the emulsion polymerisation of vinyl acetate.[20]

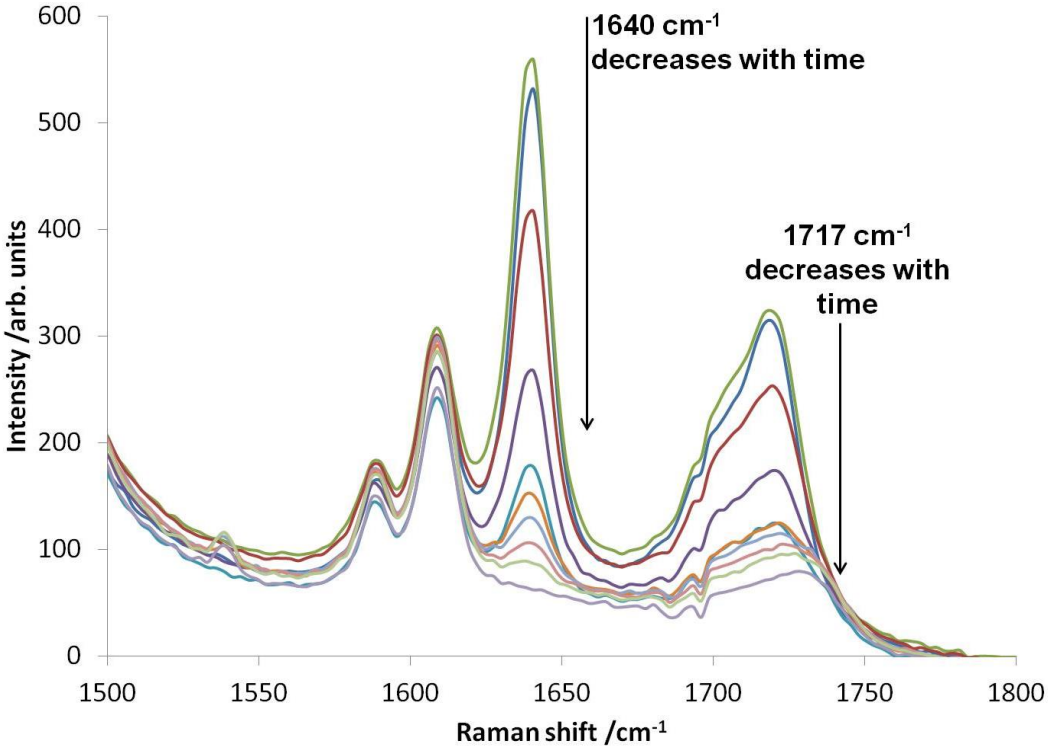

Figure 2.17. *Raman spectra showing the expanded region between 1500 to 1800 cm^{-1} for the copolymerisation of MAA and BzMA in DPG at 70°C showing the reduction in intensity of bands at 1640 cm^{-1} and 1717 cm^{-1} over time.*

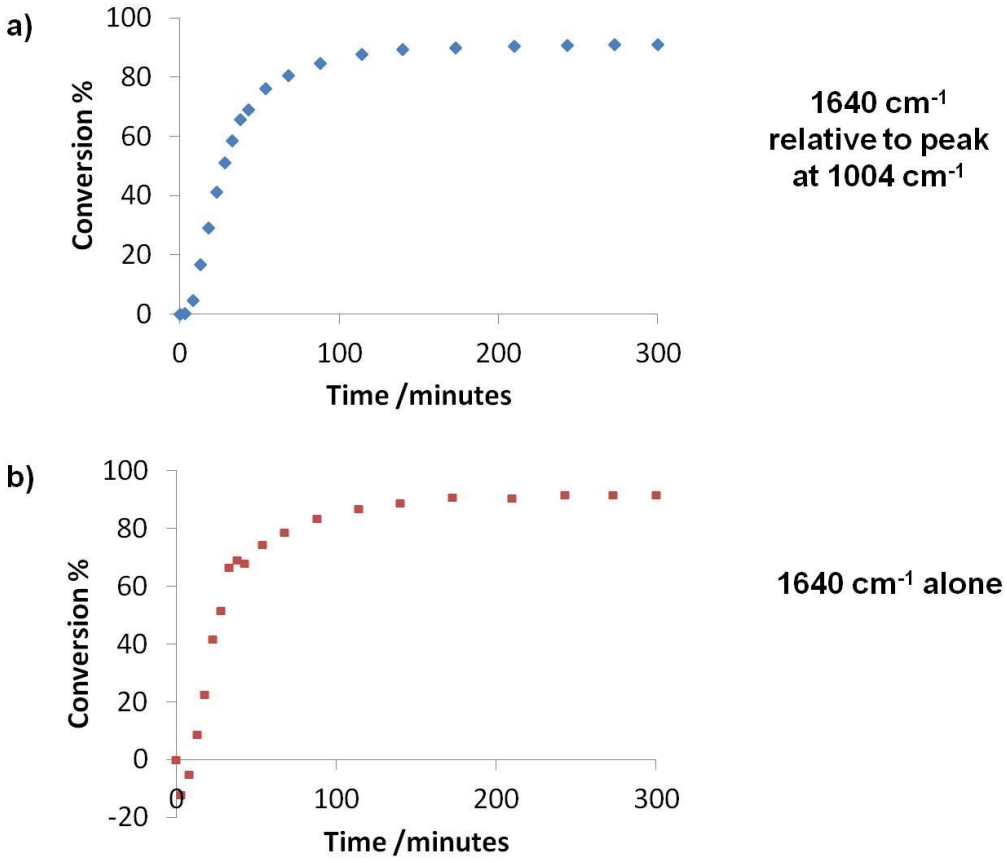

Figure 2.18. *Percentage conversion versus time for the copolymerisation of MAA and BzMA in DPG at 70°C obtained by following the change in intensity of the 1640 cm^{-1} band corresponding to C=C. The upper graph shows the change in conversion when 1640 cm^{-1} is compared to 1004 cm^{-1} and the lower graph shows the result when the 1640 cm^{-1} band is used alone.*

It can be seen from Figure 2.18a that for the copolymerisation of MAA and BzMA the copolymerisation reaches a plateau at 68 minutes, indicating that the reaction had attained reached a maximum of 88 % conversion. As the C=C band appeared at the same wavenumber for both monomer residues, it was not possible to use this feature to monitor the conversion of each monomer separately during copolymerisation. Alternatively, the 801 cm^{-1} band corresponding to the C-C bond in MAA and the 1717 cm^{-1} band corresponding to C=O bond in BzMA were monitored. Following the change in the 801 cm^{-1} band proved unsuccessful due to overlap of signals from DPG and BzMA. Following the conversion of BzMA by examining the change in intensity of the 1717 cm^{-1} band proved more informative, with its conversion versus time plot shown in Figure 2.19. In this figure, the conversion for the copolymerisation of BzMA and MAA using the change in intensity of the 1640 cm^{-1} band is shown for comparison.

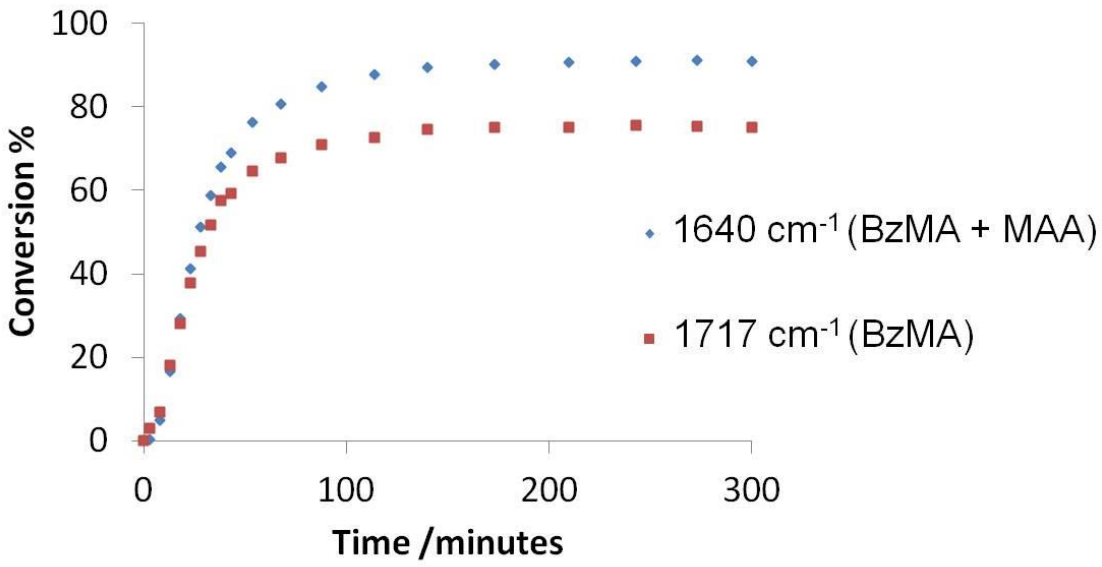

Figure 2.19. *Percentage conversion versus time for BzMA during the copolymerisation of BzMA and MAA. BzMA conversion was followed by examining the change in intensity of the Raman band at 1717 cm^{-1} corresponding to the C=O ester bond. For comparison, the conversion of BzMA and MAA is shown by following the change in intensity of the 1640 cm^{-1} band. Both sets of data were expressed relative to the internal band at 1004 cm^{-1}.*

It can be determined from the data detailed in Figure 2.19 that the maximum conversion of BzMA during the statistical copolymerisation of MAA and BzMA was 75 %. It was assumed that the MAA monomer undergoes 100 % conversion, thus yielding a final copolymer comprising 43:57 mol % MAA:BzMA (target mol % was 36:64). The calculated values concur with analysis of the ^{1}H NMR spectrum of the final copolymer, which showed the copolymer composition to be 43:57 mol % MAA:BzMA.

Following investigation of the copolymerisation of BzMA and MAA, the homopolymerisation of both MAA and BzMA was examined. The kinetic data for the homopolymerisation of MAA at 5 wt % in DPG at 70°C is shown in Figure 2.20. It was found that the kinetics of MAA could be followed by either observing the change in intensity of the Raman shift at 801 cm^{-1} or 1640 cm^{-1}. The conversion of MAA gave very similar results in each case proving that either band can be successfully used to follow the conversion of MAA. The conversion of MAA progressively increased to 50 % at 69 minutes and then increased slightly up to 63 % conversion for the remaining time. The extent of conversion was lower than expected with other MAA polymerisations described in the literature reaching 90 % conversion within a similar time.[24] It has been shown that the rate of polymerisation of MAA is dependent on the formation of hydrogen bonds

between monomer, polymer, growing radicals and solvent, which could explain why the conversion of MAA in DPG is lower than expected.[25]

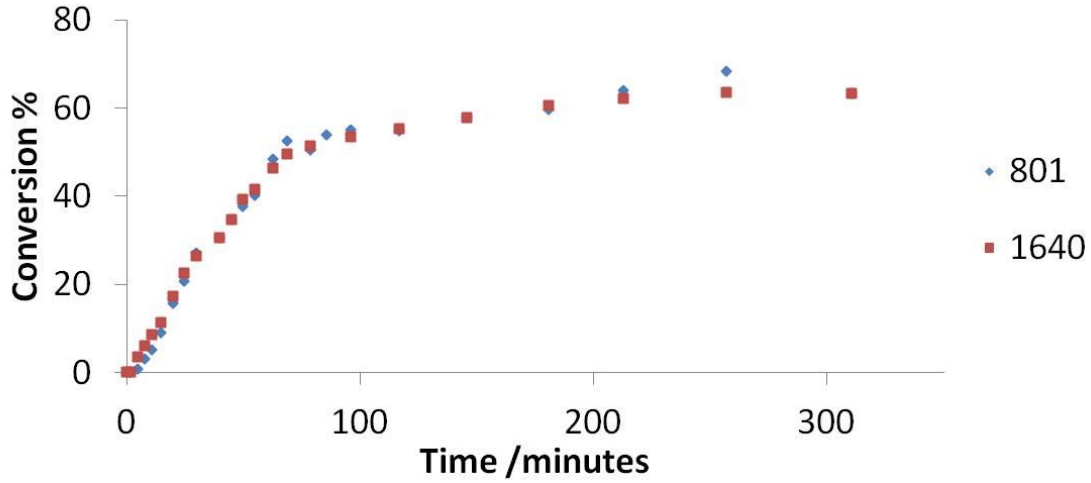

Figure 2.20. *Conversion of MAA in DPG at 70°C determined by following the change in intensity of Raman bands at 801 cm^{-1} and 1640 cm^{-1}.*

The homopolymerisation of BzMA could not be followed by Raman spectroscopy because the reaction solution became turbid after ten minutes, which prevented further Raman spectra from being obtained.

2.3 Summary

Poly(methacrylic acid-benzyl methacrylate), p(MAA-BzMA) random copolymers were successfully prepared in dipropylene glycol (DPG) by free-radical polymerisation under batch and semi-batch conditions. The target mol % of monomers compared to the actual mol % of monomer incorporated into the final copolymer differed when copolymers were prepared under batch conditions. This was explained by the differing reactivity ratios for BzMA and MAA as indicated by the linear analysis methods of Kelen-Tudos and Finemann-Ross. Kelen-Tudos analysis indicated reactivity ratios of r_1(MAA) and r_2(BzMA) to be 1.03 and 0.66 respectively and Finemann-Ross analysis gave reactivity ratios of r_1(MAA) and r_2(BzMA) of 0.93 and 0.72, respectively. These reactivity ratios indicated that the final p(MAA-BzMA) would be a random copolymer with longer blocks of MAA. Reactivity ratios calculated from the Kelen-Tudos method were subsequently used to calculate the fraction of triads along the copolymer chain and a sequence order parameter, χ. The sequence order parameter was approximately 1.1, which indicated a random copolymer with a slight tendency to alternate. The Q-e scheme predicted reactivity ratios to be 0.94 and 0.99, which would also yield a random copolymer. It was speculated that the difference between the reactivity ratios calculated from the Q-e scheme and the linear methods were due to the Q-e scheme not accounting for steric effects. The increased reactivity of MAA towards other MAA monomers as opposed to a BzMA unit was attributed to the effects of the bulky side group. ^{13}C NMR spectroscopy was used to calculate the fraction of triads along a p(MAA-BzMA) chain for comparison to the triad fractions calculated using reactivity ratios. The carbonyl groups on the MAA and BzMA units appeared as a multiplet between 174-182 ppm, indicating that they were sensitive to their environment. It was not possible to accurately quantify the fractions of triads from splitting occurring between 174-182 ppm as ^{13}C NMR was sensitive to the tacticity of monomers in addition to the sequence which resulted in an overlap of resonance signals. Raman spectroscopy was used to follow the kinetics for the batch copolymerisation of MAA and BzMA (target 36 mol % MAA) in DPG at 70°C by monitoring the change in intensity of the 1640 cm^{-1} band corresponding to the C=C bond present in the monomers. In order to produce a smooth conversion curve, the 1640 cm^{-1} band had to be compared to the 1004 cm^{-1} band corresponding to the C=C bond present in the benzene ring of BzMA. A percentage conversion versus time plot was used to demonstrate that the copolymerisation of MAA and BzMA reached 88 % conversion after 68 minutes. The kinetics for the homopolymerisation of MAA was followed using Raman

spectroscopy by monitoring the 801 cm^{-1} and 1640 cm^{-1} bands, the intensity change of each band was self-consistent. The conversion of MAA at 5 wt % solids in DPG reached 63 % after 300 minutes. The low conversion of MAA could be due to hydrogen bonds forming between monomer, polymer, growing radicals and the DPG solvent.

2.4 References

1. Gowariker, V. R.; Viswanathan, N. V.; Sreedhar, J., *Polymer Science*, New Age International Ltd Publishers: New Delhi, 1986.
2. Cowie, J. M. G.; Arrighi, V., *Polymers: Chemistry and Physics of Modern Materials*. 3rd Edition, CRC Press: Boca Raton, 2008.
3. Brandrup, J.; Immergut, E. H., *Polymer handbook*. 2nd edition, John Wiley: New York, 1976.
4. Finemann, M.; Ross, S., *Journal of Polymer Science*, **1950**, *5*, 1019-1025.
5. Kelen, T.; Tudos, F., *Journal of Macromolecular Science*, **1975**, *9*, 1-27.
6. Cohen, H. L., *Journal of Polymer Science*, **1976**, *14*, 7-22.
7. Lide, D. R., *Handbook of Chemistry and Physics*. 87th edition, CRC Press: Taylor and Francis Group: Boca Raton, 2006.
8. Mayo, F. R.; Lewis, F. M., *Journal of the American Chemical Society*, **1994**, *66*, 1594-1601.
9. Alfrey, T.; Price, C. C., *Journal of Polymer Science*, **1947**, *2*, 101-106.
10. Tidwell, P. W.; Mortimer, G. A., *Journal of Macromolecular Science Part C Polymer Reviews*, **1970**, *4*, 281-312.
11. Manju, M.; Veeraiah, M. K.; Prasannakumar, S.; Gowda, N. M.; Sherigara, B. S., *American Journal of Polymer Science*, **2012**, *2*, 22-27.
12. Lin, C.; Kuo, S.; Huang, C.; Chang, F., *Polymer*, **2010**, *51*, 883-889.
13. Lin Kusdianto, C.; Yu, F.; Chern, C. S.; *Journal of Applied Polymer Science*, **2010**, *119*, 620-628.
14. Jone Selvamalar, C. S.; Krithiga, T.; Penlidis, A.; Nanjundan, S., *Reactive and Functional Polymers*, *56*, **2003**, 89-101.
15. Papke, B. L.; Ratner, M. A.; Shriver, D. F., *Journal of Physics and Chemistry of Solids*, **1981**, *42*, 493-500.
16. Aerdts, A. M.; German, A. L., *Magnetic Resonance in Chemistry*, **1994**, *32*, 80-88.
17. Lyeria, J. R., *Journal of Research and Development*, **1977**, *21*, 111-120.
18. Merle, L.; Merle, Y., *Macromolecules*, **1982**, *15*, 360-366.
19. Blanazs, A.; Ryan, A. J.; Armes, S. P., *Macromolecules*, **2012**, *45*, 5099-5107.
20. Özpozan, T.; Schrader, B.; Keller, S., *Spectrochimica Acta Part A*, **1997**, *53*, 1-7.
21. Haigh, J.; Brookes, A.; Hendra, P.J.; Strawn, A.; Nicholas, C.; Purbrick, M., *Spectrochimica Acta Part A*, **1997**, *53*, 9-19.

22. Edwards, H. G. M.; Johnson, A. F.; Lewis, I. R., *Journal of Raman Spectroscopy*, **1993**, *24*, 475-483.
23. Nishi, N.; Nakabayashi, T.; Kosugi, K., *Journal of Physical Chemistry A*, **1999**, *103*, 10851-10858.
24. Buback, M.; Hesse, P.; Hutchinson, R. A.; Kasák, P.; Lacik, I.; Stach, M.; Utz, I., *Industrial and Engineering Chemistry Research*, **2008**, *47*, 8197-8204.
25. Beuermann, S.; Buback, M.; Hesse, P.; Kukuckova, S.; Lacik, I., *Macromolecular Symposia*, **2007**, *248*, 23-32.

CHAPTER III

Using fluorescence spectroscopy to probe the conformation of p(MAA-co-BzMA) copolymers in water

3.1 Introduction

The use of fluorescent labels and time-resolved anisotropy measurements (TRAMS) has been widely utilised to explore the conformation of polymers in solution.[1,2,3] TRAMS uses polarised light to photoselect the fluorescent labels into one specific orientation and then monitors the decay of the order by examining the emission from the excited label in the planes which lie vertical and horizontal to the polarised light. This results in an anisotropy decay curve; by fitting models to these data the correlation time of the fluorescent label can be determined and by knowing the correlation time of the label, insight into the shape and flexibility of the macromolecule being studied is gained. TRAMS is particularly useful because of its high degree of sensitivity, allowing dilute solutions of polymers to be monitored.[1] It has been described as one of 'the most powerful of all the fluorescence methods used in interrogation of the conformational behaviour of polyelectrolytes'.[4] As well as being used to monitor the conformation of polymer chains in solution, the technique has been used to examine the conformation of polymers at interfaces[5] and also higher order structures such as micelles.[6] Chan et al. used TRAMS to study the behaviour of naphthalene-labelled polystyrene-b-poly(methacrylic acid) micelles as a function of pH.[6] The naphthalene label was positioned at the end of the polystyrene block and thus resided inside the micelle core. The TRAMS data showed that the correlation time of the naphthalene label remained unchanged with pH, indicating a compact micelle core.

The work described in this chapter relates to TRAMS carried out on p(MAA-ran-BzMA) copolymers by incorporating the fluorophore acenaphthylene (ACE) into the copolymer backbone. Initially, aqueous solutions of a semi-batch prepared random copolymer of ACE-labelled p(MAA_{36}-ran-$BzMA_{64}$) were examined by studying the change in correlation time as a function of pH. Following this, two further semi-batch prepared ACE-labelled p(MAA-ran-BzMA) copolymers with BzMA contents of 36 and 55 mol % were monitored as a function of pH in order to examine the effect of different amounts of hydrophobic units on the correlation time. ACE-labelled p(MAA_{143}-b-$BzMA_n$) diblocks were synthesised by RAFT and analysed by TRAMS to probe the structure of the diblocks. Finally, TRAMS was employed to look into the effect that dipropylene glycol (DPG) has on the conformation of p(MAA_{36}-ran-$BzMA_{64}$). This was carried out by examining the change in correlation time for ACE-labelled p(MAA_{36}-ran-$BzMA_{64}$) in DPG/H_2O solutions where the wt % of DPG was varied from 0 to 100.

3.2 Experimental

3.2.1 Materials

Acenaphthylene (ACE) was purchased from Aldrich and recrystallised from ethanol and vacuum-sublimed before use. Ultrapure deionised water was used in all experiments. Methacrylic acid (MAA), benzyl methacrylate (BzMA), AIBN, trimethylsilyldiazomethane (TMS), 2-cyanoprop-2-yldithiobenzoate (CPDB) and D_2O was purchased from Aldrich and used as received. Ethanol, tetrahydrofuran (THF), hexane, methanol, and diethyl ether were purchased from Fisher and used as received.

3.2.2 Synthesis

3.2.2.1 ACE-labelled poly(methacrylic acid-random-benzyl methacrylate) p(MAA-ran-BzMA) preparation 36 mol % MAA : 64 mol % BzMA by semi-batch free-radical polymerisation.

The same protocol was used from section 2.1.2.1 in chapter II except this time ACE (1 wt % based on monomers) was additionally added into the monomer feed line. The final ACE-labelled copolymer was precipitated twice from THF into water and finally into hexane. M_n and M_w values were determined using a THF GPC equipped with a RI detector and Polymer Laboratories PL gel 5 µm Mixed-C columns. The THF eluent contained 0.05 wt % BHT and monodisperse polystyrene standards were used for calibration. The column was set at 30ºC.

3.2.2.2 ACE-labelled poly(methacrylic acid) (PMAA)

A glass ampoule with the capacity of 60 ml was charged with MAA (5.0 g, 0.058 mol), ACE (0.50 g, 3.29 mmol, 1 wt % based on monomer), AIBN (0.164 g, 1.0 mmol) and dioxane (50 ml). The reaction mixture was degassed by the freeze-thaw method three times and sealed under a high vacuum. The ampoule was then placed in a water bath at 60°C for 72 h to allow polymerisation to occur. The polymer was purified by precipitation into diethyl ether from methanol three times. M_n and M_w values were obtained by GPC

equipped with a refractive index detector and UV detector set at 295 nm. The GPC was comprised of two 600 mm DVB sulphonated Jordi Gell columns and the eluent was a mixture of 0.1 M TRIS, 0.1 M NaCL and 0.01 M sodium azide buffer set at a flow rate of 1.0 ml min^{-1}. The UV detector was set at 295 nm as this was the excitation wavelength for ACE. The UV chromatogram shows the ACE label to be evenly distributed throughout the PMAA backbone (Figure 3.1). The amount of ACE label incorporated into the backbone was calculated using UV spectroscopy.

	M_n /g mol^{-1}	M_w/g mol^{-1}	M_z/g mol^{-1}	PDI (M_w/M_n)
RI detector	323700	665700	882200	2.1
UV detector (295 nm)	362400	733600	923100	2.0

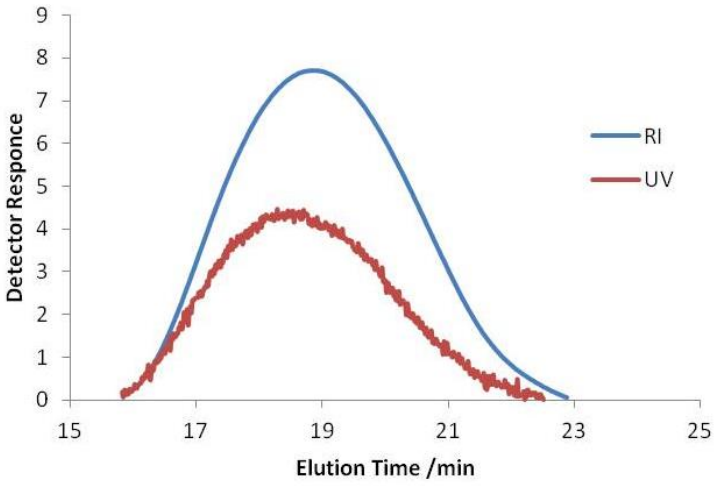

Figure 3.1. *Top: GPC data for ACE-labelled PMAA obtained using an aqueous sulphonated GPC equipped with an RI and UV detector. Bottom: Chromatograms obtained using an RI detector and a UV detector set to 295 nm.*

3.2.2.3 Synthesis of poly(methacrylic acid-block-benzyl methacrylate) p(MAA-b-BzMA) diblocks by Reversible-Addition Fragmentation Chain Transfer (RAFT) polymerisation.[12]

a) Synthesis of ACE-labelled poly(methacrylic acid) macro chain transfer agent (CTA) by RAFT.

The protocol used for the RAFT synthesis of ACE-labelled poly(methacrylic acid)

(PMAA) macro-CTA with a target degree of polymerisation (DP) of 220 was as follows. MAA (10.00 g, 0.116 mol), CPDB (0.117 g, 5.28 $x10^{-4}$ mol), AIBN (0.10 mg, 5.27 $x10^{-5}$ mol), ACE (0.10 g, 1.0 wt % based on monomer, 6.57 $x10^{-4}$ mol) and ethanol (30.00 g) were added to a round bottom flask along with a magnetic stirrer bar. The solution was purged with N_2 for 1 h before being immersed into a pre-heated oil bath at 70°C. Aliquots (typically 0.20 μl) were periodically extracted for ^{1}H NMR studies of the monomer conversion. ^{1}H NMR spectra was recorded in D_2O and the signals due to the residual vinyl protons of MAA monomer at δ 6.00 and δ 5.56 were compared with the polymer backbone protons between δ 0.00-2.40. After 6 h, the polymerisation was terminated by exposure to air. ^{1}H NMR indicated a conversion of 65 % (DP=143, M_w=12600 g mol^{-1}). The macro-CTA was precipitated into diethyl ether to remove any un-reacted monomer and dried in a vacuum oven at room temperature to give a light pink powder. Steady-state spectroscopy and UV spectroscopy confirmed the presence of ACE label in the polymer backbone.

b) Synthesis of 2nd pBzMA block

Diblocks were synthesised using the following molar ratio of reactants: [BzMA]:[pMAA macro-CTA]:[AIBN] / [n]:[1]:[0.2] where n was the target DP (50, 100, 143, 200, 300) for the BzMA block. A typical RAFT dispersion polymerisation targeting p(MAA_{143}-b-$BzMA_{143}$) at 10 wt % solids was as follows: ACE-labelled $pMAA_{143}$ macro-CTA (0.48 g, 0.0397 mmol), BzMA (1.0 g, 5.7 mmol), AIBN (1.3 mg, 0.0079 mmol) and ethanol (9.0 g) were added to a round bottom flask with a magnetic stirrer bar and purged with N_2 for 30 minutes and sealed. Polymerisations were conducted at 70°C for 24 h. The resulting diblock was analysed by ^{1}H NMR, DLS, GPC and TEM. The ^{1}H NMR spectrum was recorded in deuterated DMSO and showed no BzMA monomer peaks confirming the reaction had gone to completion.

3.2.2.4 Methylation of PMAA

For GPC studies, the carboxylic acid groups on the PMAA-based diblock copolymers and $PMAA_{143}$ macro-CTA were methylated using trimethylsilyldiazomethane (TMS), as reported by Couvreur et al.[7] Methylation was carried out in a well-ventilated fumehood by adding two drops of TMS to a solution of the polymer (10 mg) in THF (3 ml) or 1:1

MeOH/toluene (3 ml). Once added, the solutions were left to stir overnight until all the solvent had evaporated off.

3.2.3 Characterisation

3.2.3.1 Steady State

Steady state data were recorded on a FluoroMax-4 spectrofluorometer. The excitation source was a Xenon flash lamp and data were analysed using FluorEssence V3 software. ACE-labelled samples were diluted with water to 0.01 wt % and analysed in quartz cuvettes by exciting the sample at 290 nm and recording the emission between 330-500 nm.

3.2.3.2 Time-resolved anisotropy measurements (TRAMS)

Time-resolved anisotropy measurements were performed on an Edinburgh Instruments 199 fluorescence time-correlated single photon counter modified with a computer-controlled toggling polarizer accessory. The excitation source used was an IBH Nanoled operating at a repetition rate of 1 MHz and a wavelength of 295 nm. The emission wavelength (340 nm) was isolated using an interference filter. This set-up allowed selective excitation and analysis of the ACE fluorescence. Data were analysed using IBH software.

3.2.3.3 ^{1}H NMR spectroscopy

All ^{1}H NMR spectra were recorded in either D_2O or $(CD_3)_2SO$ using a 400 MHz Bruker Avance-400 spectrometer and analysed using Spinworks 3.1.8 software.

3.2.3.4 UV spectroscopy

A Specord S 600 spectrophotometer was used for recording spectra from 150 nm to 400 nm with a slit width of 1 nm.

3.2.3.5 Rheology

Viscosity measurements were carried out using a stress-controlled rheometer, TA AR-G2. A cone and plate fixture was used to measure viscosity. The cone was inverted with a conical angle of 2° and the plate had a diameter of 40 mm. The cone and plate required approximately 0.5 ml of sample for each test. Measurements were conducted under steady shear flow at 25°C between a shear rate of 1 to 1000 s^{-1}.

3.2.3.6 Dynamic Light Scattering (DLS)

A Malvern Zetasizer NanoZS instrument was used to obtain the intensity-average hydrodynamic diameter of particles via the Stokes-Einstein equation shown below.[8]

$$D = kT / 6\pi\eta R_H \qquad \textbf{Equation 3.1}$$

D is the diffusion coefficient, kT is the thermal energy (T is the absolute temperature), η is the viscosity of the continuous phase and R_H is the hydrodynamic particle radius. The p(MAA_{143}-b-$BzMA_n$) diblocks were diluted with water to obtain concentrations of around ~0.1 wt % and analysed in disposable curvettes. The results were averaged over three consecutive runs. The deionised water used in each sample was ultra-filtered through a 0.20 μm membrane to remove any dust.

3.2.3.7 Transmission Electron Microscopy (TEM)

TEM studies on the p(MAA_{143}-b-$BzMA_n$) diblocks were carried out on FEI Tecnai G2 Spirit instrument. Samples were prepared on glow-discharged carbon-coated copper grids by spotting a 12 μl solution of 0.1 wt % p(MAA_{143}-b-$BzMA_n$) in water onto the grids for 1 min and then blotting with tissue paper at the edges. This was followed by negative staining with 9 μl uranyl formate solution for 20 seconds followed by drying with a vacuum hose.

3.3 Results and Discussion

3.3.1 Using time-resolved anisotropy measurements (TRAMS) to probe the conformation of ACE-labelled p(MAA-ran-BzMA) copolymers in water.

In order to investigate the different conformations of p(MAA-ran-BzMA) adsorbed onto pigment particles, a fluorescent label was attached to the copolymer backbone. Acenaphthylene (ACE) was incorporated into p(MAA-ran-BzMA) copolymers by adding 1 wt % ACE (based on monomers) into the copolymer synthesis described in section 2.1.2.1 (see Figure 3.2).

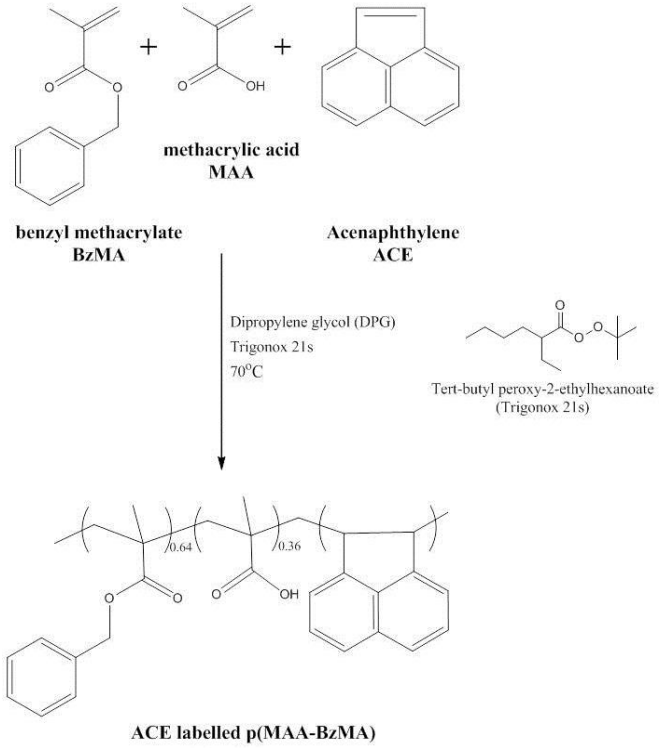

Figure 3.2. *Schematic representation of the synthesis of ACE-labelled poly(methacrylic acid-benzyl methacrylate), p(MAA-ran-BzMA) in DPG at 70°C using Trigonox 21s as initiator.*

The final copolymer had an M_n of 46300 g mol^{-1}, an M_w of 91800 g mol^{-1} and a PDI of 2. ^{1}H NMR showed that the final copolymer contained 36:64 mol % MAA:BzMA. The steady-state emission and excitation of the ACE-labelled p(MAA_{36}-ran-$BzMA_{64}$) is shown in Figure 3.3. The ACE label absorbs light at a wavelength of 295 nm and emits at a wavelength of 340 nm. The use of ACE to probe the conformation of polymers in solution has frequently been employed by Swanson and co-workers, with particular focus

on the conformational change of PMAA as a function of pH.[2,3]

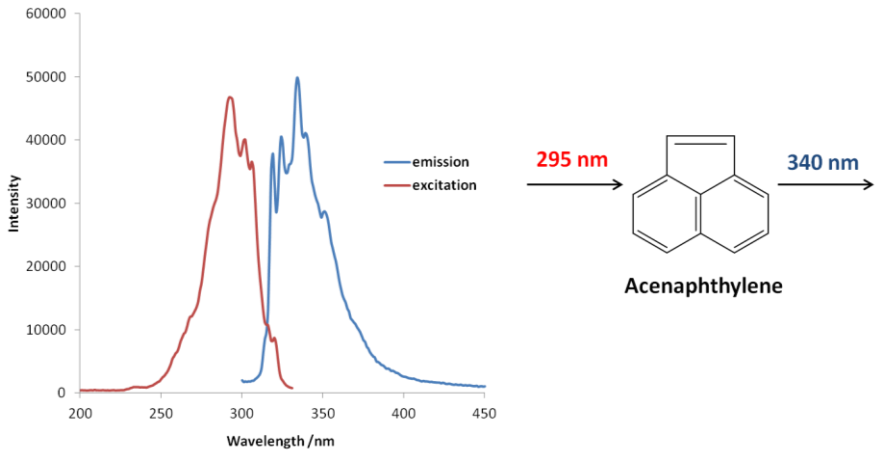

Figure 3.3. *Fluorescence excitation and emission spectra of ACE-labelled p(MAA$_{36}$-ran-BzMA$_{64}$) at 10^{-3} wt % in water at 25°C. (λ_{ex} =295 nm; λ_{em} = 340 nm).*

The amount of ACE incorporated into the copolymer backbone was determined using UV spectroscopy via the Beer-Lambert Law (Equation 3.2), which states the amount of absorbance (A) is given by the product of the concentration of the absorbing species (c), the sample thickness (l) and the molar absorption coefficient (ε).

$$A = \varepsilon l c \qquad \textbf{Equation 3.2}$$

The molar absorption coefficient was determined using a calibration curve constructed by measuring the UV absorption spectra of varying molar concentrations of acenaphthene in methanol (see Figure 3.4).

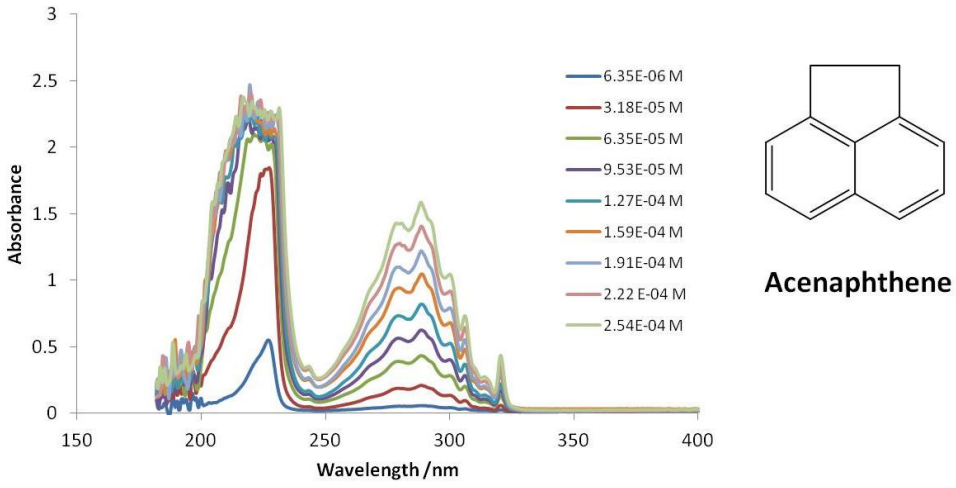

Figure 3.4. *UV absorbance spectra for acenaphthene in methanol at various molar concentrations at 298 K.*

Acenaphthene was used because its chemical structure is analogous to that of acenaphthylene once it has been polymerised into the polymer backbone. The maximum absorbance at 295 nm was then plotted against concentration. To this data set a straight line was fitted and the gradient was incorporated into the Beer-Lambert law. The concentration of ACE could then be calculated using the calibration curve shown in Figure 3.5. Using this method it was calculated that 0.98 mol % of ACE was incorporated into p(MAA_{36}-ran-$BzMA_{64}$), which is sufficiently low so that the label should not affect the polymer properties.

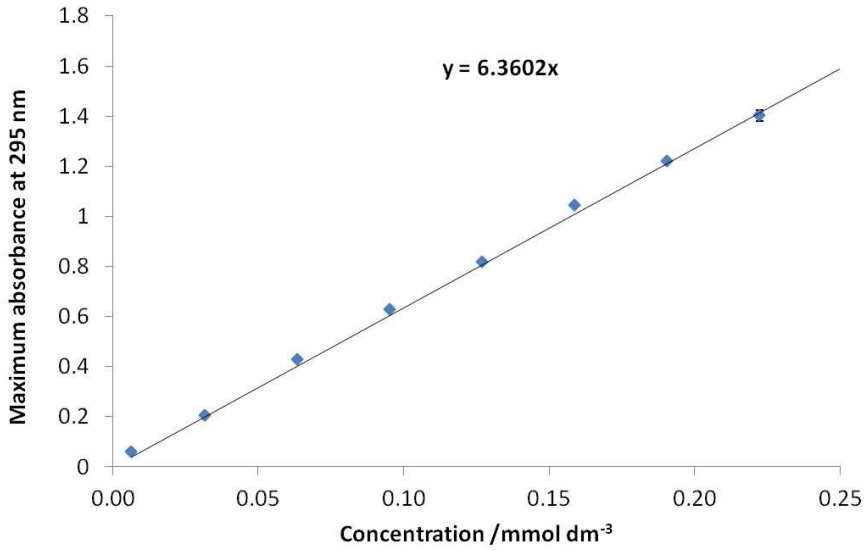

Figure 3.5. *Calibration curve for varying concentrations of acenaphthene in methanol at 298 K. The maximum absorbance reading was taken at 295 nm.*

ACE was chosen to probe the conformation of p(MAA_{36}-ran-$BzMA_{64}$) at the solid-liquid interface because its motion reflects that of the copolymer backbone.[9] Time-resolved anisotropy measurements (TRAMS) were used to detect this motion. Firstly, the conformation of p(MAA_{36}-ran-$BzMA_{64}$) in water was investigated by TRAMS between pH 5.6 and pH 11.8 (below pH 5, the copolymer precipitated out of solution). Figure 3.6 shows the aqueous electrophoresis data obtained for ACE-labelled p(MAA_{36}-ran-$BzMA_{64}$), which displays negative zeta potentials between pH 6.3-10.5. The pH at which p(MAA_{36}-ran-$BzMA_{64}$) precipitates out of water can be identified as it corresponds to a dramatic increase in mean diameter. Figure 3.7 and Figure 3.8 displays the TRAMS data for p(MAA_{36}-ran-$BzMA_{64}$) in water at pH 9.5. Figure 3.7 displays the orthogonal components of intensity analysed parallel, (I_{VV}), and perpendicular, (I_{VH}), to the plane of vertically-polarized excitation and was transformed according to equation 3.3 into the observed anisotropy, r.[10]

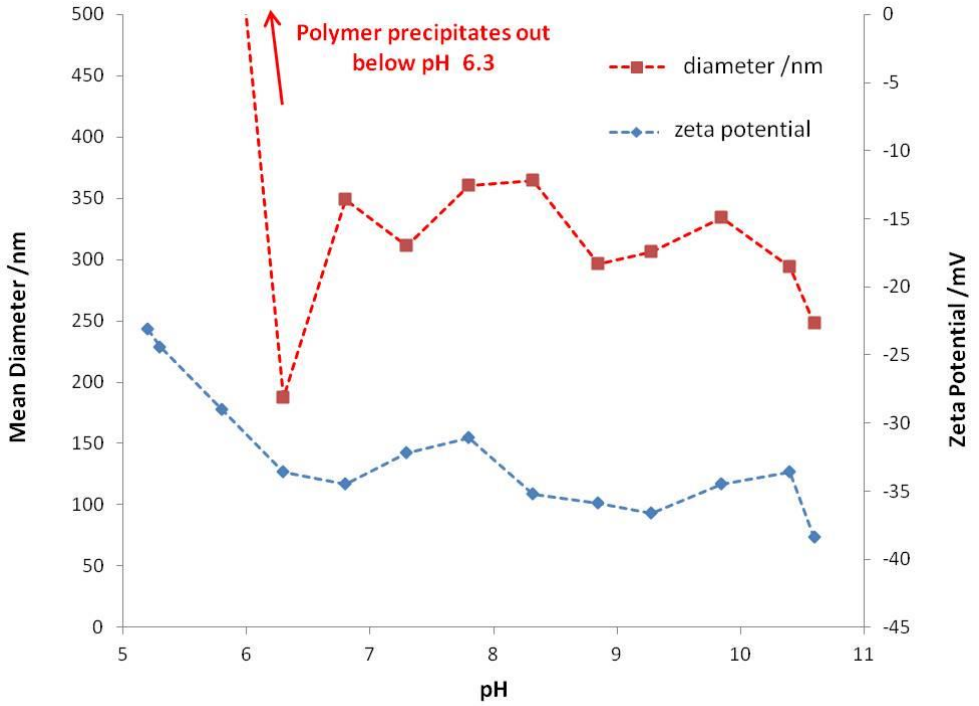

Figure 3.6. *Variation of zeta potential and mean diameter with pH for ACE-labelled p(MAA$_{36}$-BzMA$_{64}$).*

$$r = \frac{I_{VV} - I_{VH}}{I_{VV} + 2I_{VH}} \qquad \textbf{Equation. 3.3}$$

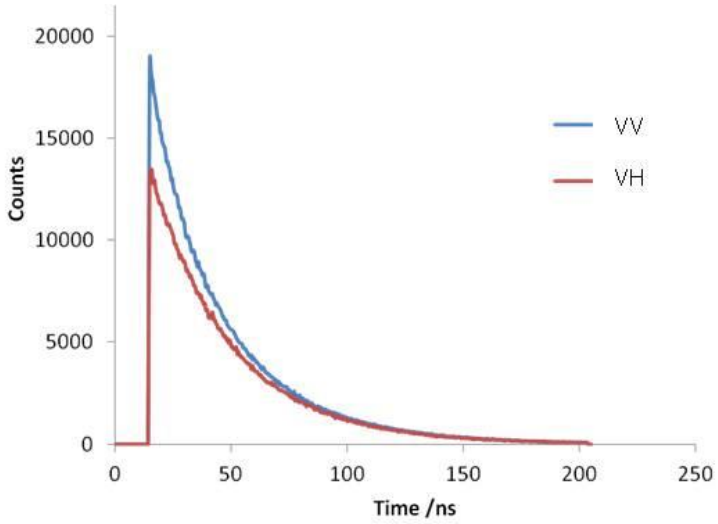

Figure 3.7. *Parallel and perpendicular fluorescence components of the time-dependent anisotropy of ACE-labelled p(MAA$_{36}$-ran-BzMA$_{64}$) (10^{-3} wt %) in water at 298 K and pH 9.5.*

The graph in Figure 3.8 displays direct analysis of the raw anisotropy data by fitting the anisotropy, r, (data points) to a single exponential decay model (solid line).[10] This model

is shown in equation 3.4, where r_0 is the intrinsic anisotropy for the individual chromophore and τ_c is the correlation time. The estimated correlation time, τ_c, at pH 9.5 was calculated to be 24 ns. The fit was deemed good in this case, as judged by the value of χ^2 being close to 1.0 and the randomly distributed residuals. The generally accepted upper limit for χ^2 is 1.3 for single exponential models.[1]

$$r(t) = r_0 \exp(-t/\tau_c) \qquad \textbf{Equation 3.4}$$

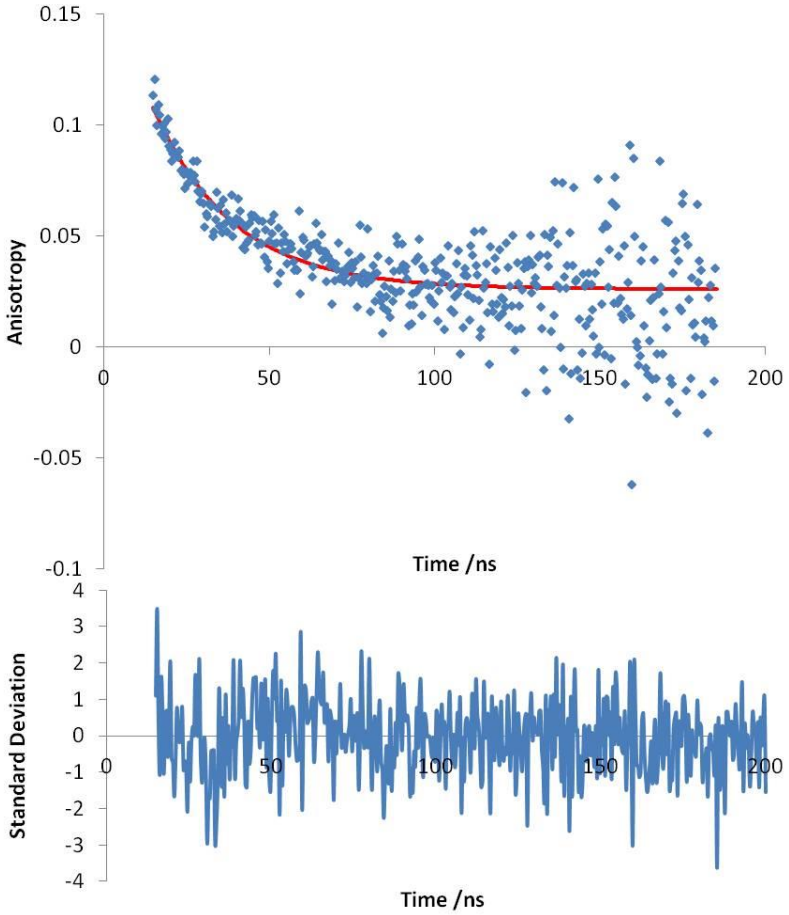

Figure 3.8. *Direct analysis of anisotropy data for ACE-labelled p(MAA$_{36}$-ran-BzMA$_{64}$) (10^{-3} wt %) in water at 298 K and pH 9.5. A single exponential fit to r(t) has been applied to fit the data. χ^2 =1.03 and τ_c= 24 x 10^{-9} seconds. The residuals are also shown.*

The τ_c values obtained for p(MAA$_{36}$-ran-BzMA$_{64}$) at varying pH are shown in Table 1 and Figure 3.9. All τ_c values were calculated using the single exponential decay model. For comparison, the behaviour of ACE-labelled PMAA in water as a function of pH is also shown. PMAA exhibits a conformational change between pH 4 and 6 going from a coiled structure to a water-swollen chain. This conformation change was similar to that

observed by Swanson and Soutar,[1] who also studied the conformation of PMAA as a function of pH using TRAMS. For PMAA, a high τ_c is obtained below pH 4 due to the coiled chains restricting the motion of the ACE label and a low τ_c is obtained above pH 6 due to ionised carboxylate groups repelling one another to give a more open chain, allowing the ACE labels to rotate more freely. From Figure 3.9 and Table 3.1 it can be seen that, between pH 5.6 and 7.3, the correlation times for p(MAA_{36}-ran-$BzMA_{64}$) are higher than the correlation times for PMAA, indicating that p(MAA_{36}-ran-$BzMA_{64}$) is in a more coiled conformation. The p(MAA_{36}-ran-$BzMA_{64}$) copolymer is more coiled than PMAA between pH 5.6-7.3 because the hydrophobic BzMA segments cluster together to minimize contact with water. These hydrophobic domains lead to p(MAA_{36}-ran-$BzMA_{64}$) being unable to unfold completely due to repulsion between the deprotonated carboxylate groups leading to a higher τ_c.

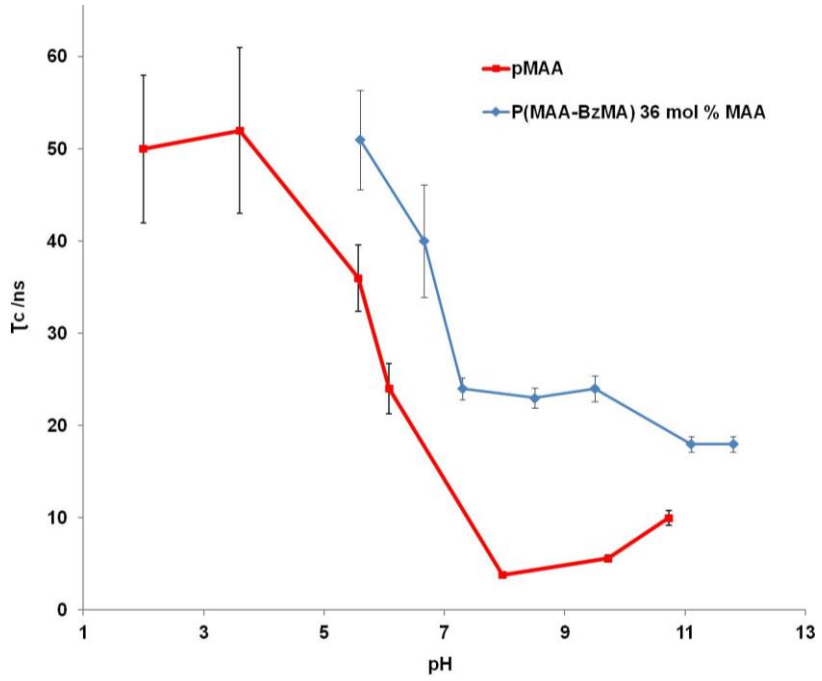

Figure 3.9. *Correlation time, τ_c vs. pH for ACE-labelled p(MAA_{36}-ran-$BzMA_{64}$) (10^{-3} wt %) in water at 298 K and ACE-labelled PMAA. The pH was adjusted with either 0.2 M HCl or 0.2 M NaOH. All correlation times were calculated from direct analysis of the raw anisotropy data using a single exponential decay model of the form: $r(t)=r_0 \exp(-t/\tau_c)$.*

Correlation time (τ_c) /ns	pH	S.D /ns	χ2
51	5.6	5.4	1.1
40	6.7	6.1	1.1
24	7.3	1.2	1.2
23	8.5	1.1	1.2
24	9.5	1.4	1.0
18	11.1	0.9	1.2
18	11.8	0.9	1.3

Table 3.1. *Correlation times, τ_c for ACE-labelled p(MAA$_{36}$-ran-BzMA$_{64}$) at varying pH via the fitting of a single exponential function model function for r(t).*

To further explore the effects of hydrophobic BzMA units on the expansion of p(MAA-ran-BzMA), two more copolymers were synthesised by the semi-batch method with 45 and 64 mol % of MAA. The TRAMS data on these copolymers at different pH is reported in Figure 3.10. This figure shows that, as the amount of MAA increases, the correlation times decrease between pH 8 and 11, indicating that the p(MAA-ran-BzMA) copolymers are able to expand into a more open conformation. The transition at which the p(MAA-ran-BzMA) copolymers switch from a coiled to a more expanded state shifts to ~pH 7 compared to pH 5 for PMAA homopolymer. The shifted transition is due to the higher degree of ionisation required to expand the copolymer and pull the BzMA hydrophobic domains apart. It was noted that increasing the BzMA content from 36 to 64 mol % did not further shift the transition to a higher pH, instead it remained at pH 7. Due to the transition occurring at a physiological pH of around 7, it was speculated that the p(MAA-ran-BzMA) copolymers could have a potential use as drug delivery polymers in the human body, whereby the hydrophobic domains could solubilise organic molecules. This could be tested in the future by utilising an environmentally sensitive probe such as pyrene, which can be used to detect the formation of hydrophobic domains.[11]

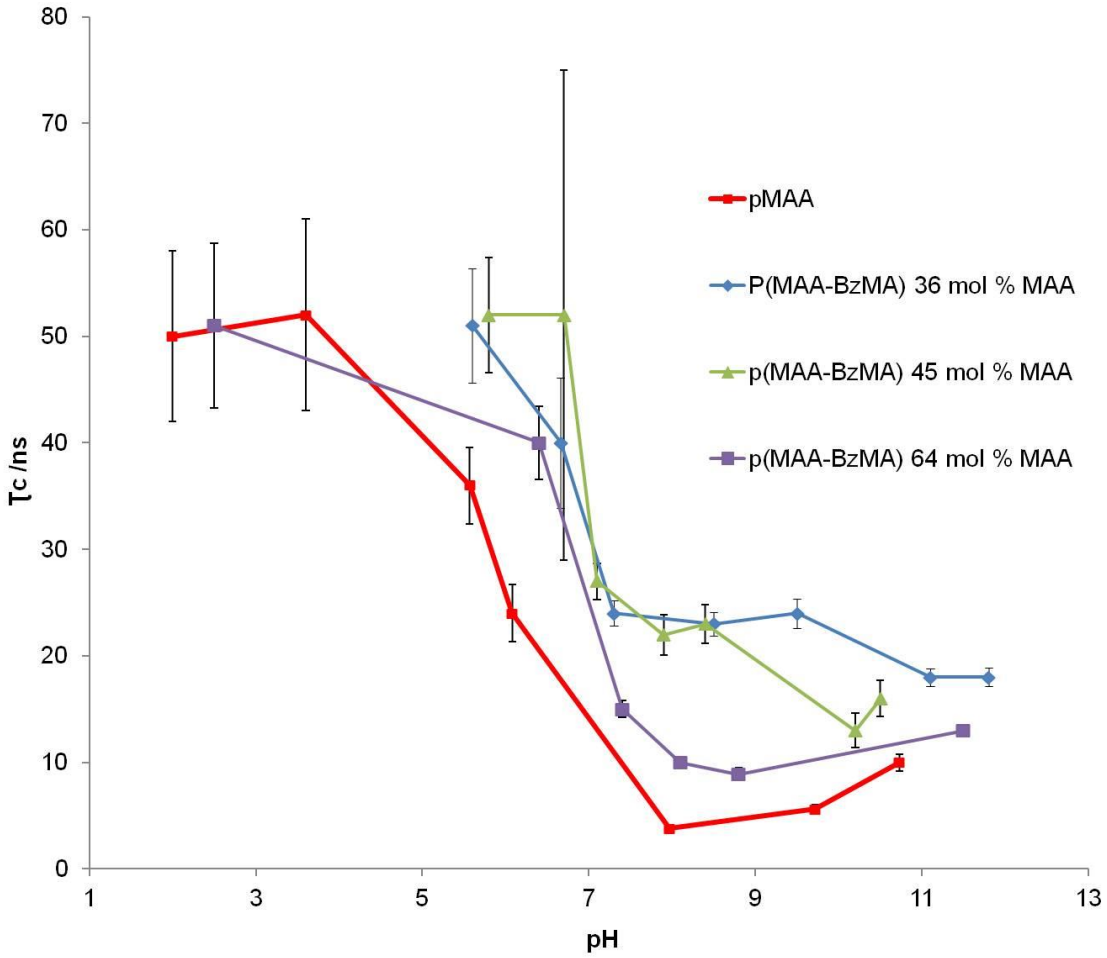

Figure 3.10. *Correlation time, τ_c vs. pH for ACE-labelled p(MAA-ran-BzMA) copolymers (10^{-3} wt %) in water at 298 K. The effect of changing the mol % of MAA incorporated into the copolymer on correlation time is shown. The pH was adjusted with either 0.2 M HCl or 0.2 M NaOH. All correlation data were calculated from direct analysis of the raw anisotropy data using a single exponential decay model of the form; $r(t)= r_0 \exp(-t/\tau_c)$. In red, correlation times for PMAA at different pH is shown for comparison. Lines have been drawn for clarity and do not reflect the exact data.*

This study on the conformation of p(MAA-ran-BzMA) copolymers can be compared to the work carried out by Ebdon et al., who studied poly(styrene-acrylic acid) (Sty-AA) and poly(methyl methacrylate-acrylic acid) (MMA-AA) copolymers in aqueous media as a function of pH using anisotropy measurements.[4] Ebdon et al. reported that, when either MMA or Sty was incorporated into the AA chain, the critical pH for the conformational transition from the acidic to neutralised copolymer to occur broadened and shifted to a higher pH, which is analogous to the p(MAA-ran-BzMA) copolymers studied in this research project. The shift in transition was due to the hydrophobic domains formed by MMA or Sty restricting the unfolding of the copolymer at higher pH. It was also found that incorporating more hydrophobic units led to a higher τ_c.

3.3.2 Using time-resolved anisotropy measurements (TRAMS) to probe the conformation of ACE-labelled p(MAA-b-BzMA) diblock copolymers in water.

3.3.2.1 Synthesis of ACE-labelled p(MAA-b-BzMA) diblock copolymers

The p(MAA-b-BzMA) diblock copolymers were synthesised by reversible addition-fragmentation chain transfer (RAFT) polymerisation. The protocol used to synthesise the diblocks was based on the synthesis used by Semsarilar et al.[12] but it was modified slightly by the incorporation of an ACE label into the PMAA block. The PMAA macro-chain transfer agent (CTA) was synthesised with 1 wt % ACE label (based on monomer) incorporated into its backbone (see Figure 3.11).

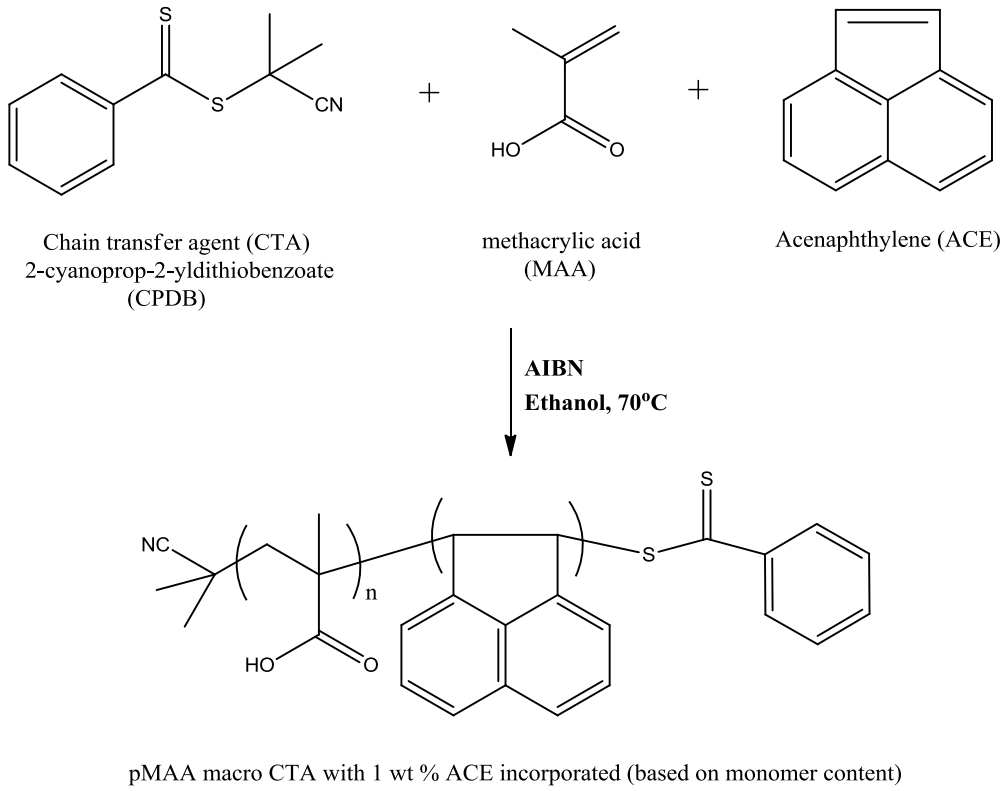

Figure 3.11. *Schematic representation showing the synthesis of PMAA macro-CTA by reversible addition fragmentation transfer (RAFT) polymerisation at 70°C in ethanol at 25 w/v % with 1 wt % of ACE incorporated (based on monomer content).*

To confirm that the ACE label was successfully incorporated into the PMAA macro-CTA polymer backbone, UV and steady-state spectroscopy were conducted on the purified macro-CTA. The emission at 340 nm proved that the ACE label was present in the PMAA backbone. By application of the Beer-Lambert law, it was determined that 1.85 mol % of ACE was incorporated into the PMAA backbone (see Figure 3.13).

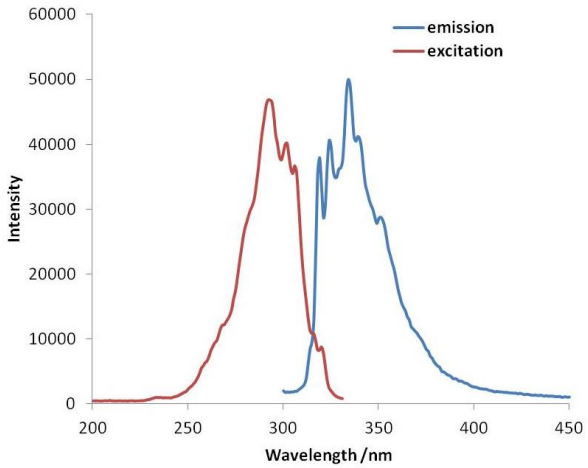

Figure 3.12. *Fluorescence excitation and emission spectra of $PMAA_{143}$-ACE macro-CTA (1 wt % ACE label incorporated based on monomer) at 10^{-3} wt % in methanol at 25 ℃. (λ_{ex} =295 nm; λ_{em} = 340 nm).*

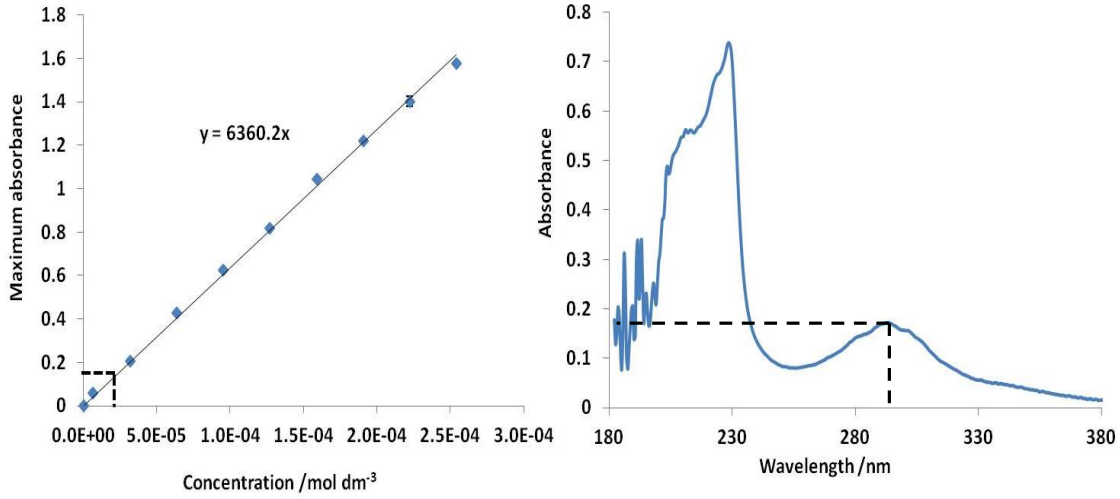

Figure 3.13. *Left) UV calibration curve for increasing concentrations of acenaphthene in methanol. Right) UV absorption spectrum for PMAA-ACE macro-CTA (10^{-3} wt %) in methanol.*

The DP of the PMAA macro-CTA was found to be 143 by comparing the integrated intensity signal from the MAA monomer peaks with the methacrylic polymer backbone at 0.1-2.5 ppm by ^{1}H NMR in D_2O. Conventionally, the mean DP is calculated by comparing the integrated intensity signal from the aromatic protons from the RAFT chain end with the methacrylic acid polymer backbone. It was not possible to calculate the mean DP via the conventional method, as the ACE label had aromatic protons that appeared in the same ppm range as the RAFT agent. GPC shows that the ACE-labelled $PMAA_{143}$

macro-CTA was obtained with a M_n of 22300 g mol^{-1} and a high polydispersity (PDI) of 1.9 (see Figure 3.14). The high polydispersity of the ACE-labelled $PMAA_{143}$ macro-CTA block is uncharacteristic of RAFT and was assumed to be due to the presence of ACE; to clarify this assumption GPC analysis was also carried out on a PMAA macro-CTA with no ACE label present synthesised under the same conditions (see Figure 3.14). The GPC shows that in the absence of ACE, the PMAA macro-CTA was obtained at a much lower PDI, supporting the hypothesis that the presence of ACE led to a higher polydispersity.

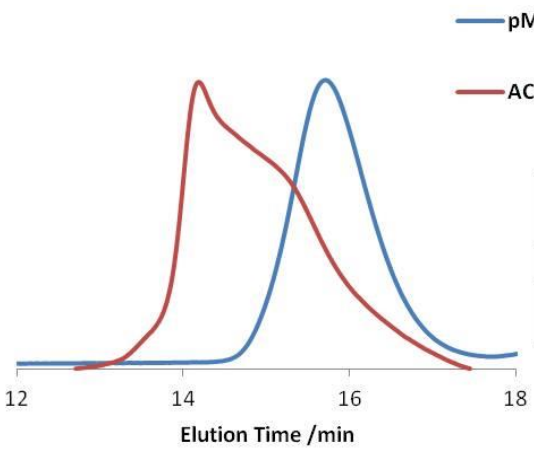

	M_w	M_n	PDI (M_w/M_n)
PMAA macro-CTA	8200	6300	1.3
ACE-labelled PMAA macro-CTA	41300	22300	1.9

Figure 3.14. *THF gel permeation chromatograms obtained for ACE-labelled $PMAA_{143}$ macro-CTA and PMAA macro-CTA synthesised via RAFT polymerisation at 70°C and 25 wt % solids.*

To understand how the presence of ACE led to the high PDI of the $PMAA_{143}$ macro-CTA, a paper by Matyjaszewski[13] was found that outlines the requirements for ensuring polymers are obtained with a low polydispersity. These are:

1) Rate of initiation is similar to the rate of propagation.
2) The terminal ends on active chains are equally inclined to reaction with monomer.
3) There is negligible chain transfer or termination.
4) Rate of depropagation is substantially lower than propagation.
5) The system is homogeneous and mixed fast.

If all five requirements are met, a polymer with a narrow molecular weight and a Poisson distribution will be obtained. The chromatogram of ACE-labelled $PMAA_{143}$ macro-CTA deviated dramatically from a Poisson distribution and it is speculated that it is due to a failure to meet requirement 2 caused by chains ending with ACE label being more or less reactive towards MAA. To explore this further, the kinetics for the RAFT synthesis of

PMAA macro-CTA with and without 1 wt % ACE label was followed at 25 wt % in ethanol at 70°C to examine if ACE had an effect on conversion (see Figure 4.15). By examining Figure 4.15, it can be seen that the polymerisation of MAA in the presence of ACE proceeded at a slightly faster rate (reaching 80 % conversion in 6 h) while the polymerisation of PMAA without ACE only reached 72 % conversion. The difference in conversion between the polymerisations is an indication that requirement two was not fulfilled.

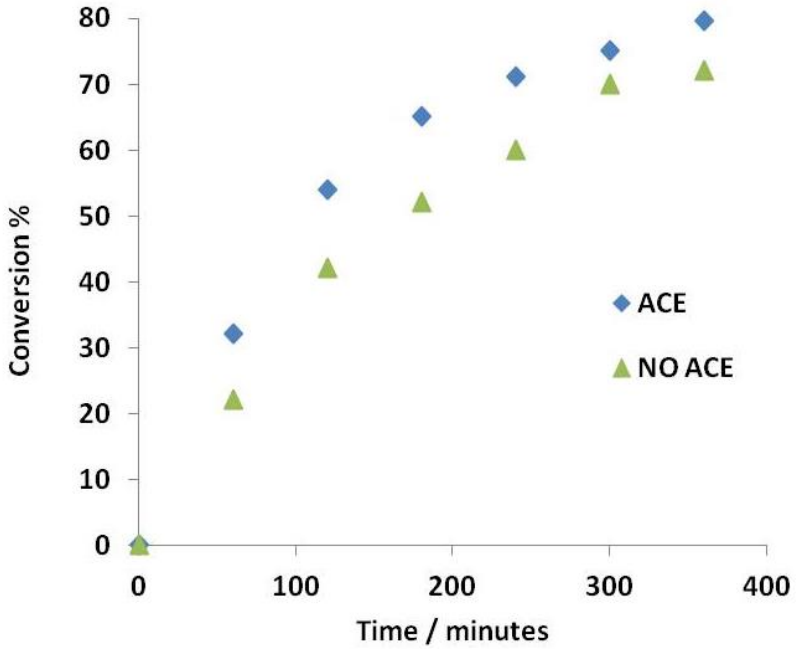

Figure 4.15. *Conversion vs. time curves for the RAFT synthesis of PMAA macro-CTA with and without 1 wt % ACE label based on monomer at 25 wt % solids at 70°C in ethanol.*

After purification, the $PMAA_{143}$-ACE macro-CTA was used for *in situ* RAFT alcoholic dispersion polymerisation of BzMA to produce a series of $PMAA_{143}$-$BzMA_n$ diblock copolymers at 10 w/v % solids. (see Table 3.2). GPC studies of the diblocks showed that they were obtained with good blocking efficiencies but with relatively high polydispersities for a living polymerisation (see Figure 3.16). It was speculated that this was due to the high polydispersity (1.9) of the $PMAA_{143}$-ACE macro-CTA block. As no monomer peaks were present in the ^{1}H NMR spectra of the p(MAA_{143}-$BzMA_n$) diblocks, it was assumed that the reaction achieved 100 % completion and the targeted BzMA DP was the final BzMA DP.

Name	Target Dp of PMAA block	Actual Dp of PMAA block[a]	Dp of pBzMA block[a]	M_n[b] (g mol^{-1})	PDI (M_w/M_n)[b]
AWR14	174	143	50	75100	1.7
AWR15	174	143	100	95400	1.8
AWR13	174	143	143	129000	1.7
AWR16	174	143	200	143200	1.8
AWR17	174	143	300	190100	2.2

Table 3.2. *Summary data for p(MAA$_{143}$-b-BzMA$_n$) diblocks synthesised by RAFT in ethanol at 70°C at 10 w/v % solids. [a]Determined by ^{1}H NMR spectroscopy [b]M_n and M_w/M_n values were determined by THF GPC against PS standards.*

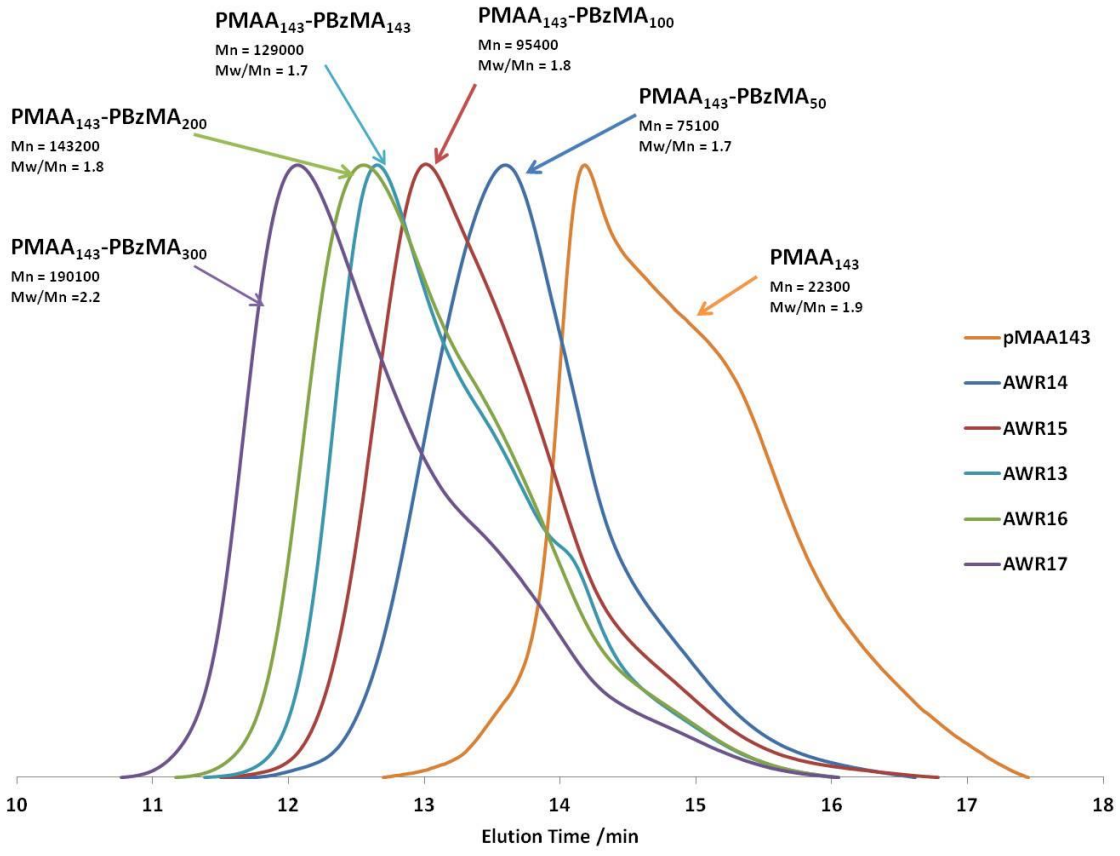

Figure 3.16. *THF gel permeation chromatograms obtained for a series of five p(MAA$_{143}$-b-BzMA$_n$) diblock copolymers synthesised by RAFT dispersion polymerisation in ethanol at 10 w/v % solids. Also shown is the corresponding PMAA$_{143}$ macro-CTA synthesised via RAFT solution polymerisation in ethanol at 70°C and 25 w/v % solids.*

It was found that these amphiphilic diblocks self-assembled into micelles during polymerisation whereby pBzMA formed the core and pMAA formed the corona.[12] This

process of self-assembly is known as polymerisation-induced self-assembly (PISA) and has been extensively researched by the Armes group who have worked on numerous diblock systems to give self-assembled structures such as micelles, vesicles and worms.[14,15] Figure 3.17 shows TEM images of the self-assembled micelles from the diblocks listed in Table 3.2. In Semsarilar's paper,[12] the diblock that self-assembled into micelles was p(MAA_{67}-b-$BzMA_{50}$) and had a PDI of 1.19, whereas the p(MAA_{143}-b-$BzMA_n$) diblocks synthesised in Table 3.2 have PDIs ranging from 1.67-2.16. This shows that even when the polydispersity of the diblocks is high, self-assembled structures still form showing that low polydispersity is not essential for the production of micelles. This has been shown previously by Adams et al., who produced poly(ethylene oxide)-block-poly(N,N-diethylaminoethyl methacrylate) diblocks with PDIs between 1.36-1.96.[16] It was found that a high PDI had no effect on the self-assembly of diblocks into micelles, worms or vesicles in solution.

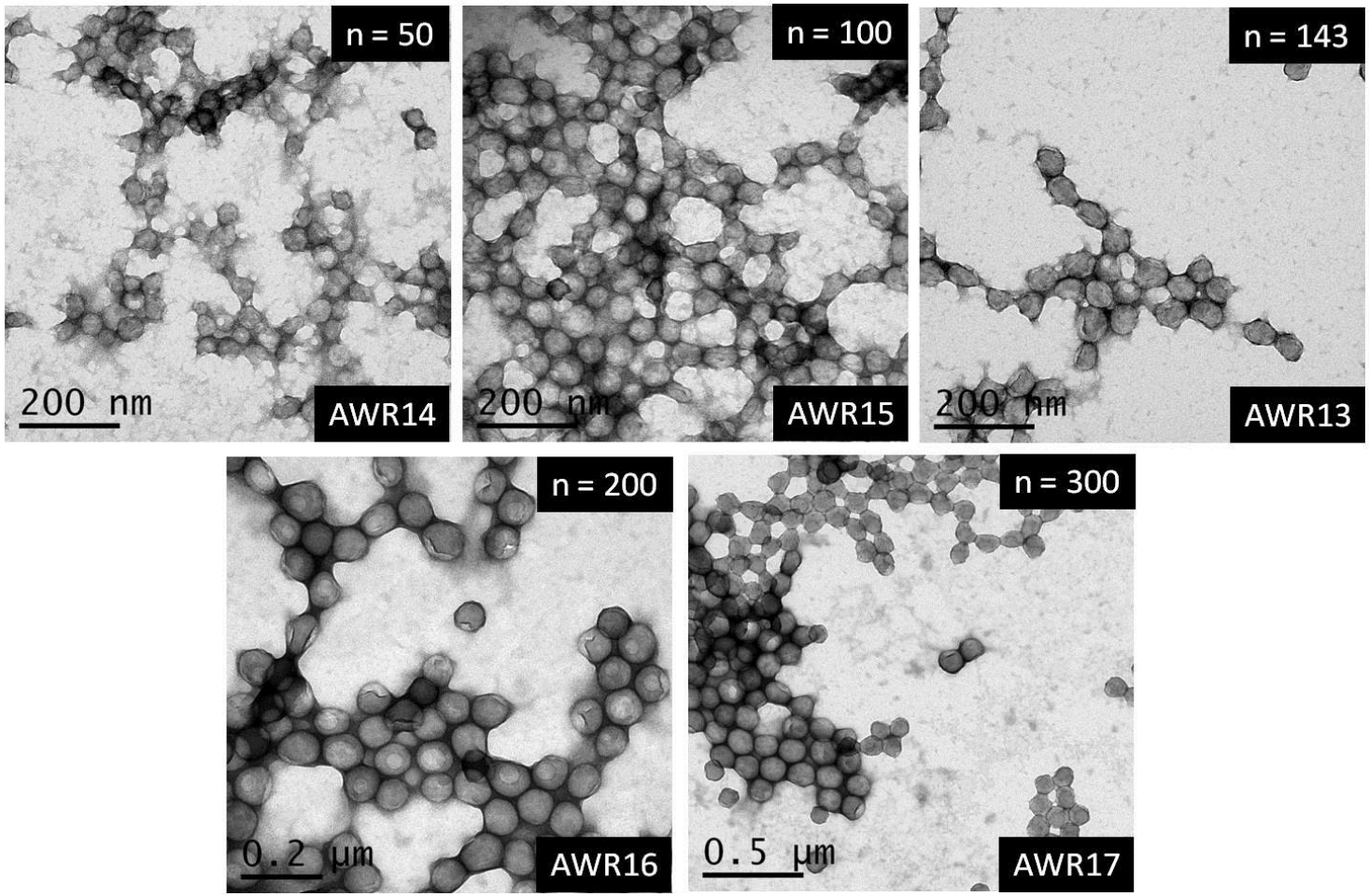

Figure 3.17. *TEM images of the diblock copolymer particles prepared by RAFT dispersion polymerisation (at >99 % conversion and 10 w/v %) for a series of five p(MAA$_{143}$-b-BzMA$_n$) block copolymers. The TEM samples were obtained by diluting the 10 w/v % reaction mixture with water to 0.1 w/v %. This gave the diblock solutions a final pH of 4.5.*

TEM was used to show that the p(MAA_{143}-b-$BzMA_n$) diblocks listed in Table 3.2 remained as micelles during a pH change from 4.5 to 11 (see Figure 3.18). Battaglia et al[17] synthesised polybutadiene-poly(methacrylic acid), p(Bd_{24}-MAA_{10}) block copolymers using sequential anionic polymerisation of butadiene and t-butyl methacrylate. The poly(t-butyl methacrylate) was hydrolysed to polymethacrylic acid by refluxing with HCl in dioxane. Battaglia et al. used TEM to show that the morphologies of the diblocks in aqueous solution could be varied as a function of pH. At a low pH, vesicles would form and, as the pH increased, the vesicles became smaller to eventually transform into worm-like micelles and then eventually form micelles at pH 10. The transformation from vesicles to micelles was driven by increasing repulsion between PMAA chains as the degree of ionisation increased. The inability of p(MAA_{143}-b-$BzMA_n$) diblocks to undergo a morphology transition with varying pH could be attributed to the p(MAA_{143}-b-$BzMA_n$) diblocks having a higher molecular weight and polydispersity, which may prevent the morphology transition.

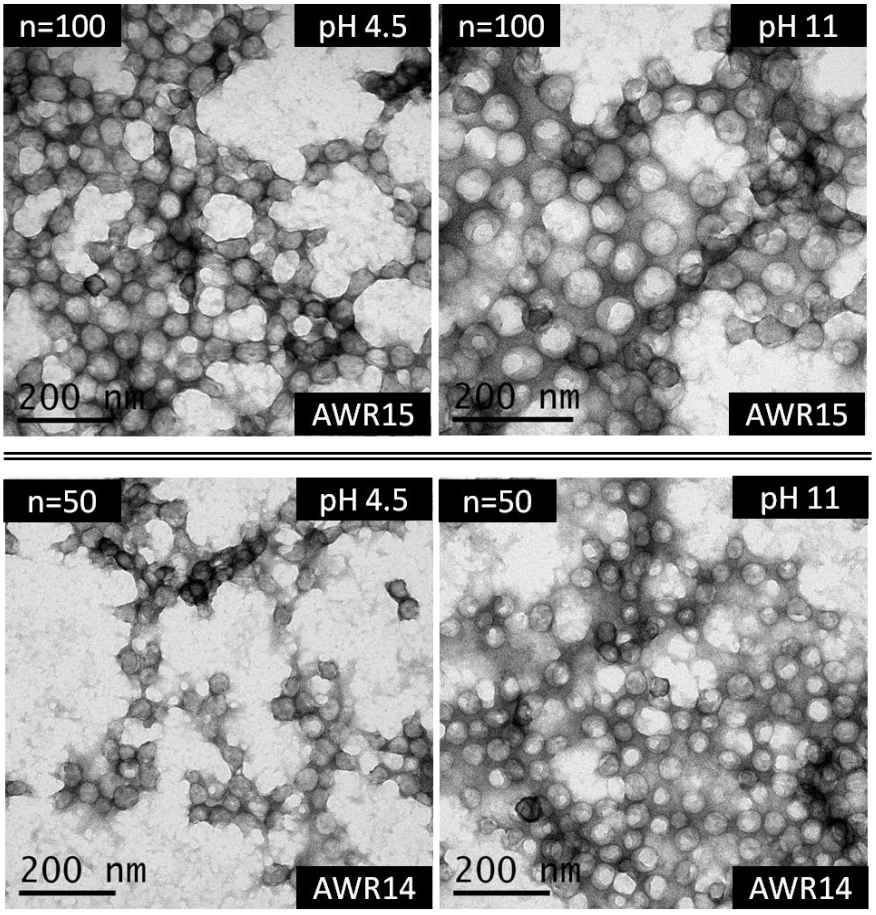

Figure 3.18. *TEM images of p(MAA_{143}-b-$BzMA_{100}$) (top row) and p(MAA_{143}-b-$BzMA_{50}$) (bottom row) at 0.1 w/v % in water at pH 4.5 and 11.*

Examination of the DLS data for the diblocks at pH 4.3 and 12 revealed that the micelles increased in diameter at higher pH. This was unsurprising as it is known that the PMAA chains in the corona should be extended due to Coulombic repulsion between the deprotonated acid groups at high pH. Also, as expected, it was observed that, as the DP of the hydrophobic block increased, the hydrodynamic radius increased due to the BzMA core becoming larger.

Sample name	DP of ACE-labelled pMAA block	DP of pBzMA block	DLS diameter /nm (PDI) at pH 4.3	DLS diameter /nm (PDI) at pH 12
AWR14	143	50	95 ± 0.8 (0.097)	168 ± 4.0 (0.037)
AWR15	143	100	111 ± 2.2 (0.070)	171 ± 0.9 (0.018)
AWR13	143	143	121 ± 1.2 (0.043)	177 ± 1.9 (0.043)
AWR16	143	200	159 ± 2.4 (0.021)	209 ± 2.0 (0.020)
AWR17	143	300	185 ± 3.3 (0.017)	243 ± 2.6 (0.075)

Table 3.3. *Summary of particle size data obtained for p(MAA_{143}-b-$BzMA_n$) diblocks prepared by RAFT dispersion polymerisation at 70°C in ethanol. Samples were run at 0.1 wt % in filtered deionised water at pH 4.3 and 12.*

3.3.2.2 TRAMS of ACE-labelled p(MAA_{143}-b-$BzMA_n$) diblocks

Due to the presence of the ACE label in the PMAA block in the p(MAA_{143}-b-$BzMA_n$) diblocks TRAMS and steady state-fluorescence spectroscopy were considered to be a useful technique for the study of the structure of the micelles. It was presumed that the ACE label could be located at any point along the PMAA chain, such as the core/corona interface, the corona/aqueous interface or at the centre of the corona. Steady-state spectroscopy was carried out on the micelles at 0.1 w/v % in water at pH 4.5 and 11. The maximum intensity seen at 335 nm due to emission from the ACE label was plotted against the DP of BzMA (see Figure 3.19). At pH 11, the steady-state intensity of the diblocks was higher than the intensity obtained at pH 4.5. This higher intensity at pH 11 could be due to the ACE label being more 'exposed' due to charged PMAA chains stretching out. It was also observed that the maximum intensity increased with increasing DP of the pBzMA block. However, as the concentration of ACE label in each diblock solution can differ, giving a different maximum intensity, no conclusion could be drawn from this data.

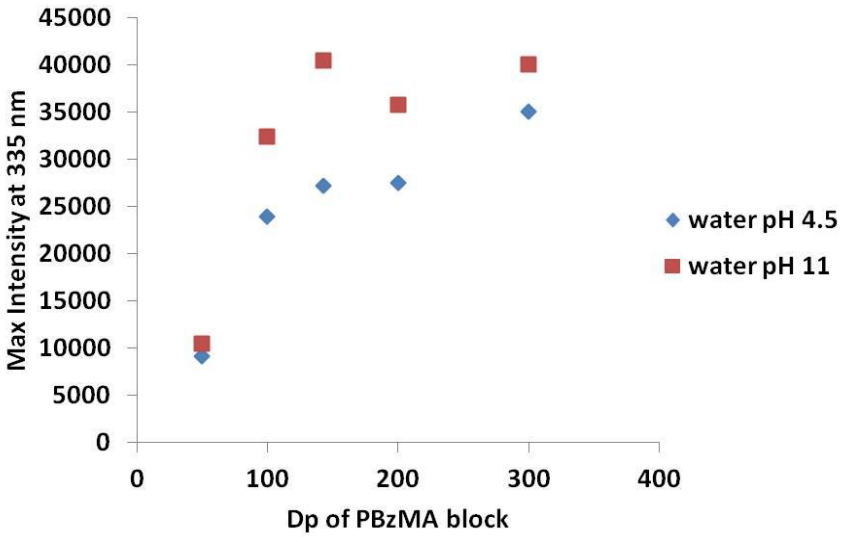

Figure 3.19. *Maximum intensity of emission at 335 nm from the steady-state emission spectra obtained for p(MAA$_{143}$-b-BzMA$_n$) diblocks (0.1 w/v % in water) at pH 4.5 and 11.*

TRAMS measurements were also performed on 0.1 w/v % aqueous solutions at pH 4.5 and 12. The data were fitted with a single exponential fit and the corresponding τ_c values are shown in Table 3.4. It was not possible to conduct TRAMS measurements on samples AWR16 and AWR17 due to the TRAMS instrument being decommissioned before the project was completed. It can be seen from Table 3.4 that the correlation time decreased with increasing pH, which was expected because the PMAA corona chains stretch out at a high pH due to repulsion between the chains (see Figure 3.20). The higher τ_c values at pH 4.5 suggest that the ACE labels attached to the PMAA chains are in a more restricted environment but can still move relatively freely, suggesting the PMAA chains in the corona are not coiled up tightly but just slightly retracted. The inability of the PMAA chains to coil up tightly could be attributed to steric hindrance at the corona. There seems to be no correlation between τ_c and the DP of the pBzMA block, but due to limited TRAMS data collected on the diblocks, no strong conclusions could be drawn about the structure of the micelles; further investigation would be required.

Sample name	Dp of ACE-labelled PMAA block	Dp of PBzMA block	τ_c /ns at pH 4.5 FIT 1	χ^2	τ_c /ns pH 12 FIT 1	χ^2
AWR14	143	50	7.1 ± 1.6	1.4	2.5 ± 0.3	1.3
AWR15	143	100	8.6 ± 4.1	1.2	2.4 ± 0.5	1.1
AWR13	143	143	4.5 ± 0.7	1.6	2.2 ± 0.1	1.3

Table 3.4. *Summary of TRAMS data obtained for p(MAA_{143}-b-$BzMA_n$) diblocks prepared by RAFT at 70°C in ethanol whereby the PMAA block was ACE labelled. All samples were run at 0.1 w/v % in ultrapure water and the pH was changed with either 0.2 M HCl or 0.2 M NaOH.*

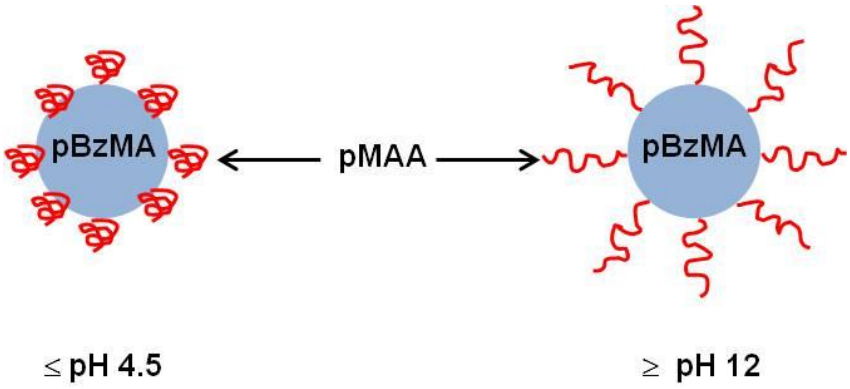

Figure 3.20. *Schematic representation showing the retraction and stretching of PMAA chains in the micelle corona at different pH.*

3.3.3 Using TRAMS to explore the adsorption of random copolymers and diblock copolymers of methacrylic acid and benzyl methacrylate onto colloid particles.

In order to gain insight into the conformation of polymeric dispersants on pigment particles, the conformation of p(MAA-ran-BzMA) copolymers adsorbed onto colloid particles can be investigated using TRAMS. Due to the decommissioning of the TRAMS instrument, it was not possible to obtain measurements to examine the change in correlation time when either the ACE-labelled random copolymer p(MAA_{36}-ran-$BzMA_{64}$) or ACE-labelled p(MAA_{143}-$BzMA_n$) diblocks were adsorbed onto colloid particles. It was speculated that if the TRAMS measurements were carried out a large increase in τ_c would occur upon adsorption and a double exponential function would be needed to fit the anisotropy data due to the ACE label being located in loop and train

segments. It is difficult to predict what conclusions could be drawn from TRAMS data for the adsorption of p(MAA_{143}-b-$BzMA_n$) micelles as there is uncertainty regarding the TRAMS data obtained for the non-adsorbed micelles.

3.3.4 Effect of dipropylene glycol on the correlation time of the feed-prepared random copolymer p(MAA_{36}-ran-$BzMA_{64}$)

Often used in the formulation of inkjet printing inks is a solvent called dipropylene glycol (DPG). DPG was introduced in Chapter II where it was used as a solvent for the free-radical copolymerisation of MAA and BzMA. DPG is a desirable solvent in industry as it is not toxic and has a high boiling point. It was noted that, during mixing of water and DPG, the temperature of the system increased by approximately 5°C. It has been reported that DPG is slightly hygroscopic[18] (holds onto water molecules) and it was speculated that the interaction between the water and DPG resulted in an elevation in temperature. The interaction of DPG with p(MAA_{36}-ran-$BzMA_{64}$) was explored by performing TRAMS on 0.1 wt % p(MAA_{36}-ran-$BzMA_{64}$) in various ratios of DPG and H_2O. The data were fitted using a single exponential fit and is shown as a function of DPG wt % in Table 3.1 and Figure 3.21.

		FIT1			
I.D	DPG wt %	τc /ns	S.D	χ2	pH
aw068	100	33	3.5	1.3	9.6
aw077	90	35	3.8	1.3	9.4
aw076	80	35	2.3	1.2	9.6
aw069	70	34	1.8	1.3	9.1
aw070	50	28	2.2	4.7	9.2
aw071	40	27	1.1	1.8	9.3
aw072	30	26	1.6	1.3	8.9
aw073	20	22	0.1	1.4	9.1
aw074	10	23	1.2	1.2	8.9
aw075	0	28	1.0	1.4	9.2

Table 3.1. *Correlation times for 0.1 wt % ACE-labelled p(MAA_{34}-ran-$BzMA_{64}$) obtained via TRAMS in different ratios of water and dipropylene glycol (DPG). The pH was unaltered.*

Figure 3.21 displays τ_c as a function of DPG wt %. At 20 wt % DPG, τ_c is at its lowest value at 22 ns and then steadily increases with increasing DPG content up to 35 ns. The increase in correlation time with increasing DPG concentration could simply be due to the overall greater solution viscosity, which would lead to slower rotation of p(MAA_{36}-ran-$BzMA_{64}$) and hence a higher τ_c. Viscosity measurements on the same samples that were analysed by TRAMS were carried out to test this hypothesis. It was found that viscosity did indeed increase with increasing DPG content (see Figure 3.22). However, Raman studies described in Chapter 2 show that DPG hydrogen bonds with methacrylic acid. Thus the increasing τ_c values could be attributed to the DPG molecules forming hydrogen bonds with the MAA groups in p(MAA_{36}-ran-$BzMA_{64}$), leading to the chain being held in a more rigid conformation and giving a slower decay in anisotropy.

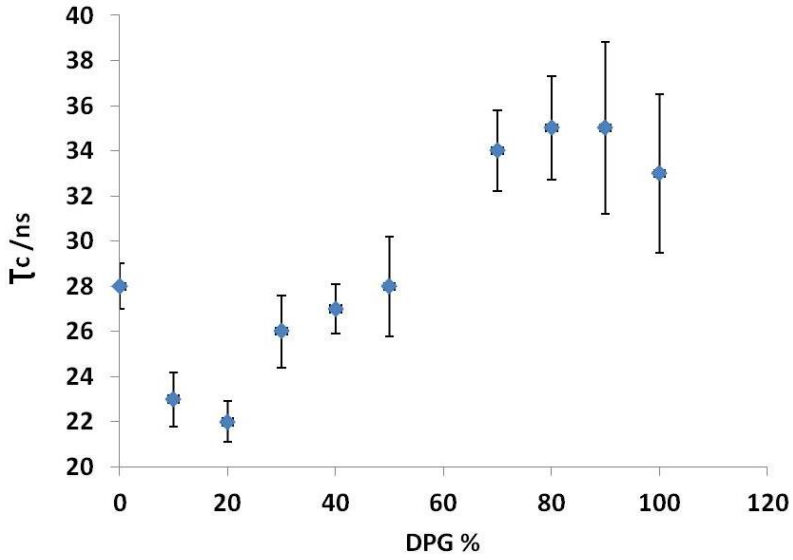

Figure 3.21. *Correlation times for ACE-labelled p(MAA_{36}-ran-$BzMA_{64}$) (0.1 wt %) in different mixtures of DPG and water. All correlation times were calculated from direct analysis of the raw anisotropy data using a single exponential decay model of the form:* $r(t) = r_0 \exp(-t/\tau_c)$.

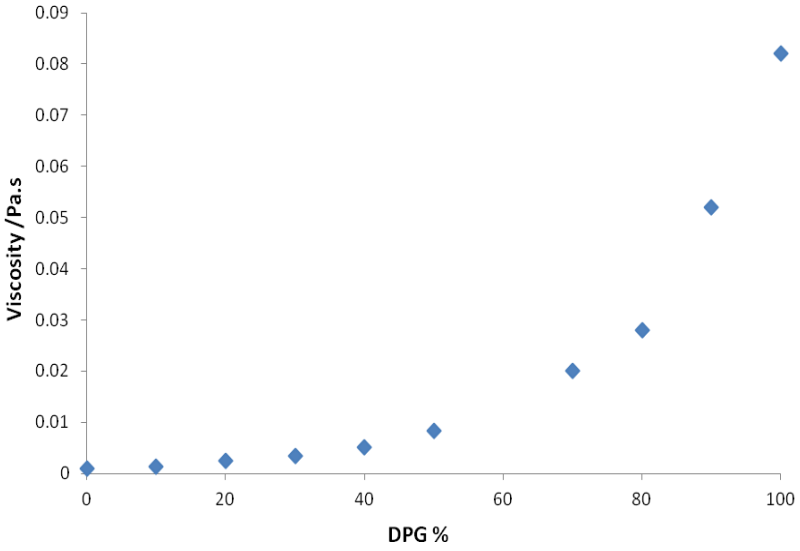

Figure 3.22. *Viscosity vs DPG wt % for ACE-labelled p(MAA$_{36}$-ran-BzMA$_{64}$) (0.1 wt %) in different mixtures of water and DPG.*

3.4 Summary

The ACE-labelled p(MAA_{36}-ran-$BzMA_{64}$) copolymer was successfully prepared using semi-batch, free-radical polymerisation. Steady-state fluorescence and UV spectroscopy confirmed the presence of ACE label in the copolymer backbone at 0.98 mol %. TRAMS performed on p(MAA_{36}-ran-$BzMA_{64}$) in water as a function of pH using a single exponential decay model to extract τ_c values showed that p(MAA_{36}-ran-$BzMA_{64}$) undergoes a conformation change at pH~7. Below pH 7, p(MAA_{36}-ran-$BzMA_{64}$) is coiled, while above pH 7 it adopts a more open structure due to repulsion between deprotonated acid groups. p(MAA_{36}-ran-$BzMA_{64}$) cannot fully uncoil like PMAA between pH 8-11 due to the hydrophobic BzMA units clustering together to minimise its interaction with water. The conformation change of PMAA from a coiled to water-swollen chain occurs at pH 5-6, showing that the incorporation of BzMA groups in p(MAA_{36}-ran-$BzMA_{64}$) restricts the unfolding of the copolymer and requires a higher degree of ionisation to induce a conformation switch. Two further semi-batch synthesis of ACE-labelled p(MAA-ran-BzMA) copolymers containing 45 and 64 mol % MAA were synthesised to explore the effect of the amount of hydrophobic units on τ_c. It was shown that, as more BzMA units were present in the copolymer backbone, the less the copolymer could unfold between pH 8-11. This was due to the Coulombic repulsion between the neutralised PMAA groups not being sufficient to break apart the hydrophobic domains formed by the BzMA units.

ACE-labelled p(MAA_{143}-b-$BzMA_n$) diblocks were synthesised using RAFT alcoholic dispersion polymerisation based on the protocol reported by Semsarilar et al.[12] The ACE-label was incorporated in the PMAA block and was found to increase the PDI of the PMAA macro-CTA as shown by GPC (when compared to a PMAA macro-CTA with no ACE present). TEM studies showed the p(MAA_{143}-b-$BzMA_n$) diblocks existed as micelles in water and remained intact with a pH change from 4.5 to 11. DLS studies showed that the micelles increased in diameter from pH 4.5 to pH 11 due to coulombic repulsion between the PMAA chains in the corona. TRAMS on the diblocks p(MAA_{143}-b-$BzMA_n$) (n=50, 100, 143) at pH 4.5 and 12 showed that a lower τ_c was obtained at pH 12, indicating that the ACE label was in a less restricted environment. This was attributed to be the result of expansion of the PMAA chains, which was supported by the DLS data.

TRAMS exploring the conformation of p(MAA_{36}-ran-$BzMA_{64}$) in DPG/water mixtures revealed that the τ_c increased with increasing DPG content. It was speculated that this occurred for two reasons: (i) the DPG molecules were hydrogen bonding to p(MAA_{36}-

ran-$BzMA_{64}$) leading to the copolymer chain being held rigid and (ii) the viscosity increased with increasing DPG content leading to slower rotation of p(MAA_{36}-ran-$BzMA_{64}$) and hence a slower anisotropy decay.

3.5 References

1. Soutar, I.; Swanson, L., *Macromolecule*, **1994**, *27*, 4304-4311.
2. Chee, C. K.; Rimmer, S.; Soutar, I.; Swanson, L., *Polymer*, **1997**, *38*, 483-486.
3. Soutar, I.; Swanson, L., *Macromolecules*, **1996**, *29*, 4931-4936.
4. Ebdon, J. R.; Hunt, B. J.; Lucas, D. M.; Soutar, I.; Swanson, L.; Lane, A. R., *Canadian Journal of Chemistry*, **1995**, *73*, 1982-1994.
5. Smith, T. A.; Irwanto, M.; Haines, D. J.; Ghiggino, K. P.; Millar, D. P., *Colloid Polymer Science*, **1998**, *276*, 1032-1037.
6. Chan, J.; Fox, S.; Kiserow, D.; Ramireddy, C.; Munk, P.; Webber, S. E., *Macromolecules*, **1993**, *26*, 7016-7023.
7. Couvreur, L.; Lefay, C.; Belleney, J.; Charleux, B.; Guerret, O.; Magnet, S., *Macromolecules*, **2003**, *36*, 8260-8267.
8. Lascelles, S. F.; Malet, F.; Mayada, R.; Billingham, N. C.; Armes, S. P., *Macromolecules*, **1999**, *32*, 2462-2472.
9. Soutar, I.; Swanson, L.; Thorpe, G.; Zhu, C., *Macromolecules*, **1996**, *29*, 918-924.
10. Lakowicz, J. R., *Principles of Fluorescence Spectroscopy*, 3rd Edition, **2010,** Springer.
11. Webber, S. E., *Macromolecular Symposia*, **1999**, *143*, 359-370.
12. Semsarilar, M.; Jones, E. R.; Blanazs, A.; Armes, S. P., *Advanced Materials*, **2012**, *24*, 3378–82.
13. Qiu, J.; Charleux, B.; Matyjaszewski, K., *Progress in Polymer Science* **2001**, *26*, 2083-2134.
14. Ladmiral, V.; Semsarilar, M.; Canton, I.; Armes, S. P., *Journal of the American Chemical Society*, **2013**, *135*, 13574-13581.
15. Fielding, L. A.; Derry, M. J.; Ladmiral, V.; Rosselgong, J.; Rodrigues, A. M.; Ratcliffe, L. P. D.; Sugihara, S.; Armes, S. P., *Chemical Science*, **2013**, *4*, 2081-2087.
16. Adams, D. J.; Butler, M. F.; Weaver, A. C., *Langmuir*, **2006**, *22*, 4534-4540.
17. Fernyhough, C.; Ryan, A. J.; Battaglia, G., *Soft Matter*, **2009**, *5*, 1674-1682.
18. Chiao, T.; Thompson, A. R., *Analytical Chemistry*, **1957**, *29*, 1678-1681.

CHAPTER IV

Using Poly(methacrylic acid-co-benzyl methacrylate) Copolymers as Dispersants for Pigments

4.0 Introduction

Polymers are frequently used in industry as dispersants to produce stable dispersions for the use in a range of products including pharmaceuticals, cosmetics and paints.[1] Polymeric dispersants stabilise particles via either electrostatic, steric or electrosteric stabilisation by adsorbing onto the particle surface by physisorption or chemisorption. Stable dispersions can be prepared either by condensation or dispersion. The condensation method relies on the process of nucleation to build up particles, as seen in the formation of polystyrene by aqueous emulsion polymerisation of styrene in the presence of a polymeric stabiliser.[2] The dispersion method, which is the method employed by ink-jet ink manufacturers, involves the mixing of pre-formed pigment particles with an aqueous solution of polymeric stabiliser to give a final dispersion with the desired properties (particle size, viscosity) (see Figure 4.1). To create the stable dispersion and prevent re-aggregation of pigment, the dispersant must be able to firmly attach to the particle surface at a high level of adsorption so that a thick dispersant layer is obtained.[3]

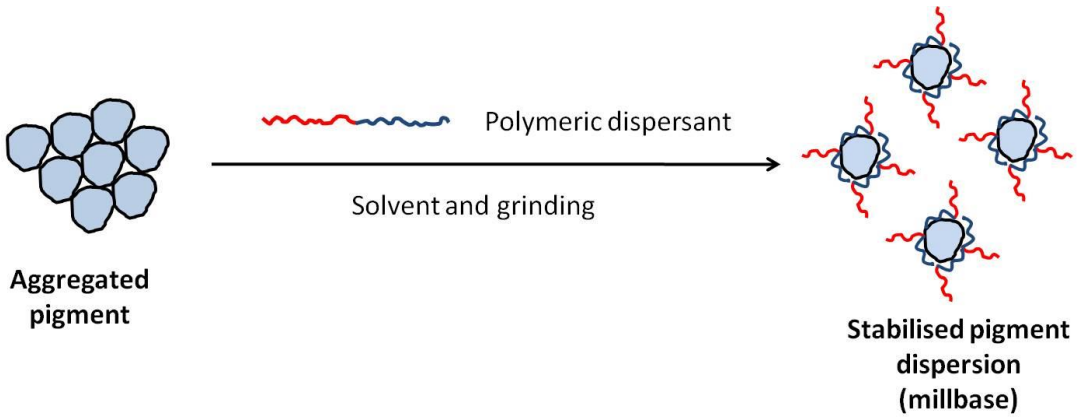

Figure 4.1. *Schematic representation showing the formation of stable pigment dispersions using a polymeric dispersant.*

Random copolymers are commonly used as polymeric dispersants as they can be synthesised with relative ease. Random copolymer dispersants are produced by the free-radical polymerisation of two or more different types of monomer: one monomer with a high affinity for the pigment surface and another that will provide steric, electrostatic or electrosteric stabilisation. Alternatively, diblocks can be used as dispersants but these are more challenging and time-consuming to prepare, requiring synthesis via polymerisation

methods such as anionic or RAFT polymerisation. This is not always viable in a commercial environment and as such diblocks are rarely used as polymeric dispersants in industry.

The work described in Chapter Four focuses on the examination of the properties of pigment dispersions stabilised using p(MAA-co-BzMA) copolymers. Adsorption isotherms for the adsorption of semi-batch-prepared p(MAA_{39}-ran-$BzMA_{61}$) on black, yellow, cyan and magenta pigments in water were constructed using the depletion method. The effect of changing the loading of p(MAA_{39}-ran-$BzMA_{61}$) dispersant on pigment particles was examined by DLS, TGA, rheology and sedimentation experiments. IR spectroscopy was used to analyse any interactions occurring between adsorbed polymer and the surface of pigments. Use of analytical centrifugation allowed for a comparison of adsorption efficiency between p(MAA-b-BzMA) diblocks and the random copolymer p(MAA_{39}-ran-$BzMA_{61}$).

4.1 Experimental

4.1.1 Materials

Carbon black, magenta, cyan and yellow pigments were provided by Fujifilm Imaging colorants. Potassium hydroxide was purchased from Aldrich and used as received. Deionised water was used in all experiments. Two polymeric dispersants have been used in this chapter:

(i) The random copolymer p(MAA_{39}-ran-$BzMA_{61}$) prepared by semi-batch free-radical polymerisation (see section 2.1.2) **M_w= 86200 g mol^{-1}, M_n=47800 g mol^{-1}, PDI=1.8.**

(ii) p(MAA_{143}-b-$BzMA_{300}$) diblock prepared by alcoholic dispersion RAFT polymerisation (see section 3.2.2.3) **M_w=410000 g mol^{-1}, M_n=190000 g mol^{-1}, PDI=2.2.**

4.1.2 Adsorption Isotherm construction

Adsorption isotherms were constructed using the depletion method whereby un-adsorbed polymeric dispersant is separated by centrifuge and quantified to calculate the amount of adsorbed polymeric dispersant on the surface. The polymeric dispersant used was semi-batch-prepared p(MAA_{39}-ran-$BzMA_{61}$) and the surface for adsorption was either black, cyan, magenta or yellow pigment. The following protocol was used to prepare the adsorption isotherm. Neutralised solutions of p(MAA_{39}-ran-$BzMA_{61}$) were made by dissolving precipitated p(MAA_{39}-ran-$BzMA_{61}$) in aqueous KOH with stirring and heating at 80°C so that 100 % of the MAA groups were ionised. These solutions were added to the desired quantity of pigment and mixed using a Soniprep 150 Sanyo sonic probe at 10 µm for 1 h. After sonication, the dispersion was centrifuged at 12,000 rpm for 3 h and the supernatant was separated and analysed by UV spectroscopy to determine the concentration of un-adsorbed dispersant. The adsorbed amount per unit area, Γ (mg m^{-2}), was calculated using equation 4.1, by dividing the difference between the initial concentration of polymeric dispersant (C_i) and the concentration in the supernatant (C_{eq}) by the total surface area of the particles, A. The isotherm was repeated three times to get an average.

$$\Gamma(\text{mg m}^{-2}) = \frac{C_i(\text{mg}) - C_{eq}(\text{mg})}{A\ (\text{m}^2)} \qquad \textbf{Equation 4.1}$$

A UV calibration plot was determined for p(MAA$_{39}$-ran-BzMA$_{61}$) to calculate the concentration of dispersant remaining in the supernatant. A UV calibration curve was obtained by plotting concentration of dispersant versus absorbance at 258 nm due to the aromatic ring on the BzMA residue (Figure 4.2). Figure 4.3 displays the UV calibration curve for semi-batch prepared p(MAA$_{39}$-ran-BzMA$_{61}$).

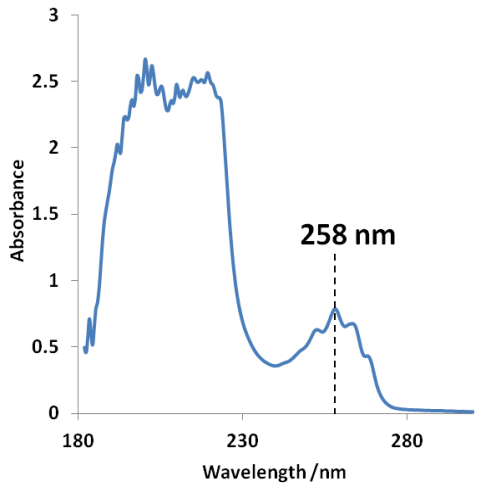

Figure 4.2. *UV absorption curve for 0.1 w/w % p(MAA$_{39}$-ran-BzMA$_{61}$) in water. The absorbance at 258 nm is from the aromatic group of the BzMA repeat units.*

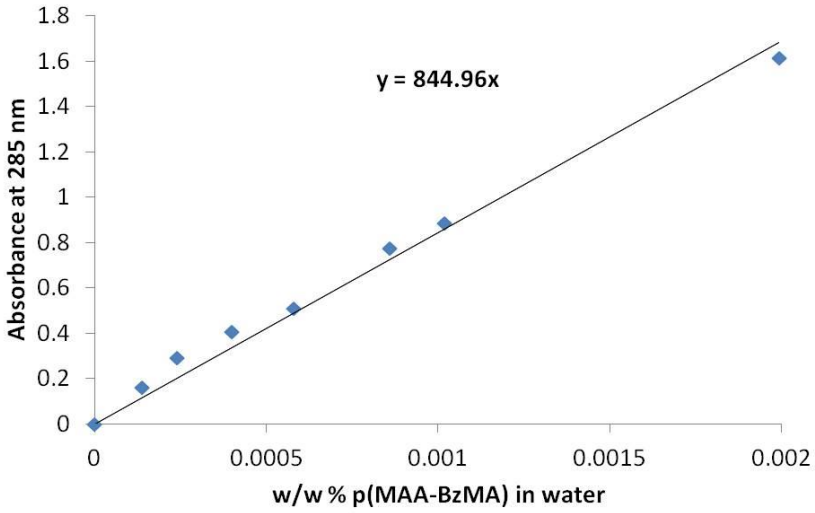

Figure 4.3. *UV calibration curve for varying concentrations of p(MAA$_{39}$-ran-BzMA$_{61}$) in water at 298 K. The absorbance reading was taken at 258 nm.*

4.1.3 Characterisation

4.1.3.1 UV spectroscopy

A Specord S 600 spectrophotometer was used for recording spectra from 150 nm to 400 nm with a slit width of 1 nm. Samples were recorded in sample cells with a path length of 1 cm.

4.1.3.2 Dynamic Light Scattering (DLS)

Intensity-average hydrodynamic diameter measurements of pigment dispersions were carried out using a Malvern Zetasizer NanoZS instrument. Pigment dispersions were diluted with water to obtain carbon black concentrations of ~0.1 w/w % and analysed in disposable curvettes. The results were averaged over three consecutive runs. The deionised water used in each sample was ultra-filtered through a 0.20 µm membrane to remove any dust.

4.1.3.3 Fourier Transform Infrared (FTIR) Spectrosocopy

FTIR spectra were recorded using a Thermo Scientific, Nicolet iS10 instrument equipped with an ATR accessory. Background was run for 64 scans before the sample was run and the sample was run for 64 scans.

4.1.3.4 BET surface area analysis

The specific surface area of the pigment particles was determined using the Brunauer-Emmett-Teller (BET) method.[4] BET measurements were performed on a Quantachrome, NOVA 1000e instrument using nitrogen as an adsorbate. Samples were dried at 100°C under vacuum prior to analysis to remove any moisture that might affect nitrogen adsorption. Samples were run twice and an average value was taken.

4.1.3.5 Thermal Gravimetric Analysis (TGA)

TGA was used to assess the amount of adsorbed polymer on the pigment surface using a

TA TGAQ500 instrument. TGA analysis was performed on centrifuged pigment that had been washed three times with water and dried at room temperature. Pigments were analysed over the temperature range of 100°C to 500°C in N_2 at a heating rate of 10°C min^{-1}.

4.1.3.6 Helium Pycnometer

Density measurements were determined at 20ºC using a Micromeritics AccuPyc 1330 helium pycnometer using either a 0.1 cm^3 or 1 cm^3 sample cell. Measurements were carried out on pigment that had been dried for 24 h in an oven at 100°C to remove any water. Calibration was performed before every measurement.

4.1.3.7 Analytical centrifugation (LUMiSizer®)

Carbon black diameters were determined using a LUMiSizer® analytical photocentrifuge (LUM GmbH, Berlin, Germany) at 25ºC. Measurements were carried out on 5 wt % carbon black dispersions in water prepared at 1-50 wt % loading of p(MAA_{39}-ran-$BzMA_{61}$) on carbon black. The measurements were carried out at a centrifugation rate of 2000 rpm using 2 mm path length polyamide cells. The densities of carbon black and water were taken to be 1.9 g cm^{-3} and 1.0 g cm^{-3}, respectively. The LUMiSizer® is a microprocessor-controlled analytical centrifuge and is particularly convenient for the analysis of p(MAA_{39}-ran-$BzMA_{61}$) stabilized carbon black dispersions because it enables the stability of the dispersion to be assessed. The LUMiSizer® employs STEP™-Technology (Space- and Time-resolved Extinction Profiles) allowing the measurement of the intensity of transmitted light as a function of time and position over the entire sample length simultaneously. The progression of the transmission profiles contains the information on the kinetics of the separation process and therefore allows particle size characterisation.

4.1.3.9 Rheology

Rheology measurements were carried out using the same protocol as described in section 3.2.3.5.

4.2 Results and Discussion

4.2.1 Characterisation of yellow, cyan, magenta and carbon black pigments.

Four pigment types are commonly used to produce the range of colours available in an ink-jet printer; yellow, magenta, cyan and carbon black (see Figure 4.4). The structure of carbon black is not shown in the Figure but is thought to exist as an amorphous quasi-graphitic structure. Each of the four pigments were analysed by elemental analysis to check that the actual composition of the pigments matched the proposed structure. The amount of carbon, hydrogen and nitrogen present in the pigments was determined by elemental analysis. For the yellow, magenta and carbon black pigments any mass not accounted for by CHN analysis was attributed to oxygen. Elemental data for the pigments is presented in Table 4.1.

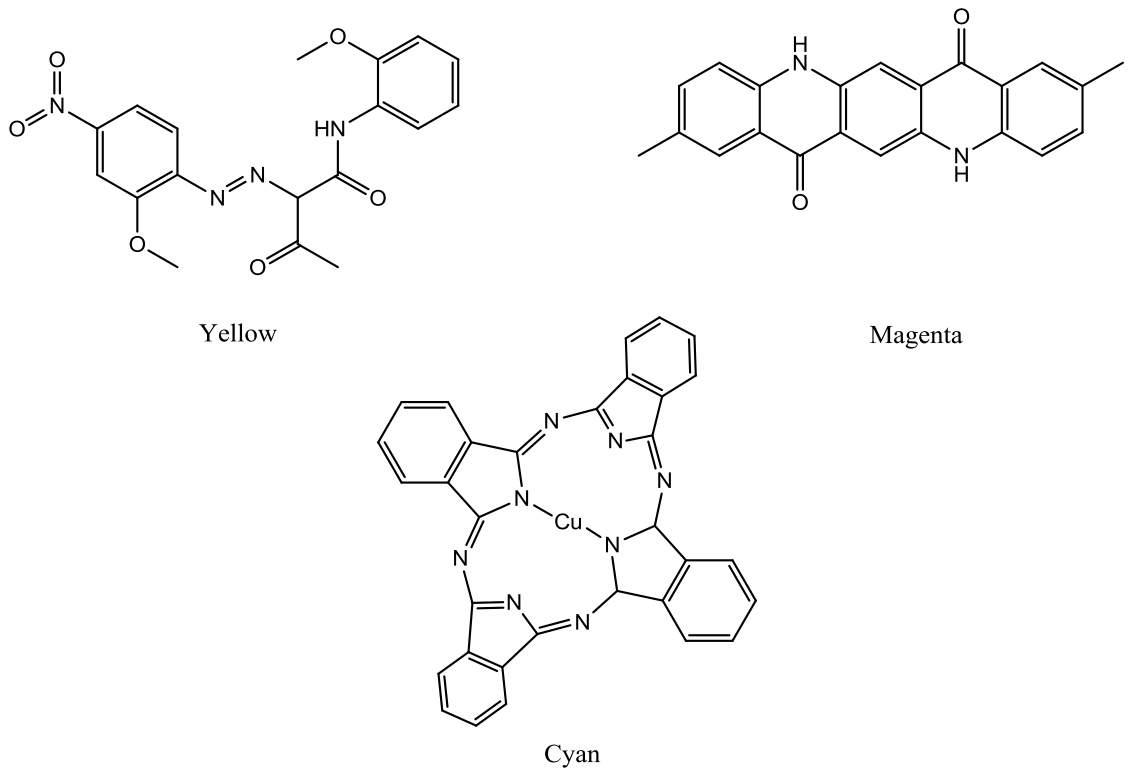

Figure 4.4. *Schematic representation of the structures of cyan, magenta and yellow pigments used in ink-jet printing inks.*

Pigment		Calculated composition from structures given in Figure 4.4 /wt %	Composition given by elemental analysis /wt %
Cyan	C %	66.7	58.9
	H %	2.8	2.1
	N %	19.5	18.6
Yellow	C %	56.0	56.2
	H %	4.7	4.2
	N %	14.3	14.3
Magenta	C %	77.6	70.7
	H %	4.7	4.2
	N %	8.2	7.7
Black	C %	-	93.4
	H %	-	0.4
	N %	-	0

Table 4.1. *C, H and N % elemental analysis of cyan, yellow, magenta and carbon black pigment particles.*

The specific surface area and density of the pigment particles was obtained using BET surface analysis and helium pycnometry, respectively (see Table 4.2). Using these measured specific surface area and density values, an average particle radius was calculated for each pigment using equation 4.1, where ρ is the particle density and A_s is the specific surface area. This radius is only an average value because equation 4.1 assumes the particles to be spherical and non-porous, which is not the case for the four pigments.

$$A_s = \frac{3}{\rho . R} \qquad \textbf{Equation 4.1}$$

Pigment particle	Specific Surface Area /m^2 g^{-1}	Density /g cm^{-3}	Calculated radius /nm
Black	240	1.9	7
Magenta	71	1.4	29
Cyan	88	1.6	21
Yellow	19	1.4	116

Table 4.2. *Specific surface area, density and average radius (calculated using equation 4.1) for black, magenta, cyan and yellow pigment particles.*

4.2.2. Adsorption of semi-batch-prepared p(MAA_{39}-ran-$BzMA_{61}$) on yellow, cyan, magenta and carbon black pigments in water.

To create stable aqueous pigment dispersions, the semi-batch-prepared random copolymer p(MAA_{39}-ran-$BzMA_{61}$) was used as a polymeric dispersant. This copolymer is a successful dispersant for pigments because the BzMA residues adsorb onto the pigment particles via hydrophobic interactions and the MAA groups provide electrosteric stabilisation, preventing re-aggregation of the pigment particles.

Adsorption isotherms were plotted for the adsorption of p(MAA_{39}-ran-$BzMA_{61}$) on carbon black, yellow, cyan and magenta pigment using the depletion method described in section 4.1.2. Prior to constructing the adsorption isotherms, it was speculated that, because the copolymer consisted of 61 mol % of hydrophobic BzMA, the copolymer would have low solubility in water leading to any un-adsorbed polymer being sedimented to the bottom of the centrifuge tube along with pigment resulting in inaccurate data. To test the theory that un-adsorbed polymer would be sedimented during centrifugation, a 1 w/w % neutralised solution of p(MAA_{39}-ran-$BzMA_{61}$) was centrifuged at 12000 rpm for 3 h and the top and bottom of the solution was analysed by UV spectroscopy to examine whether any of the copolymer had become sedimented. Figure 4.5 shows that this was not the case, with the top and bottom of the solution having an almost identical UV spectrum, confirming that copolymer is not sedimented during centrifugation.

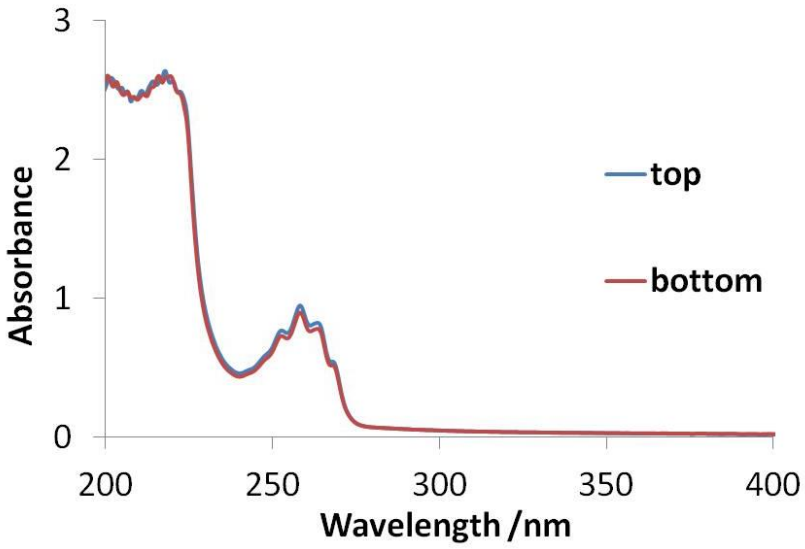

Figure 4.5. *UV spectra of the bottom 1 cm^3 and top 1 cm^3 of a 1 w/w % neutralised solution of p(MAA$_{39}$-ran-BzMA$_{61}$) centrifuged for 3 h at 12000 rpm.*

The adsorption isotherm for the adsorption of p(MAA$_{39}$-ran-BzMA$_{61}$) on carbon black in water is shown in Figure 4.6. Monolayer coverage of p(MAA$_{39}$-ran-BzMA$_{61}$) on carbon black was achieved at 13 wt % loading on carbon black. After monolayer coverage was achieved, a plateau is formed as a result of the carbon black surface becoming saturated. This adsorption isotherm follows the same shape as a Langmuir isotherm indicating that, as more surface sites are reached, it becomes more difficult for p(MAA$_{39}$-ran-BzMA$_{61}$) to adsorb onto carbon black.[5] Figure 4.6 shows the change in hydrodynamic diameter of the corresponding dispersions with different wt% loadings of p(MAA$_{39}$-ran-BzMA$_{61}$) on carbon black, as determined by DLS. The point at which monolayer coverage is achieved, 13 wt % loading of p(MAA$_{39}$-ran-BzMA$_{61}$) on pigment, coincides with a reduction in diameter from 1400 nm to around 220 nm. This indicates that, to create a stable carbon black dispersion that will not re-aggregate, monolayer coverage of p(MAA$_{39}$-ran-BzMA$_{61}$) on the surface is required at a minimum.

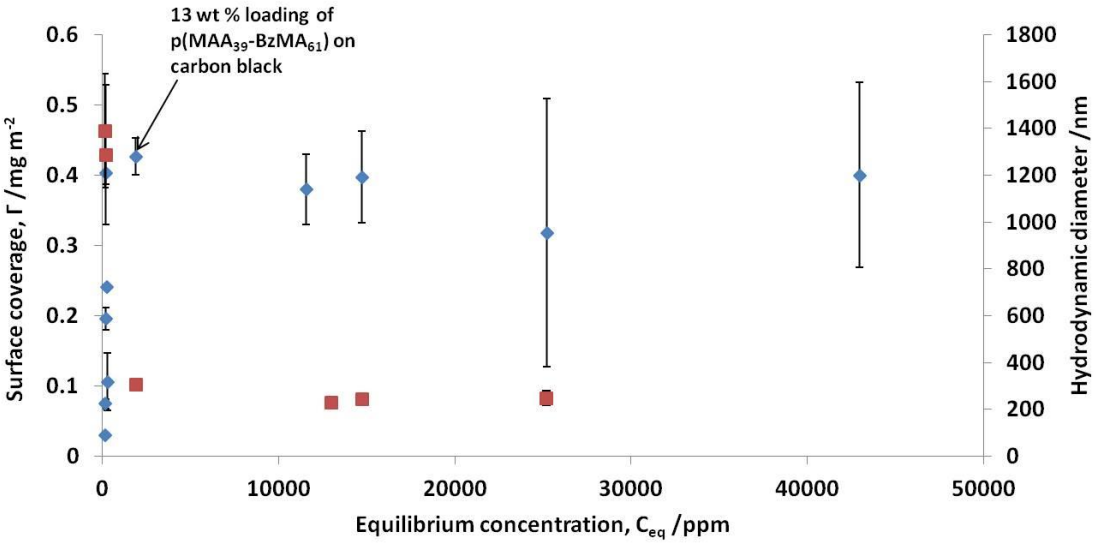

Figure 4.6. *Adsorption isotherm of p(MAA$_{39}$-ran-BzMA$_{61}$) on carbon black pigment in water (◊) and the hydrodynamic diameter of the dispersions determined by DLS (□).*

In addition to the depletion method, thermogravimetric analysis (TGA) was used to directly analyse the amount of adsorbed p(MAA$_{39}$-ran-BzMA$_{61}$) on carbon black (see Figure 4.7). A plot of the TGA data followed a similar shape to the isotherm determined by the depletion method, although the TGA measurements did not reach a plateau, indicating that the adsorbed amount continued to increase with increasing loading of p(MAA$_{39}$-ran-BzMA$_{61}$). TGA was found to be an effective means of constructing an adsorption isotherm, allowing the point of monolayer coverage to be determined.

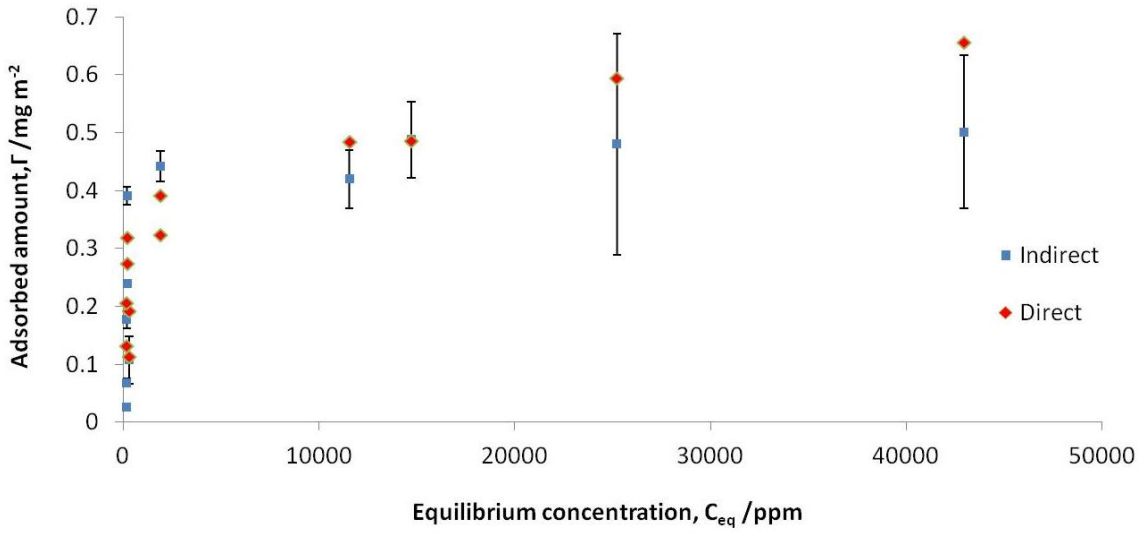

Figure 4.7. *Adsorption isotherms constructed using direct (TGA) and indirect (centrifugation) analysis for the adsorption of p(MAA$_{39}$-ran-BzMA$_{61}$) on carbon black in water.*

Infra-red (IR) spectroscopy was used to determine how p(MAA$_{39}$-ran-BzMA$_{61}$) interacted with the carbon black surface during adsorption (see Figure 4.8). The IR spectra show that adsorption of p(MAA$_{39}$-ran-BzMA$_{61}$) onto carbon black led to a 13 cm^{-1} decrease in shift of the carbonyl bond present on the surface of carbon black. This decrease is indicative of hydrogen bonding between the C=O groups on the black pigment and COOH groups present in p(MAA$_{39}$-ran-BzMA$_{61}$). Chevalier et al.[6] made a similar observation and reported that the C=O bond was displaced from 1734 cm^{-1} to 1701 cm^{-1} when the alkyl ester of polycaprolactone was adsorbed onto carbon black. It has been shown that all carbon black pigments have oxygen species chemisorbed to their surface.[7]

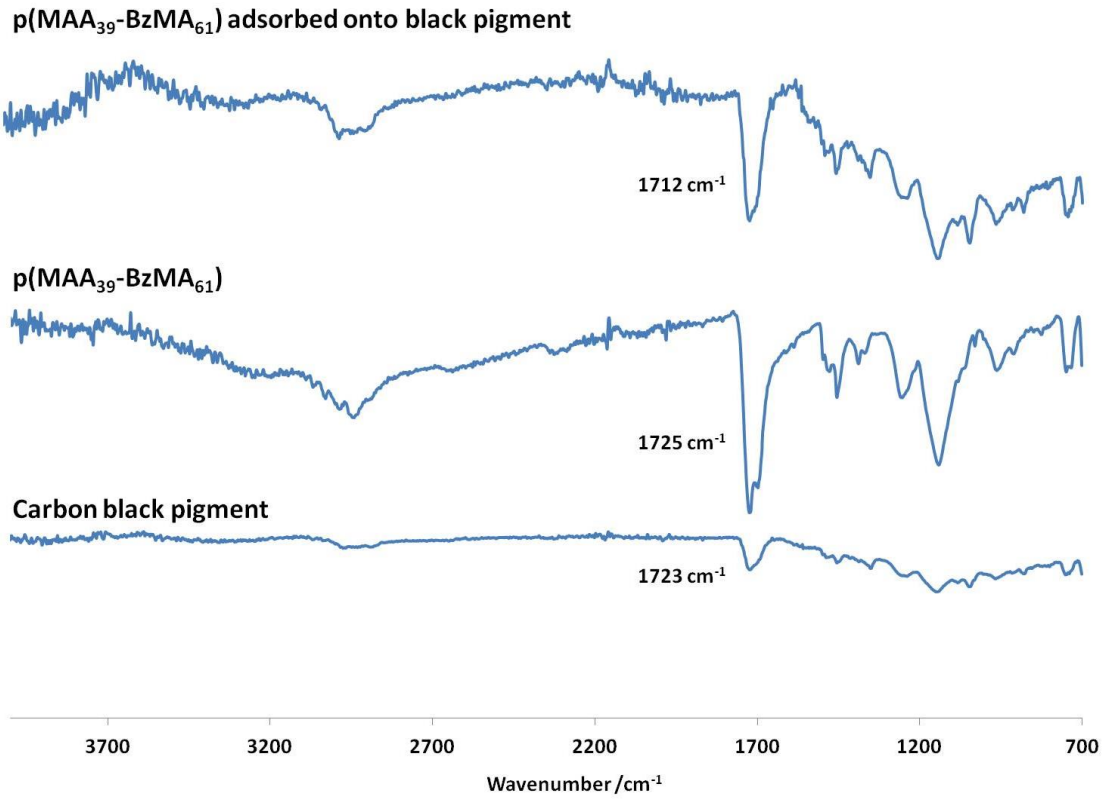

Figure 4.8. *IR spectra for carbon black, p(MAA$_{39}$-ran-BzMA$_{61}$) and p(MAA$_{39}$-ran-BzMA$_{61}$) adsorbed onto carbon black.*

In order to understand the effect that adsorbed p(MAA$_{39}$-ran-BzMA$_{61}$) has on the stability of carbon black, steady-state shear viscosity measurements were performed. Measurements were conducted on carbon black dispersions at a fixed pigment concentration of 5 wt % and a p(MAA$_{39}$-ran-BzMA$_{61}$) loading varying from 6 to 50 wt % (see Figure 4.9).

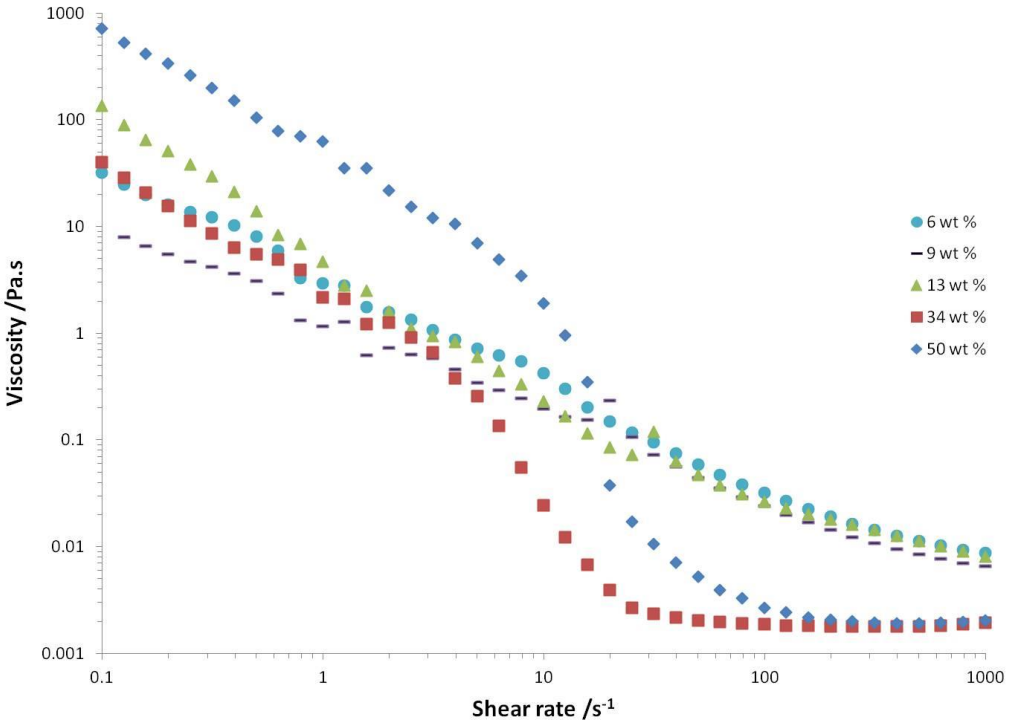

Figure 4.9. *Viscosity versus shear rate for carbon black dispersions stabilised with either 6, 9, 13, 34 and 50 wt % p(MAA$_{39}$-ran-BzMA$_{61}$) loading on carbon black in water.*

At p(MAA$_{39}$-ran-BzMA$_{61}$) loadings of 13 wt % and below, the dispersions displayed shear-thinning behaviour. Above 13 wt % loading, where non-adsorbed p(MAA$_{39}$-ran-BzMA$_{61}$) is present in the dispersion, shear-thinning is observed but it is accompanied by a sudden drop in viscosity at approximately 10 s^{-1}. After this drop in viscosity, Newtonian behaviour is observed between a shear rate of 100 to 1000 s^{-1}. The difference in behaviour of the dispersions which contain non-adsorbed p(MAA$_{39}$-ran-BzMA$_{61}$) could be attributed to the non-adsorbed copolymer forming a network with the adsorbed polymer which is broken down by shear forces created by the rheometer. The breakdown of the network manifests itself as a sudden reduction in viscosity. The hypothesis that a polymer network is occurring is supported by Figure 4.10, which shows the shear rate dependence on viscosity for varying concentrations of p(MAA$_{39}$-ran-BzMA$_{61}$) in water. All the copolymer solutions show Newtonian behaviour across the range of shear rates and they display an increase in viscosity with increasing concentration. Above 25 wt % copolymer the viscosity increases drastically, indicating that the copolymer chains interact and form a weak polymer network or form aggregates. It is speculated that the interactions are a result of the hydrophobic benzyl groups on the polymer associating together to minimise their interactions with water molecules. The rheological behaviour observed here is

similar to the observations made by Barrie and co-workers who studied aqueous carbon black dispersions stabilised by a low molecular weight (Mw~8500 g mol^{-1}) poly(acrylate).[8] Barrie and co-workers found that carbon black dispersions in the presence of non-adsorbed polymer displayed similar viscosity versus shear rate curves to the 34 and 50 wt % loading dispersions investigated in this research; these results are shown in Figure 4.9. Barrie and co-workers attributed this behaviour to the non-adsorbed polymer forming a weak network with adsorbed polymer.

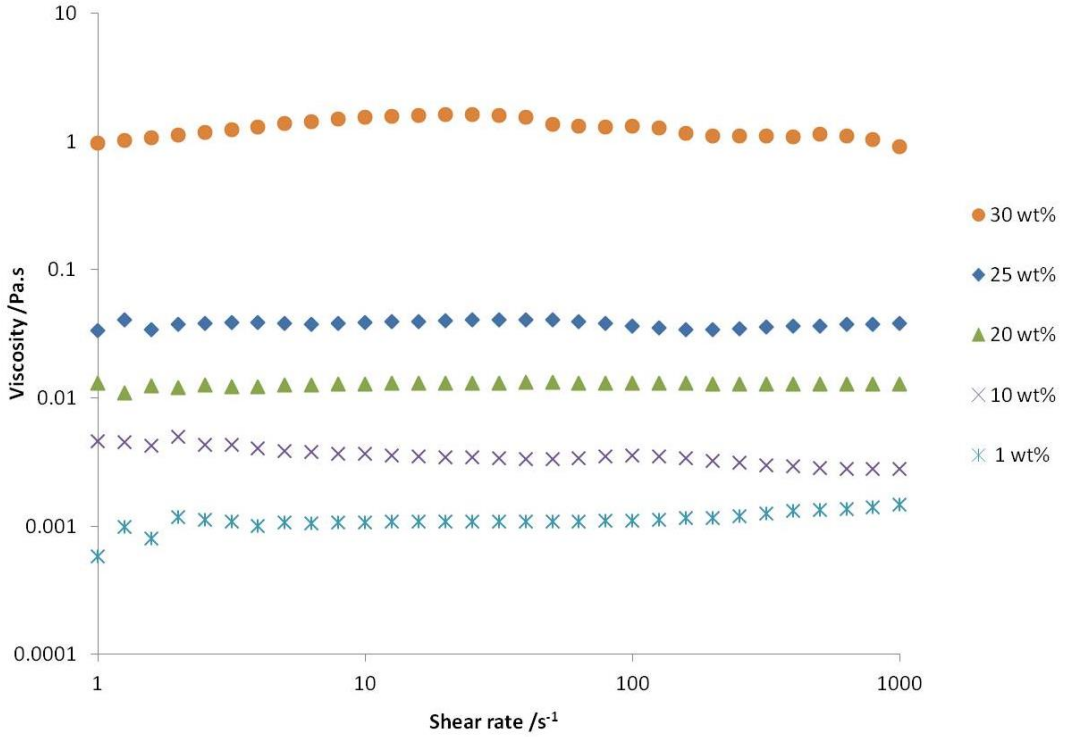

Figure 4.10. *Viscosity versus shear rate for varying wt % of p(MAA_{39}-ran-$BzMA_{61}$) in water.*

It can be seen from Figure 4.9 that, once monolayer coverage of carbon black has been achieved, the viscosity of the dispersions between 100-1000 s^{-1} drops to ~2.0 mPa.s. This drop in viscosity is attributed to the formation of a stable carbon dispersion whereby any large aggregates have been broken down. A reduction in viscosity, appearing at the start of the plateau of the adsorption isotherm, was also observed by Zaman et al.[9] who studied the viscosity of kaolin particles dispersed in water by Na-poly(acrylic acid). Occasionally, after monolayer coverage is achieved, the viscosity begins to increase with increasing concentration of non-adsorbed polymer.9 It is clear from looking at Figure 4.9 that this was not occurring in the systems under scrutiny, with the same viscosity being obtained for the dispersions prepared at 34 and 50 wt % loading of p(MAA_{39}-ran-$BzMA_{61}$).

Analytical centrifugation was conducted on the carbon black dispersions to study the effect of different loadings of p(MAA_{39}-ran-$BzMA_{61}$) on the stability of the dispersions (see Figure 4.11). This was achieved by centrifuging the dispersions at 2000 rpm and measuring the intensity of transmitted light through the cell as a function of time and position over the entire sample length simultaneously. In Figure 4.11 the position in mm is the distance along the sample tube where 109 mm corresponds to the filling height of the dispersion in the sample cell and 130 mm corresponds to the bottom of the sample cell. The transmission represents the particle concentration in the cell, a low transmission indicates a high particle concentration and a high transmission indicates a low particle concentration. By monitoring the progression of the transmission profiles, information on the rate of sedimentation and therefore particle size can be obtained. The earliest recorded data is shown in red and the most recent data is shown in green.

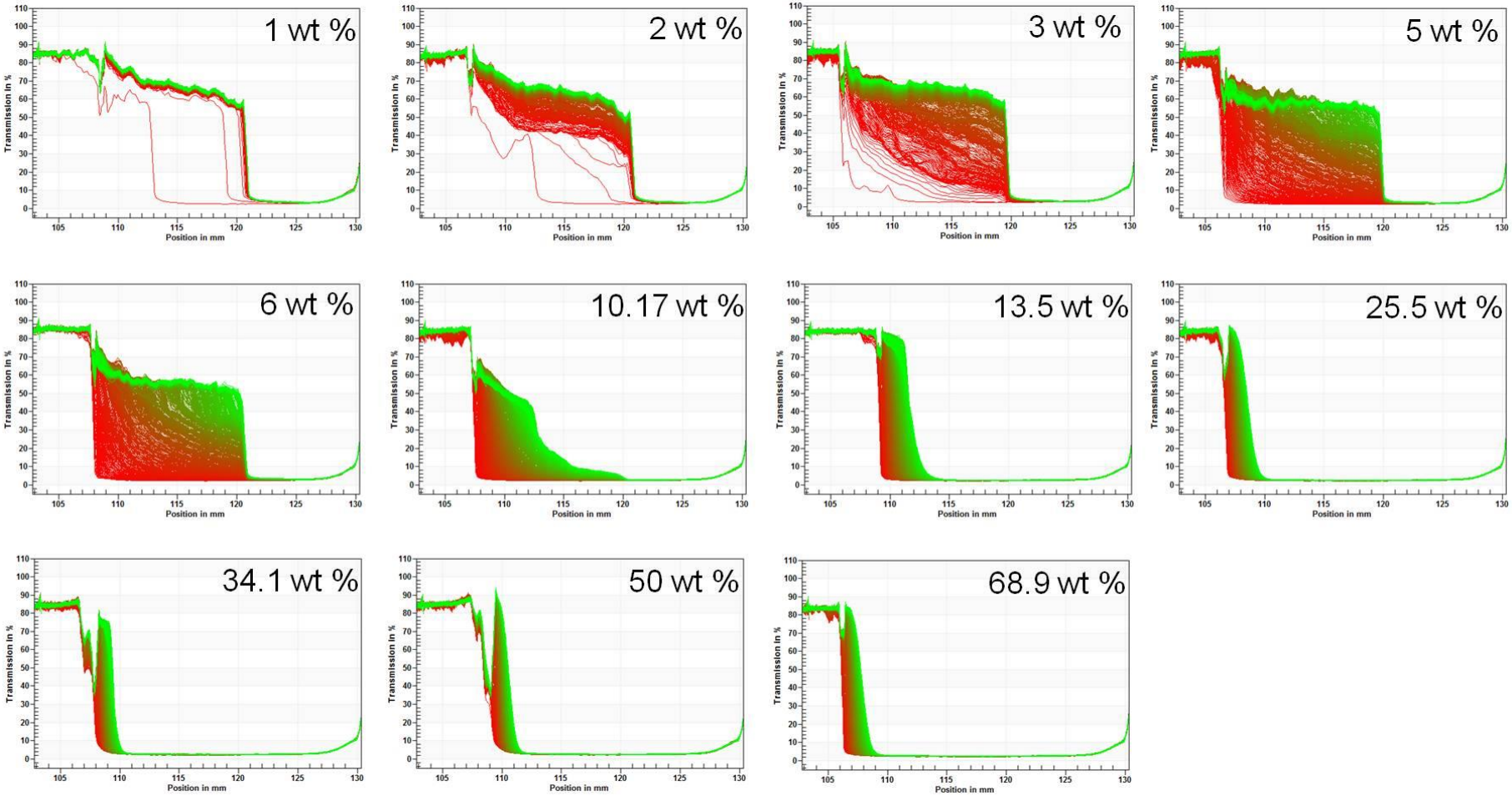

Figure 4.11. *LUMisizer transmission plots depicting how far the carbon black dispersion sediments down the sample tube in mm when centrifuged at 2000 rpm. The wt % in the top right-hand corner is the wt % loading of p(MAA$_{39}$-ran-BzMA$_{61}$) on carbon black. The mean diameter for the dispersions extracted from the above plots is shown in Table 4.3. Green plots represent the most recent transmission data whilst red represents the earliest recorded transmission plot.*

It can be seen from Figure 4.11 that for 1 wt % loading of p(MAA_{39}-ran-$BzMA_{61}$) the carbon black particles are centrifuged immediately to the bottom of the sample cell. This is shown by the high transmission between 109 – 121 mm which indicates the solution is clear and the time sequence indicates this happened relatively quickly. The low value of transmission observed above 121 mm is due to the carbon black being centrifuged to the bottom of the tube. The quick sedimentation of the carbon black at 1 wt % loading is due to the carbon black particles being present as large agglomerates and is indicative of an unstable dispersion. It can be seen from the transmission plots that, at p(MAA_{39}-ran-$BzMA_{61}$) loadings of 13 wt % and above, the transmission is almost 0 % above 114 mm, showing the carbon black remains dispersed during the centrifugation process, indicating that the dispersion is stable. From the transmission plots, the mean diameter of the dispersions was extracted and the results summarised in Table 4.3. Once monolayer coverage had been achieved at 13 wt % loading of p(MAA_{39}-ran-$BzMA_{61}$), the average diameter of the stabilised carbon black particles was approximately 200 nm. Further addition of p(MAA_{39}-ran-$BzMA_{61}$) had little effect on the particle diameter and colloidal stability of the dispersions.

Wt % loading of p(MAA_{39}-ran-$BzMA_{61}$) on carbon black	**Median /nm**	**Mean /nm**
1.0	9280	8612 ± 1468
2.0	8995	6702 ± 2179
3.0	7157	4069 ± 2813
5.0	902	829 ± 979
6.0	642	628 ± 381
10.2	384	368 ± 79
13.5	223	222 ± 31
25.5	199	196 ± 35
34.1	182	182 ± 33
50.0	173	176 ± 23
68.9	196	198 ± 50

Table 4.3. *Mean and median diameters extracted using analytical centrifugation of carbon black dispersions where the wt % loading of p(MAA_{39}-$BzMA_{61}$) has been varied from 1 to 69 wt %.*

It was not possible to obtain adsorption isotherms for yellow, cyan and magenta pigments using the indirect or direct method. The relatively low densities of these three pigments made it impossible to induce sedimentation through centrifugation and as such it would not be possible to accurately analyse the concentration of un-adsorbed copolymer left in the supernatant. TGA could not be used to analyse the amount of adsorbed copolymer as yellow, cyan and magenta pigments are pyrolysed at the same temperature as the p(MAA_{39}-ran-$BzMA_{61}$) dispersant. As discussed earlier, once monolayer coverage has been achieved any aggregates present break down, resulting in a decrease in particle diameter. If time had permitted, analytical centrifugation and DLS would have been used to reveal the point of monolayer coverage.

4.2.3 Adsorption of ACE-labelled p(MAA_{143}-b-$BzMA_{300}$) diblock on carbon black in water.

The capability of p(MAA-b-BzMA) diblock copolymer to act as a polymeric dispersant for carbon black was explored. The diblock used was ACE-labelled p(MAA_{143}-b-$BzMA_{300}$), which was synthesised by reversible addition-fragmentation chain transfer (RAFT) polymerisation (see section 3.2.2.3). As p(MAA_{143}-b-$BzMA_{300}$) exists as micelles, an adsorption isotherm for the adsorption of the diblock onto carbon black could not be generated via the depletion method because centrifugation would cause the copolymer micelles to sediment with the carbon black particles. As an alternative to centrifugation, analytical centrifugation was employed to examine the dispersion stability when using a diblock as a polymeric dispersant. The dispersions were prepared by mixing 5 wt % carbon black in water and varying the loading of diblock from 1.1 to 27 wt %. Images of the prepared dispersions are shown in Figure 4.12. At diblock loadings of 5.6 wt % and less the carbon black particles immediately sedimented and at 11 wt % loading and above of diblock the carbon black appeared to stay fully dispersed. Analytical centrifugation was performed on the dispersions prepared at 11, 16 and 27 wt % loading of diblock using a centrifugation rate of 3000 rpm (see Figure 4.13 and Table 4.4).

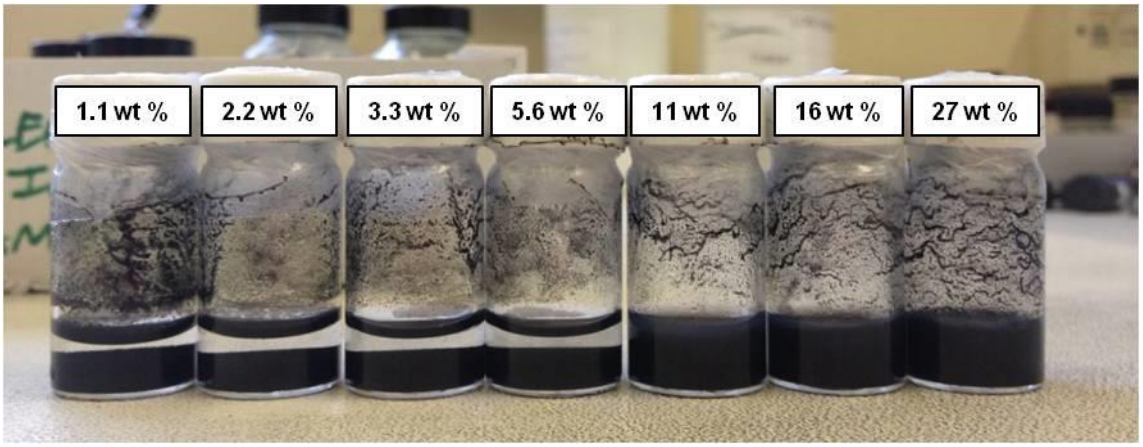

Figure 4.12. *Photograph of carbon black dispersions prepared with 1.1 to 27 wt % loading of p(MAA$_{143}$-b-BzMA$_{300}$) diblock in water. The wt % of carbon black was kept constant at 5 wt % for all dispersions. Dispersions containing 1.1, 2.2, 3.3 and 5.6 wt % loading of p(MAA$_{143}$-b-BzMA$_{300}$) immediately sedimented upon standing at 20ºC.*

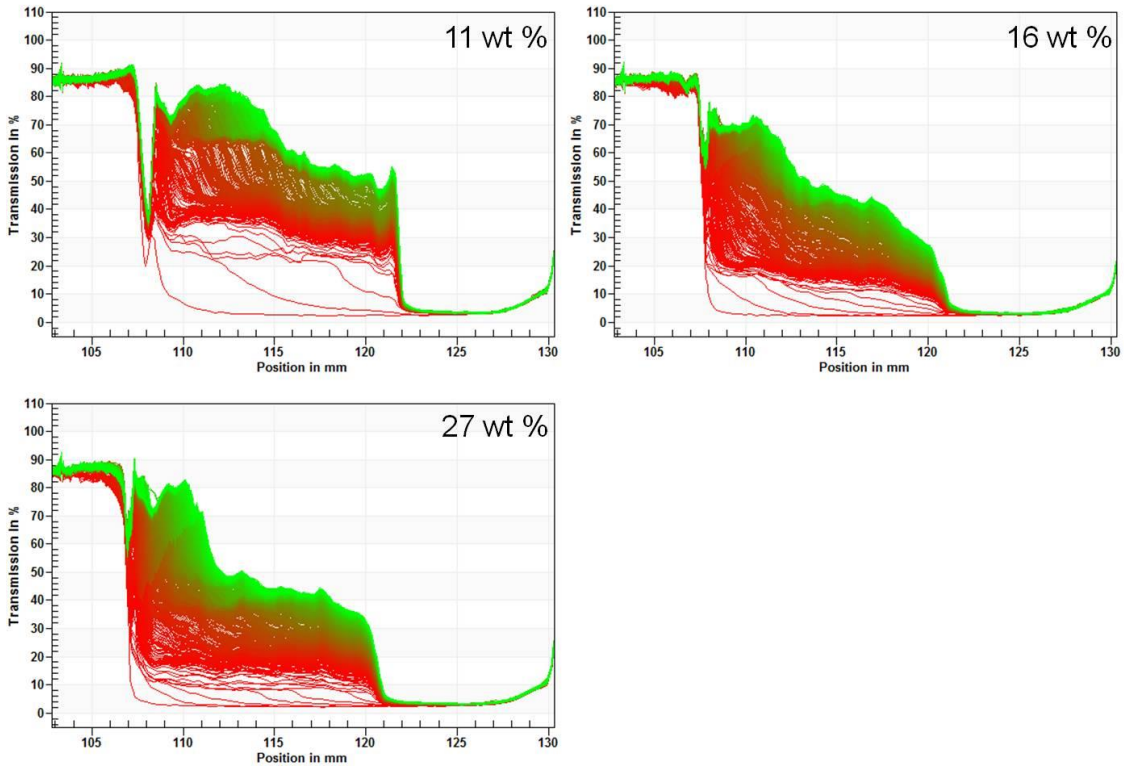

Figure 4.13. *LUMisizer transmission plots depicting how far the carbon black dispersion moved down the sample tube in mm when being centrifuged at 3000 rpm for 45 minutes at 25ºC. The wt % in the top right hand corner is the wt % loading of p(MAA$_{143}$-b-BzMA$_{300}$) on carbon black. The mean diameter for the dispersions extracted from the above plots is shown in Table 4.4.*

Wt % loading of p(MAA_{143}-b-$BzMA_{300}$) on carbon black	Median /nm	Mean /nm	SD /nm
11	1184	325	584
16	954	386	419
27	960	363	391

Table 4.4. *Mean and median diameter of carbon black dispersions when the loading of the diblock p(MAA_{143}-b-$BzMA_{300}$) is 11, 16 and 27 wt %.*

It can be seen from Figure 4.13 and Table 4.4 that p(MAA_{143}-b-$BzMA_{300}$) adsorbs onto the carbon black surface, creating a stable carbon black dispersion; as indicated by the reduced mean diameter and the dispersion not fully sedimenting during centrifugation. However, the diblock is not as effective as the random copolymer dispersant p(MAA_{39}-ran-$BzMA_{61}$). It can be seen from the transmission plots (see Figure 4.11) that the stable dispersions do not sediment at all. It is speculated that the diblock is not as effective as the analogous random copolymer dispersant due to the diblock copolymers existing as micelles. The p(MAA_{143}-b-$BzMA_{300}$) diblock may adsorb onto carbon black either (i) as unimers or (ii) as micelles (see Figure 4.14). The adsorption of unimers is feasible as micelles can be viewed as 'reservoirs' of unimers with an equilibrium existing between micelles and unimers. In the presence of pigment, unimers can adsorb onto the pigment surface via the pBzMA block and the pMAA block can provide an electrostatic barrier towards flocculation. This shifts the equilibrium to unimers hence reducing the number of micelles, but copolymer will still be present as micelles. The other potential route for adsorption is via the micelle rearranging to expose the pBzMA core for adsorption onto the carbon black surface. The adsorption of the diblock onto carbon black could be examined using SANS, TEM and DLS.

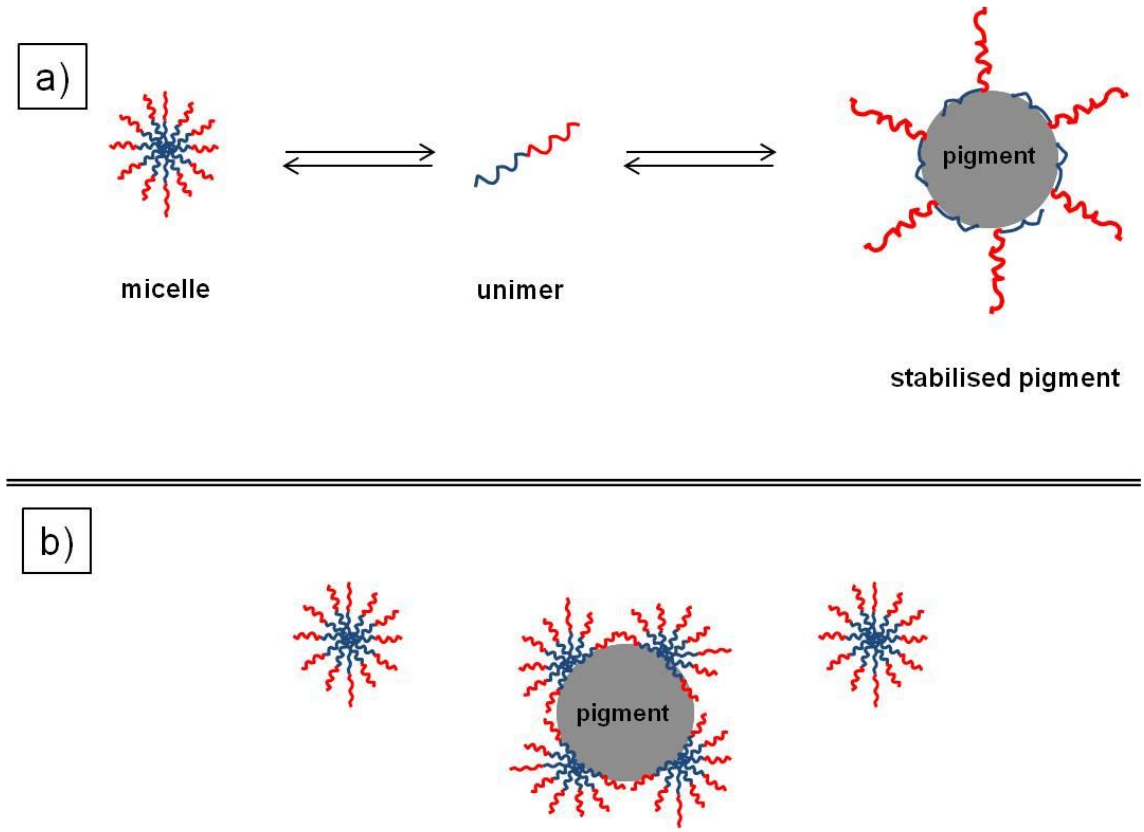

Figure 4.14. *Schematic representation of the two possible ways in which the diblock p(MAA_{143}-b-$BzMA_{300}$) could be adsorbing onto carbon black. a) unimers adsorb onto the pigment surface or b) micelles adsorb onto the pigment surface.*

4.2.4 Summary

Isotherms for the adsorption of p(MAA_{39}-ran-$BzMA_{61}$) on carbon black were obtained using UV spectroscopy and TGA. It was determined that monolayer coverage was achieved at 13 wt % loading of copolymer. DLS measurements on the same dispersions revealed a reduction in mean diameter of the dispersion from 1400 to 220 nm, indicating the formation of a stable dispersion that would not re-aggregate. It can be seen from steady-state viscosity measurements that dispersions containing non-adsorbed p(MAA_{39}-ran-$BzMA_{61}$) display a sharp reduction in viscosity when a shear rate of approximately 10 s^{-1} was applied. This decrease in viscosity was attributed to networks between the non-adsorbed and adsorbed copolymer breaking down under a certain applied force. IR spectroscopy was used to confirm the presence of p(MAA_{39}-ran-$BzMA_{61}$) on carbon black. A shift in the carbon black carbonyl bond of 13 cm^{-1} was attributed to carbonyl bonds on carbon black forming hydrogen bonds with the COOH groups present along the p(MAA_{39}-ran-$BzMA_{61}$) backbone.

Analytical centrifugation was used to compare the performance of the p(MAA_{143}-b-$BzMA_{300}$) diblock to act as a polymeric dispersant for carbon black in water with that of p(MAA_{39}-ran-$BzMA_{61}$)**.** The diblock was found to adsorb and aid the dispersion of carbon black in water but was not as effective as using p(MAA_{39}-ran-$BzMA_{61}$) as a dispersant. It has been hypothesised that the p(MAA_{143}-b-$BzMA_{300}$) diblock was adsorbing onto carbon black either as unimers or micelles. DLS and TEM are two analytical techniques which could be used to determine the precise mode of adsorption.

4.4 References

1. Urban, D.; Takamura, K., *Polymer Dispersions and Their Industrial Applications*, Wiley: Weinheim, 2002.
2. Walsh, A.; Thompson, K. L.; Armes, S. P.; York, D. W., *Langmuir*, **2010**, *26*, 18039-18048.
3. Vincent, B.; Whittington, S. G., *Surface and Colloid Science*, Plenum Press, New York, 1982, Vol 12.
4. Brandauers, S.; Emmett, P. H.; Teller, E., *Journal of the American Chemical Society*, **1938**, *60*, 309-319.
5. Farrokhpay, S., *Advances in Colloid and Interface Science*, **2009,** *151*, 24-32.
6. Nsib, F.; Ayed, N.; Chevalier, Y., *Progress in Organic Coatings*, **2006**, *55*, 303-310.
7. Boehm, H. P., *Carbon*, **2002**, *40*, 145-149.
8. Barrie, C. L.; Griffiths, P. C.; Abbott, R. J.; Grillo, I.; Kudryashov, E.; Smyth, C., *Journal of Colloid and Interface Science*, **2004**, *272*, 210-217.
9. Zaman, A. A.; Tsuchiya, R.; Moudgil, B. M., *Journal of Colloid and Interface Science*, **2002**, *256*, 73-78.

CHAPTER V

Small-Angle X-ray Scattering (SAXS) and Small-Angle Neutron Scattering (SANS) of Carbon Black Dispersions

5.0 Introduction

Carbon black is a fine powder of elemental carbon formed from the vapour phase pyrolysis of hydrocarbons.[1] Its main commercial use is as reinforcing filler and colourant in rubber components such as car tyres.[2] However, its high optical density makes it perfect as a tint for inks and paints.[3] The economic importance of carbon black has led to numerous studies being carried out to characterise its morphology and improve its performance.[4,5,6] However, the structure of carbon black is difficult to determine and is thought to be intermediate between the ordered structure of graphite and a completely amorphous material.[7] Commonly, its structure is described on three levels: primary particles, aggregates and agglomerates (see Figure 5.1). The primary particles (10-100 nm) fuse together during pyrolysis to form aggregates (50-500 nm) which cluster together to form agglomerates (> 5 μm).[8] The agglomerates are a complex statistically determined structure and are often described by a fractal dimension, D. The concept of fractal dimensions was developed by Mandelbrot to describe structures that are self-similar over different length scales.[9] If particles cluster together through random motion, the process is called diffusion-limited cluster aggregation[10] (DLCA) and results in a D value of approximately 1.7-1.8.[11] This value indicates an open, low density structure and is common for the aggregation of colloids such as carbon black.

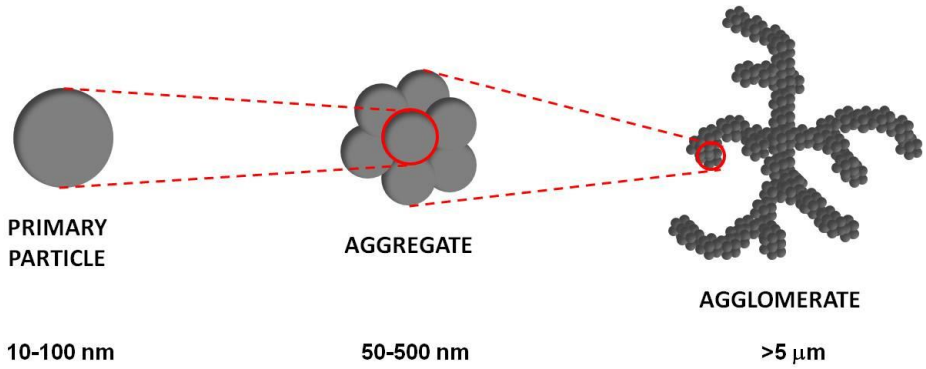

Figure 5.1. *Schematic demonstrating the hierarchy of structures of carbon black from primary particle to agglomerate.*

The two main techniques used to probe the properties of carbon black are electron microscopy[12,13] and small-angle scattering.[14,15] Small-angle scattering is useful for analysing the structure of carbon black as this probes several length scales, covering both aggregates and the primary particles. Small-angle X-ray scattering (SAXS) has been used to investigate the morphology of carbon black as powders and within composites.[6,14]

The use of carbon black in the paint and ink industry requires the presence of a dispersant at the carbon black/liquid interface to produce a fine homogeneous dispersion.[3] The interaction and conformation of the dispersant is important in ensuring the production of a stable dispersion which is not susceptible to destabilisation during storage. A vast array of dispersants have successfully been used to stabilise carbon black including: diblocks,[15,16] homopolymers,[17] and surfactants.[18,19] The structure of adsorbed polymers at the solid-liquid can be investigated using small-angle neutron scattering (SANS). Alexandridis et al. have used SANS to study the adsorption of PEO-PPO-PEO triblocks[16] and graft copolymers[8] on carbon black.

The results detailed in Chapter IV indicate that stable aqueous carbon black dispersions can be obtained by adsorbing the random copolymer p(MAA_{39}-ran-$BzMA_{61}$) at the pigment/liquid interface, which then provides electrosteric stabilisation. The results presented in this Chapter relate to the characterisation of aqueous carbon black dispersions using small-angle neutron scattering (SANS) and small-angle X-ray scattering (SAXS). Initially, SANS was used to calculate the radius of gyration (R_g) of p(MAA_{39}-ran-$BzMA_{61}$) in D_2O and the effect of changing the mol % of MAA in these copolymers on R_g was studied. The consequence of changing the p(MAA_{39}-ran-$BzMA_{61}$) concentration in the preparation of aqueous carbon black dispersions was investigated by examining either contrast-matched carbon black or contrast-matched p(MAA_{39}-ran-$BzMA_{61}$) dispersions using SANS. SAXS was used in conjunction with SANS to probe the carbon black dispersions at a higher q range. The effect of temperature and different milling techniques on the preparation of carbon black dispersions was investigated using SANS.

5.1 Experimental

5.1.1 Materials

Sodium deuteroxide (NaOD) (30 wt % in D_2O) and D_2O were purchased from Aldrich and used as received. Deuterated DMSO ($(CD_3)_2SO$) was purchased from Fisher and used as received. Deionised water was used in all experiments. Carbon black was supplied by FujiFilm Imaging Colorants.

5.1.2 Synthesis of p(MAA-BzMA) random copolymers with MAA content varying from 39 to 79 mol %.

p(MAA-BzMA) copolymers with MAA varying from 39-79 mol % MAA were synthesised by batch free-radical polymerisation in DPG at 70°C. A detailed description of this synthesis is given in section 2.1.2.1 in Chapter II.

5.1.3 Preparation of carbon black dispersions stabilised by p(MAA_{39}-$BzMA_{61}$) at the University of Sheffield.

All carbon black dispersions mentioned in this Chapter were stabilised with semi-batch prepared p(MAA_{39}-ran-$BzMA_{61}$), [M_n=47800 g mol^{-1}, M_w=86200 g mol^{-1} and M_w/M_n=1.8]. Dispersions were prepared by first making up 5.0 g solutions of p(MAA_{39}-ran-$BzMA_{61}$) by adding dry p(MAA_{39}-ran-$BzMA_{61}$) into D_2O and NaOD followed by heating at 80°C until a homogeneous solution was obtained. NaOD was added in amounts so that 100 % of the acid groups on MAA were neutralised. The concentration of p(MAA_{39}-ran-$BzMA_{61}$) varied depending on the final target wt % p(MAA_{39}-ran-$BzMA_{61}$) relative to carbon black. The solution of neutralised p(MAA_{39}-ran-$BzMA_{61}$) was added to pre-weighed carbon black so that the overall wt % of carbon black in the sample was 5 wt %. This was shaken by hand in a vial for 30 seconds and then mixed further by a sonic probe for 1 h using a Sanyo Soniprep 150 at 10 μm amplitude. Samples were sonicated in an ice bath to minimise heating. THF GPC analysis was carried out on p(MAA_{39}-$BzMA_{61}$) before and after sonication to assess whether the copolymer was degraded during sonication. Table 5.1 shows that there was little difference between M_n and M_w values before and after sonication, showing that the copolymer was not degraded.

	M_w/ g mol^{-1}	M_n/ g mol^{-1}	PDI (M_w/M_n)
Before sonication	86200	47800	1.8
After sonicating for 1 h	84200	48000	1.7

Table 5.1. *THF GPC data for p(MAA_{39}-ran-$BzMA_{61}$) before and after being subjected to sonication for 1 h. Before analysis p(MAA_{39}-ran-$BzMA_{61}$) was methylated using trimethylsilyldiazomethane (further details in 3.2.2.3).*

5.1.4 Preparation of carbon black dispersions stabilised by p(MAA_{39}-ran-$BzMA_{61}$) at 6, 13 and 50 wt % polymer on pigment. (Dispersions were formulated by Chris Potter at Fujifilm Imaging Colorants).

Dried p(MAA_{39}-ran-$BzMA_{61}$), NaOD (30 wt % in D_2O) and D_2O were weighed out into a beaker and heated to 80°C whilst stirring until a clear solution was obtained. Three p(MAA_{39}-ran-$BzMA_{61}$) solutions were made up at 0.32, 0.68 and 2.63 wt %. NaOD was added in amounts so that 100 % of MAA groups were neutralised. Neutralised p(MAA_{39}-ran-$BzMA_{61}$) solutions were mixed with carbon black using one of the following three techniques: a red devil paint shaker, Blackley mill and a sonic mill. Dispersions milled using the Blackley mill or sonic mill had to be mixed on the Red Devil paint shaker beforehand to break up any large aggregates that might otherwise clog up the mills.

- **Preparation of Dispersions Using Red Devil Paint Shaker**

28.5 g of neutralised p(MAA_{39}-ran-$BzMA_{61}$) solution (0.32, 0.68 or 2.63 wt %) and 1.5 g of carbon black were added to 60 ml glass jars so that polymer on pigment was obtained at 6, 13 and 50 wt %. To each jar 60 g of 3 mm glass beads were added and then agitated for 6 hours on a Red Devil paint shaker.

- **Preparation of Dispersions Using Blackley Bead Mill**

A sample of pre-milled 6 wt % p(MAA_{39}-ran-$BzMA_{61}$) on pigment dispersion mixed on the Red Devil paint shaker was added to a Blackley Mill pot along with 0.4-0.6 mm diameter Ermil ceramic beads. The stirrer was positioned to be just off the bottom of the

pot. Milling was carried out for two hours and beads were separated from the dispersion with a 50 μm filter cloth. This process was repeated for the 13 and 50 wt % p(MAA_{39}-ran-$BzMA_{61}$) loading on pigment dispersions created from the Red Devil paint shaker.

- **Preparation of Dispersions Using a Branson Digital Sonifier Sonic Mill**

A sample of pre-milled 6 wt % p(MAA_{39}-ran-$BzMA_{61}$) on pigment dispersion mixed on the Red Devil paint shaker was added to a 30 ml glass jar and subjected to ultrasound using a dual horn Branson Digital S45OD Ultrasonifier sonic mill at 60 % amplitude. The sample was milled for two hours whilst the jar was submerged in an ice bath to reduce heating. This process was repeated for the 13 and 50 wt % p(MAA_{39}-ran-$BzMA_{61}$) loading on pigment dispersions created from the Red Devil paint shaker.

5.1.5 Small-angle Neutron Scattering (SANS)

SANS measurements were carried out on three different instruments:

1) Sans2d at ISIS in Oxford
2) LENS at the Centre of Exploration of Energy and Matter in Bloomington, USA
3) D11 at I.L.L in Grenoble

Sans2d and LENS uses a spallation source to produce a pulsed beam of neutrons and I.L.L uses nuclear fission to produce a constant beam of neutrons. The measurements performed on each instrument are described below.

- **Radius of Gyration (R_g) measurement**

SANS measurements to determine the R_g of p(MAA-ran-BzMA) copolymers with MAA content varying from 39-79 mol % were performed at LENS at the Centre for Exploration of Energy and Matter in Bloomington, USA. The q-range was 0.008-0.27 $Å^{-1}$ and sample cells were 2 mm Helma quartz 'banjo' cells. Measurements were carried out on 1 wt % solutions of neutralised p(MAA-ran-BzMA) in D_2O. The copolymers were neutralised by adding NaOD (30 wt % in D_2O) and stirring at 80°C until a homogeneous solution was obtained.

- **Contrast matching and measurements of p(MAA_{39}-ran-$BzMA_{61}$) stabilised carbon black in 27:73 D_2O:H_2O volume % solvent**

SANS was used to determine the contrast match point for carbon black. Contrast matching experiments were carried out on 5 wt % dispersions of carbon black in 0:100 H_2O:D_2O, 10:90 H_2O:D_2O and 41:59 H_2O:D_2O volume % solvent. Measurements were performed on the D11 beamline at the Institut Laue-Langevin (I.L.L) in Grenoble. The q-range of 0.004-0.05 $Å^{-1}$ was achieved by setting the distance between sample and detector to 13 m and the distance between sample and moderator to 13.5 m. The capability of D11 to reach a lower q was exploited by also measuring scattering from p(MAA_{39}-ran-$BzMA_{61}$)-stabilised carbon black dispersions whereby p(MAA_{39}-ran-$BzMA_{61}$) was contrast-matched in 27:73 D_2O:H_2O volume % solvent. The access to a higher q range meant any large-scale structures present would also be detected. All samples were run in Helma 2 mm quartz 'banjo' cells and scattering data were normalised for sample transmission and background.

- **SANS measurements of carbon black dispersions stabilised by p(MAA_{39}-ran-$BzMA_{61}$) in 100 % D_2O.**

SANS measurements of carbon black dispersions stabilised by p(MAA_{39}-ran-$BzMA_{61}$) in 100 % D_2O so that carbon black was contrast-matched were performed at Sans2d in ISIS. Samples were run in 2 mm Helma quartz 'banjo' cells over a q range of 0.0045-0.79 $Å^{-1}$.

5.1.6 Small-angle X-ray Scattering (SAXS)

SAXS measurements were carried out on a Bruker AXS Nanostar using a Hi-STAR 2D detector. X-rays were generated by a Cu-Kα source giving a wavelength of 1.54 Å. X-rays were focused by two cross-coupled Gobel mirrors and a 'pin hole' collimated to provide a defined beam of known wavelength and diameter (0.5 mm). Bruker AXS software was used to collect and process the data frames. A detector set at 106.1 cm from the sample was used with a semi-transparent beam stop mounted between the two to protect the detector from the direct beam and to allow normalisation of intensities. Samples were injected between two ruby mica discs (15 mm diameter, 25 μm thickness) mounted on the sample holder. Samples were ran for 1 h and an empty and solvent background were ran for 12 h each. Scattering from the sample was corrected by

normalising data for the counts observed through the sample and beamstop, followed by subtraction of the solvent and empty cell background.

5.1.7 Rheology

Viscosity measurements were carried out using the same protocol described in section 3.2.3.5 in Chapter III.

5.2 Results and Discussion

5.2.1 Measuring the Radius of Gyration (R_g) of poly(methacrylic acid-random-benzyl methacrylate) copolymers in D_2O

The radius of gyration (R_g) of a polymer is defined as the root mean square, mass-weighted average distance of the monomer repeat units from their centre of mass.[20] R_g only gives an average size of the polymer chain for two reasons: (i) polymer coils are constantly undergoing random thermal motion so will always be changing shape and volume and (ii) polymer chains exist in a variety of lengths leading to each chain occupying a different volume.[21] R_g can be determined using small-angle X-ray or neutron scattering[22] or by collating data from static light scattering and constructing a Zimm plot.[23]

The R_g for p(MAA_{39}-ran-$BzMA_{61}$) gave an insight into the adsorption process for the copolymer adsorbing onto the carbon black surface. Knowing the average size of p(MAA_{39}-ran-$BzMA_{61}$) allowed for the determination of whether the copolymer chain was bigger, smaller or similar in size to the carbon black particles and enabled examination of whether or not p(MAA_{39}-ran-$BzMA_{61}$) changed size upon adsorption. Small-angle neutron scattering (SANS) was used to calculate the R_g of the p(MAA_{39}-ran-$BzMA_{61}$) dispersant used in the preparation of carbon black dispersions. In addition, the R_g of other p(MAA-ran-BzMA) copolymers prepared by batch free-radical polymerisation in DPG at 70°C (with MAA mol % varying from 47 to 79 %) was calculated for comparison. These copolymers are listed in Table 5.2.

name	M_n /g mol^{-1}	M_w /g mol^{-1}	PDI	Target mol % MAA	Actual mol % MAA[a]
AW40	19800	39600	2.0	36	39
AW41	24500	37700	1.5	36	47
AW42	33000	47300	1.4	45	54
AW43	19300	34500	1.8	54	61
AW44	18000	43200	2.4	75	79

Table 5.2. *Summary of p(MAA-ran-BzMA) copolymers synthesised by free-radical polymerisation in DPG at 70°C for 6 h. a) Calculated by ^{1}H NMR in $(CD_3)_2SO$.*

SANS measurements were performed on the copolymers at 1 wt % in D_2O (100 % neutralised by sodium deuteroxide (NaOD)). SANS data for the p(MAA-ran-BzMA) copolymers listed in Table 5.2 are presented in Figure 5.2 as Guinier plots where the natural log of intensity, ln (I) is plotted against the scattering variable squared, q^2. Guinier analysis allowed R_g to be extracted from the slope at low q, which is equal to $R_g^2/3$.

The R_g values obtained from the Guinier plots in Figure 5.2 are listed in Table 5.3. To check that the R_g values extracted from the Guinier plots were physically reasonable, R_g values were also calculated by theoretical means using equation 5.1 where b is the statistical segment length (Kuhn length) and N is the degree of polymerisation. Statistical length gives a measure of chain stiffness, essentially the distance between two points where the orientation of the chain changes appreciably.[20] As there is no literature value of statistical segment length for p(MAA-ran-BzMA) copolymers, an average value was calculated using the statistical lengths calculated for pMAA and pBzMA homopolymers. The statistical length used for pMAA was 3 Å,[24] which is approximately the same size as a single pMAA monomer unit. The statistical length of pBzMA could not be found, thus, as polystyrene has a similar structure to pBzMA the statistical length of polystyrene, which is 6.9 Å, was used as a substitute.[25] R_g values calculated by SANS and Equation 5.1 are shown in Table 5.3.

$$R_g^2 \sim \frac{Nb^2}{6} \qquad \textbf{Equation 5.1}$$

Sample name	M_n /g mol^{-1}	Mol % MAA	N	b /Å	R_g theoretical /Å	R_g experimental /Å
AW40	19800	39	137	5.5	26	21
AW41	24500	43	182	5.7	28	23
AW42	33000	54	257	4.8	31	17
AW43	19300	61	158	4.5	23	16
AW44	18000	79	165	3.9	21	5.7

Table 5.3. *R_g values of p(MAA-ran-BzMA) copolymers calculated experimentally using SANS using Guinier analysis and theoretically using equation 5.1. Corresponding statistical length, b and number of repeat units, N parameters are also shown. All samples were run at ~pH 10.*

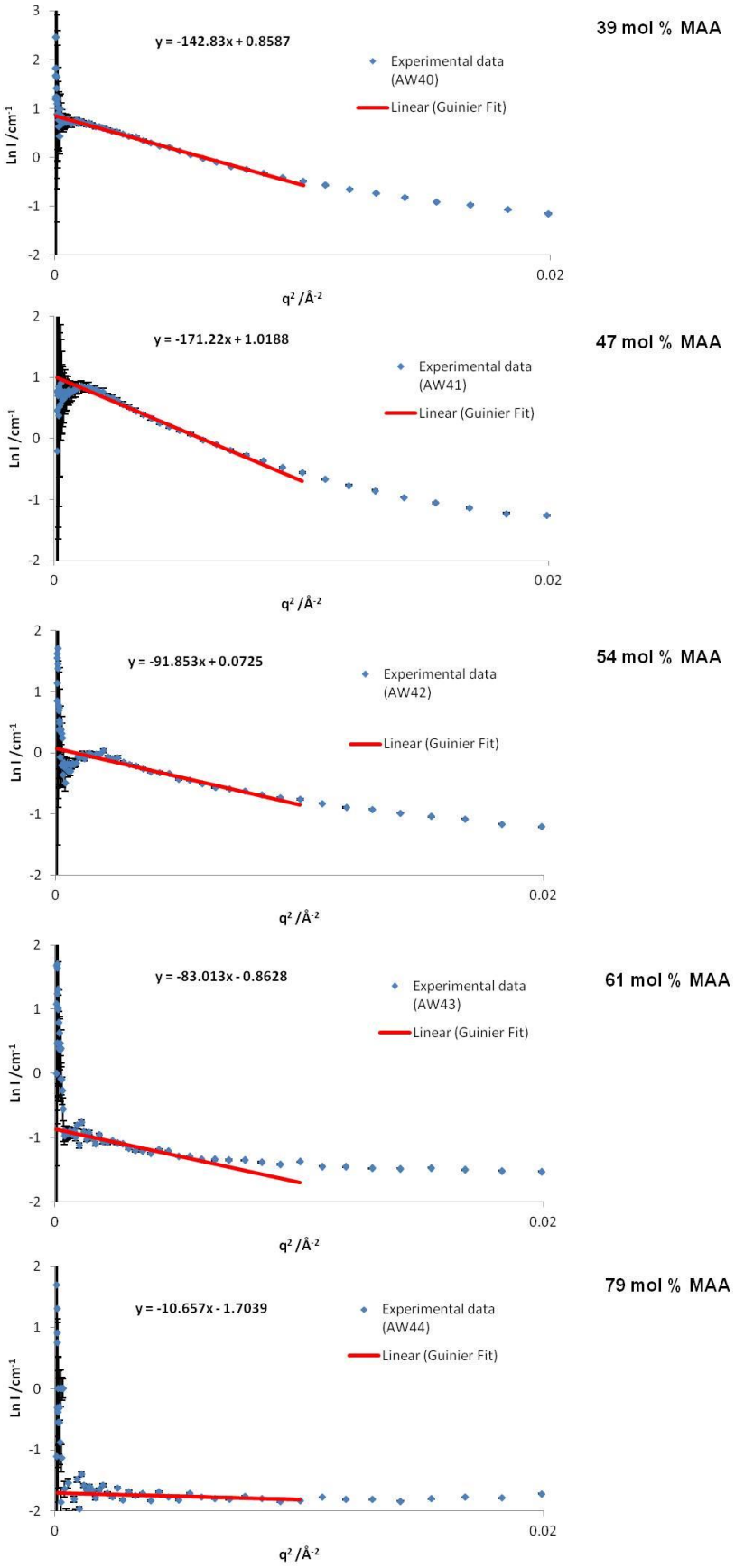

Figure 5.2. *Ln I vs. q^2 Guinier plots for 1 wt % solutions of p(MAA-ran-BzMA) copolymers in D_2O, pH 10, whereby the mol % of MAA has been varied from 39 to 79. Each plot is fitted with a straight line at low q where the slope is equivalent to $-R_g^2/3$. Further information on the copolymers is listed in Table 5.2.*

R_g of p(MAA_{39}-ran-$BzMA_{61}$) determined by SANS was 21 Å and the theoretical value calculated using equation 5.1 was 26 Å. The theoretical R_g value is slightly higher as an estimated statistical length, b was used. Nevertheless, it offers some assurance that the R_g of p(MAA_{39}-ran-$BzMA_{61}$) obtained from the Guinier plot was reasonable. It can be seen in Table 5.3 that the R_g values obtained from SANS for samples AW42-AW45 are significantly lower than the R_g values obtained by equation 5.1, which is not consistent with expectations. It was expected that, as the amount of MAA in the copolymer increased, the R_g would increase as deprotonated MAA groups would push the chain apart. Observation of the scattering curves for samples AW42-AW45 in Figure 5.2 reveal minimal scattering. It is speculated that the weak scattering observed for the copolymers with high MAA content was the result of the copolymer swelling and being outside the range for Guinier analysis which is $qRg < \sqrt{3}$ leading to inaccurate R_g values. (see Figure 5.3).

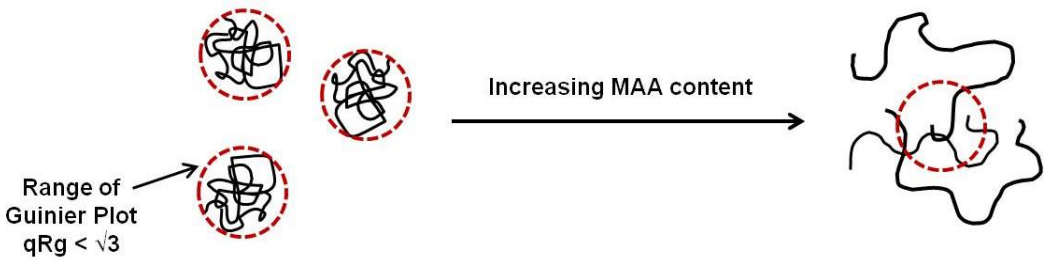

Figure 5.3. *Schematic representation of the swelling of p(MAA-ran-BzMA) chains with increasing MAA content.*

Rheology was used to test the theory that copolymers were more swollen with increasing MAA content. If swelling occurred an increase in viscosity should be observed. Figure 5.4 shows a plot of viscosity versus mol % MAA for the copolymers. The viscosity of p(MAA-ran-BzMA) increases with increasing MAA as expected, supporting the argument that copolymers with 54 mol % MAA or above are sufficiently swollen to lie outside the range for Guinier analysis.

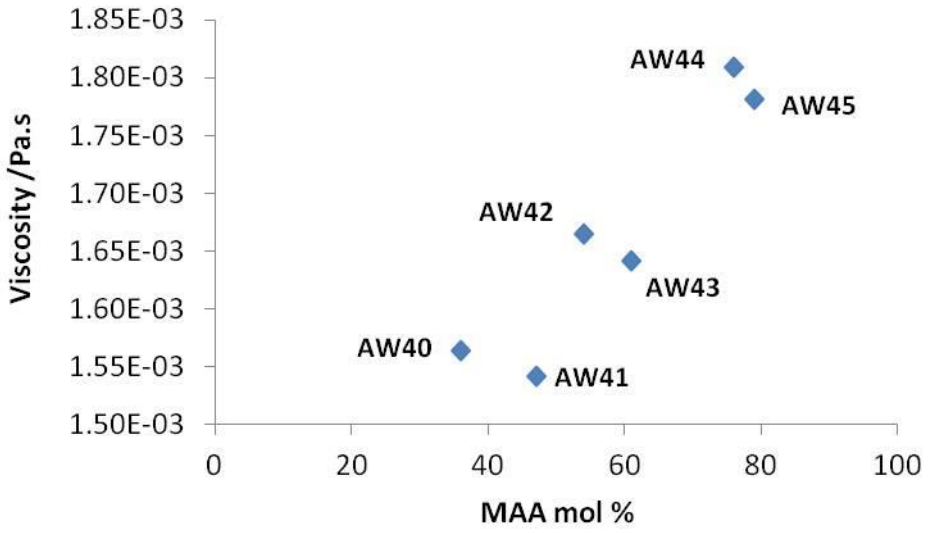

Figure 5.4. *Viscosity of various p(MAA-ran-BzMA) copolymers at 1 wt % in water with MAA mol % varying from 39 to 79. Further details of the copolymers are provided in Table 5.1.*

5.2.2 Contrast matching carbon black and p(MAA_{39}-ran-$BzMA_{61}$)

Neutron scattering is nuclear-dependent and scattering occurs at different scattering lengths depending on the nucleus. SANS is an incredibly powerful technique as it is capable of distinguishing between two isotopes of the same element such as ^{1}H and ^{2}D, with the two isotopes having different scattering lengths. Contrast-matched conditions arise when the scattering length density, ρ, of the solvent can be matched to the scattering length density of one component of the sample, rendering it 'invisible'. Contrast matching was used to make either carbon black or p(MAA_{39}-ran-$BzMA_{61}$) invisible in p(MAA_{39}-ran-$BzMA_{61}$)-stabilised carbon black dispersions. This was achieved by changing the scattering length density of the solvent by mixing H_2O and D_2O in suitable quantities. The scattering length densities for carbon black and p(MAA_{39}-ran-$BzMA_{61}$) were calculated using equation 5.2 and are shown in Table 5.5. In equation 5.2 N_A is Avogadro's constant, M is the molecular weight, δ is the bulk density of the molecule and b_i is the coherent neutron scattering length of nucleus i.

$$\rho = N \cdot \sum_i b_i = \frac{\delta N_A}{M} \cdot \sum_i b_i \qquad \textbf{Equation 5.2}$$

When calculating ρ for homopolymers, only the ρ for one repeat unit needs to be calculated as this is what constitutes a scattering centre. In the case of calculating ρ for

p(MAA_{39}-ran-$BzMA_{61}$), two scattering centres (BzMA and MAA) were taken into account and an average was taken.

Element	**H**	**D**	**C**	**O**
Coherent scattering length, b_i /10^{-15} m	-3.741	6.671	6.646	5.803

Table 5.4. *Coherent scattering lengths for elements used in equation 5.2.*

Sample	**M /g mol^{-1}**	**b_i (10^{-15} m)**	**δ/ g cm^{-3}**	**ρ (10^{10} cm^{-2})**
Carbon black	257	135	1.87	5.90
MAA	88.06	15.7	1.015	1.09
BzMA	176.21	39.8	1.04	1.42
p(MAA_{39}-co-$BzMA_{61}$)	-	-	-	1.29

Table 5.5. *Parameters used to calculate the scattering length density of carbon black and p(MAA_{39}-ran-$BzMA_{61}$) using equation 5.2. b_i was calculated using values listed in Table 5.4.*

Table 5.5 shows that the scattering length density of carbon black is 5.9 x 10^{10} cm^{-2} which would require a 93:7 vol % of D_2O:H_2O to obtain the contrast-matched point, ø (see equation 5.3).

$$\emptyset = \frac{\rho_{CB} - \rho_{H_2O}}{\rho_{D_2O} - \rho_{H_2O}} \qquad \textbf{Equation 5.3}$$

As the contrast-matched point is a theoretical value, the scattering length density was confirmed by creating a contrast match plot using neutron scattering data. The total intensity of three carbon black samples in different D_2O:H_2O mixtures was plotted against H_2O volume % and a parabolic curve fitted, whereby the lowest part of the curve was the contrast match point (see Figure 5.5). It can be seen from Figure 5.5 that low intensity is observed between 0-10 volume % of H_2O. For ease of preparation, carbon black was contrast-matched in 100 % D_2O for future SANS experiments.

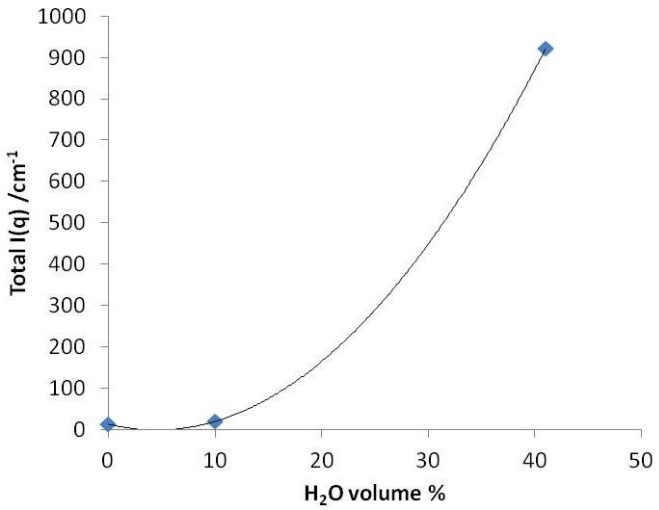

Figure 5.5. *Contrast match point determination of carbon black by plotting total scattering intensity against H_2O volume content in various D_2O/H_2O mixtures.*

Using equation 5.3, it was calculated that a 27:73 volume % D_2O:H_2O mixture would be required to contrast-match p(MAA_{39}-ran-$BzMA_{61}$). This calculated match point was not checked using SANS as any scattering from p(MAA_{39}-ran-$BzMA_{61}$) would be obscured by strong scattering from the carbon black. The schematic presented in Figure 5.6 summarises the two contrast matching conditions used to analyse the carbon black dispersions stabilised with p(MAA_{39}-ran-$BzMA_{61}$).

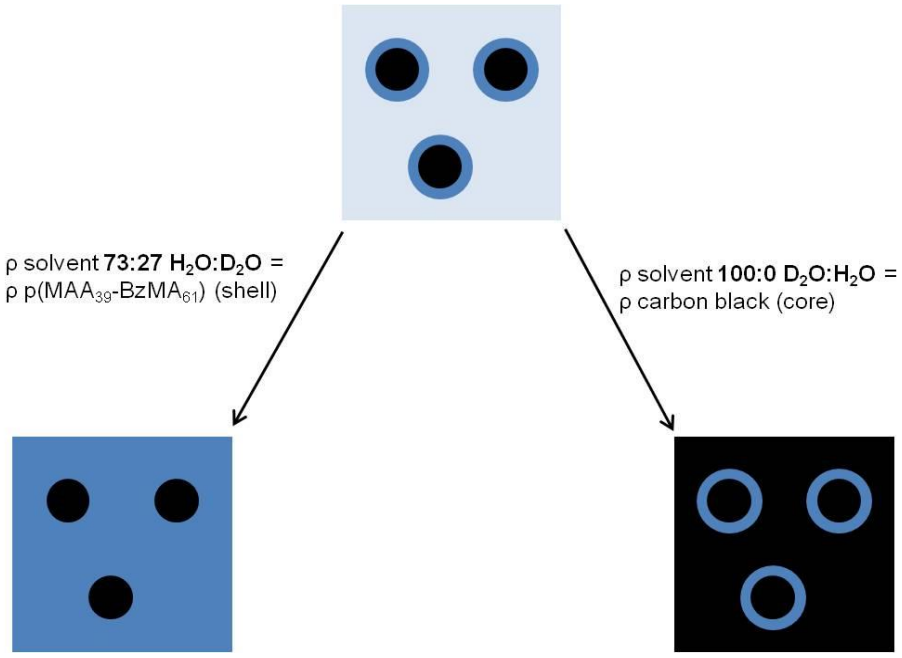

Figure 5.6. *Schematic representation for the two contrast matching experiments carried out to analyse p(MAA_{39}-ran-$BzMA_{61}$)-stabilised carbon black dispersions by SANS. Left) contrast-matched p(MAA_{39}-ran-$BzMA_{61}$) in 73:27 volume % H_2O:D_2O and right) contrast-matched carbon black in 100 % D_2O.*

5.2.3 SANS and SAXS measurements of carbon black and p(MAA_{39}-$BzMA_{61}$) dispersions with contrast matched p(MAA_{39}-$BzMA_{61}$) in 27:73 volume % D_2O:H_2O.

SANS measurements were carried out on three carbon black dispersions prepared at either 6, 13 or 50 wt % p(MAA_{39}-$BzMA_{61}$) loading on carbon black in 27:73 volume % D_2O:H_2O so that p(MAA_{39}-$BzMA_{61}$) was contrast-matched. The three wt % loading were chosen as they targeted three specific points on the adsorption curve previously constructed from Chapter IV (see Figure 5.7). At a loading of 6 wt % p(MAA_{39}-$BzMA_{61}$), the carbon black surface was not completely covered, at 13 wt % p(MAA_{39}-$BzMA_{61}$) a monolayer coverage of p(MAA_{39}-$BzMA_{61}$) on carbon black was achieved and at 50 wt % excess p(MAA_{39}-$BzMA_{61}$) is present in the dispersion. A summary of the SANS data for each of the dispersions analysed is given in Table 5.6 and the SANS scattering curves are presented in Figure 5.8.

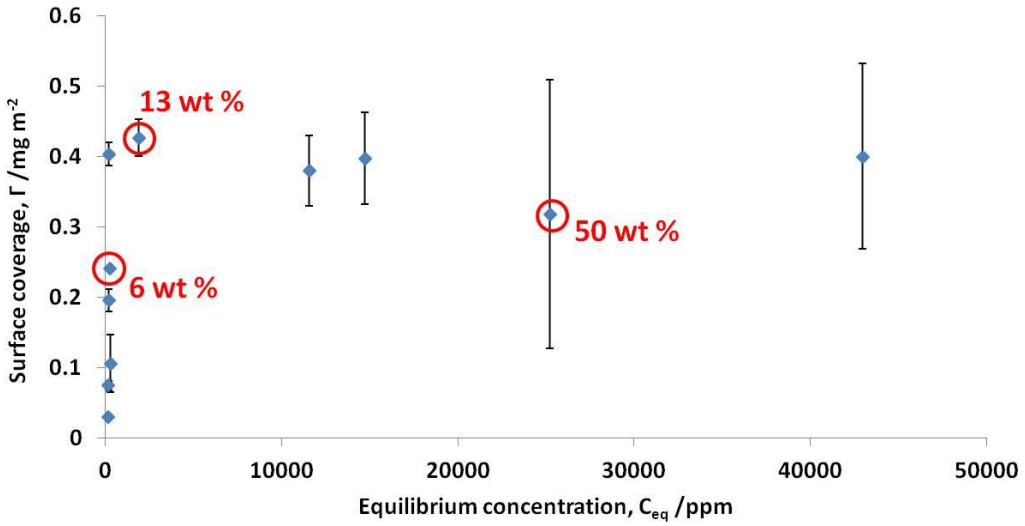

Figure 5.7. *Isotherm obtained for the adsorption of p(MAA_{39}-ran-$BzMA_{61}$) on carbon black in water. Circled points are the wt % loadings of p(MAA_{39}-ran-$BzMA_{61}$)on carbon black used for SANS measurements where p(MAA_{39}-ran-$BzMA_{61}$) has been contrast-matched.*

Name	Carbon black wt %	Wt % p(MAA_{39}-$BzMA_{61}$) on pigment	Solvent	pH
PCM_06SS	5	6	27:73 D_2O:H_2O	10.2
PCM_13SS	5	13	27:73 D_2O:H_2O	10.9
PCM_50SS	5	50	27:73 D_2O:H_2O	10.5

Table 5.6. *Summary of carbon black dispersions run at 6, 13 and 50 wt % p(MAA_{39}-ran-$BzMA_{61}$) on carbon black in 73:27 D_2O:H_2O so that p(MAA_{39}-ran-$BzMA_{61}$) was contrast-matched. PCM= p(MAA_{39}-ran-$BzMA_{61}$) contrast-matched, SS =sonicated at Sheffield.*

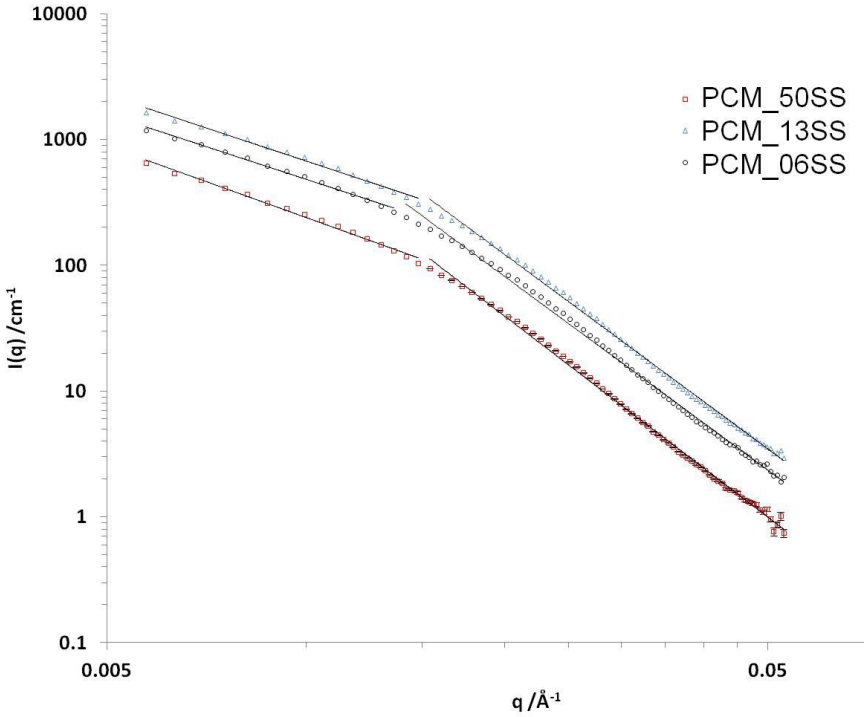

Figure 5.8. *SANS data obtained for three carbon black and p(MAA$_{39}$-ran-BzMA$_{61}$) dispersions, obtained at D11 at the I.L.L, whereby the concentration of p(MAA$_{39}$-ran-BzMA$_{61}$) was 6, 13 and 50 wt % based on carbon black. Carbon black is 5 wt % in all three samples in a 27:73 D_2O:H_2O volume % of solvent so p(MAA$_{39}$-ran-BzMA$_{61}$) was contrast-matched. The black solid lines are least-square fits to a power law equation. Data extracted from the fits are shown in Table 5.7.*

Three features are displayed in the log I(q) vs log q plots, presented in Figure 5.8, which are characteristic of a fractal aggregate: (i) at high q there is a power law, $I(q) \sim q^P$ region corresponding to the surface scattering from the primary particles (Porod law); (ii) at low q there is a power law $I(q) \sim q^P$ region corresponding to scattering from aggregates; and (iii) there is a curved cross-over region between the two power laws that occurs at q values of the order 1/a, where a is the diameter of the primary particles. A summary of the power law exponents extracted from Figure 5.8 are shown in Table 5.7.

Name	Exponent at low q (0.005-0.015), p_1 (D_m)	Exponent at high q (0.015-0.05), p_2	$D_s=6+p_2$
PCM_06SS	-1.7	-3.9	2.1
PCM_13SS	-1.7	-3.9	2.1
PCM_50SS	-1.9	-4.0	2.0

Table 5.7. *Exponents extracted from the power law fits to the data presented in Figure 5.8 whereby D_s = surface fractal dimension, D_m = mass fractal dimension.*

Between 0.015-0.05 $Å^{-1}$ the Porod law applies. For 50 wt % p(MAA_{39}-ran-$BzMA_{61}$) the Porod exponent is -4, indicating that the carbon black has a smooth surface with a sharp interface. For 6 and 13 wt % p(MAA_{39}-ran-$BzMA_{61}$) the Porod exponent is slightly lower at -3.9, signifying a slightly rougher surface. From the Porod exponent, the surface fractal dimension, D_s, of the primary particles can be obtained using $D_s=6+p_2$. In general, if D_s is 2 then the surface is smooth and, as D_s approaches 3, the surface is becoming rough. D_s was found to lie between 2.0-2.1 for the three dispersions, indicating smooth primary particles. These D_s values are reasonable because some grades of carbon black have primary particles with a partially graphitic surface, which would give a smooth texture.[26] The exponent extracted at low q (0.005-0.015 $Å^{-1}$) gives the mass fractal dimension, D_m. A value of D_m close to 1.8 indicates an open structure. For 6 and 13 wt % p(MAA_{39}-ran-$BzMA_{61}$) D_m was 1.7, which is in agreement with previous scattering studies conducted on carbon black composites and powders.[11] For 50 wt % p(MAA_{39}-ran-$BzMA_{61}$) D_m was slightly higher at 1.9, indicating that the carbon black structure has become more compact. This higher D_m value could be attributed to the agglomerate structure of carbon black being broken down.

SAXS was used to analyse the same carbon black dispersions in order to investigate the structure of the dispersions at higher q. The SANS and SAXS data for the 50, 13 and 6 wt % p(MAA_{39}-ran-$BzMA_{61}$) on carbon black dispersions are presented in Figure 5.9. The SAXS data at high q followed a power law of q^{-4} indicating a sharp smooth interface, which is consistent with the SANS data.

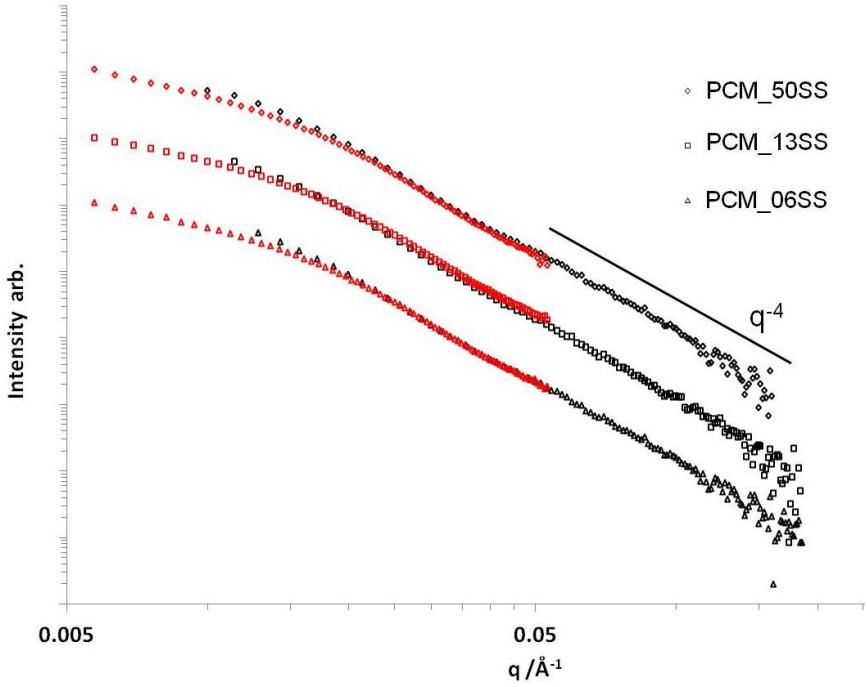

Figure 5.9. *SANS (red, low q) and SAXS (black, high q) data obtained for three carbon black and p(MAA$_{39}$-ran-BzMA$_{61}$) dispersions for which the concentration of p(MAA$_{39}$-ran-BzMA$_{61}$) was varied to give 6, 13 and 50 wt % on carbon black. Carbon black is 5 wt % in all three samples in a 27:73 D_2O:H_2O volume ratio of solvent so p(MAA$_{39}$-ran-BzMA$_{61}$) is contrast-matched for SANS.*

5.2.4 SANS measurements of carbon black and p(MAA$_{39}$-ran-BzMA$_{61}$) dispersions with contrast-matched carbon black in 100 % D_2O.

The conformation of p(MAA$_{39}$-ran-BzMA$_{61}$) on carbon black was studied by SANS by contrast matching carbon black in 100 % D_2O. Six carbon black dispersions were analysed at 6, 9, 13, 25, 34 and 50 wt % loadings of p(MAA$_{39}$-ran-BzMA$_{61}$) on carbon black and a summary of these compositions is given in Table 5.8. The log I(q) versus log q plots for the contrast-matched carbon black dispersions are shown in Figure 5.10.

Name	Carbon black wt %	Wt % p(MAA_{39}-ran-$BzMA_{61}$) on pigment	Solvent	pH
CMCB_06SS	5	6	100 % D_2O	11.0
CMCB_09SS	5	9	100 % D_2O	11.5
CMCB_13SS	5	13	100 % D_2O	10.9
CMCB_25SS	5	25	100 % D_2O	10.8
CMCB_34SS	5	34	100 % D_2O	10.8
CMCB_50SS	5	50	100 % D_2O	10.4

Table 5.8. *Summary of carbon black dispersions ran at various p(MAA-ran-BzMA) wt % whereby carbon black has been contrast-matched in 100 % D_2O. CMCB=contrast-matched carbon black and SS=sonicated at Sheffield.*

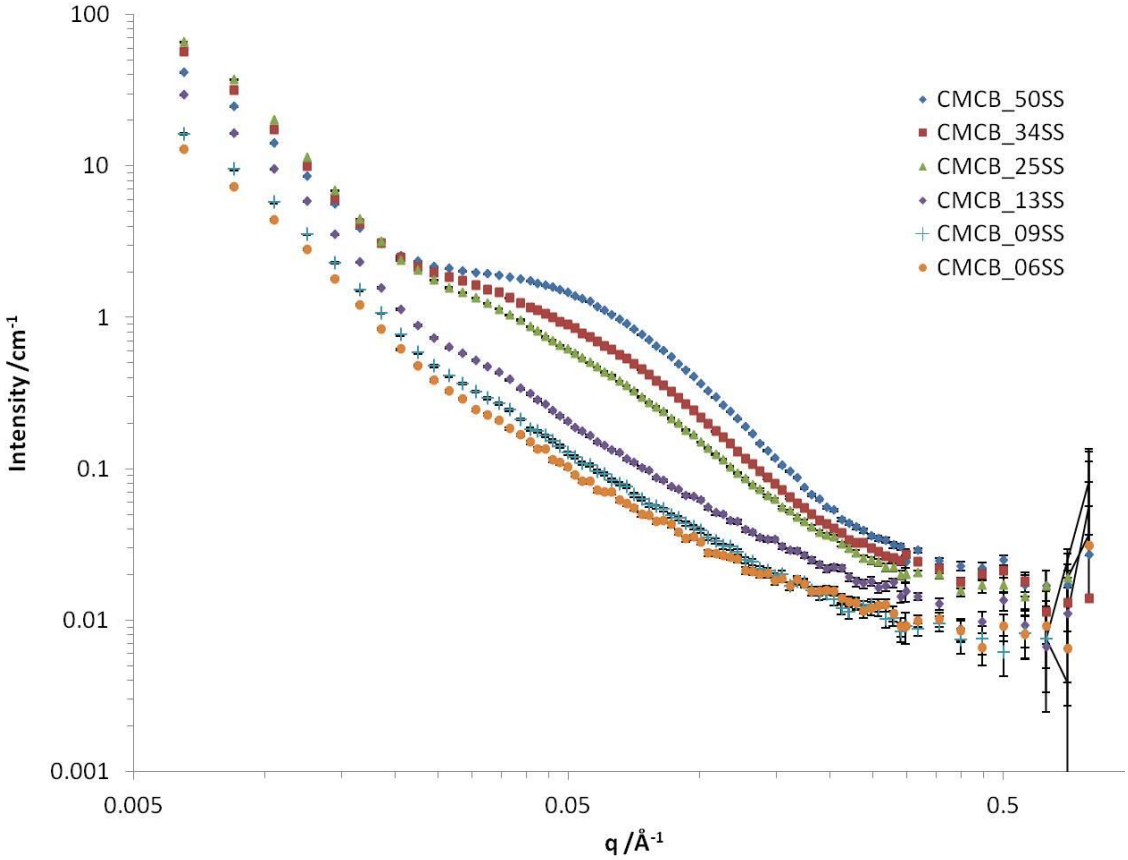

Figure 5.10. *SANS data obtained for six carbon black and p(MAA_{39}-ran-$BzMA_{61}$) dispersions whereby the concentration of p(MAA_{39}-ran-$BzMA_{61}$) has been varied to give 6, 9, 13, 25, 34 and 50 wt % loading on carbon black. Carbon black is 5 wt % in all six samples and has been contrast-matched in 100 % D_2O so only p(MAA_{39}-ran-$BzMA_{61}$) was visible by SANS.*

It can be seen from Figure 5.10 that above 13 wt % p(MAA_{39}-ran-$BzMA_{61}$) loading a broad peak appears at ~0.08 Å and increases in intensity with increasing concentration of p(MAA_{39}-ran-$BzMA_{61}$). The point at which this peak occurs is after monolayer coverage of the carbon black is achieved, as shown by the adsorption isotherm in Figure 5.7. The presence of the broad peak has been attributed to scattering from un-adsorbed copolymer. To understand what shape and size the adsorbed and un-adsorbed p(MAA_{39}-ran-$BzMA_{61}$) was adopting, information was extracted from the scattering curves by fitting to a model. It was found that a single model was inadequate for fitting of the SANS data and instead two combined Gaussian coil and mass fractal models were required. The Gaussian coil model calculates scattering from a polydisperse coil (the free polymer in solution) in a good solvent and the mass fractal model calculates scattering from fractal-like aggregates (the carbon black) composed of spherical building blocks. The scattering curves for the dispersions listed in Table 5.8 are shown in Figure 5.11, along with the combined model fits. The parameters extracted from these fits are listed in Table 5.9.

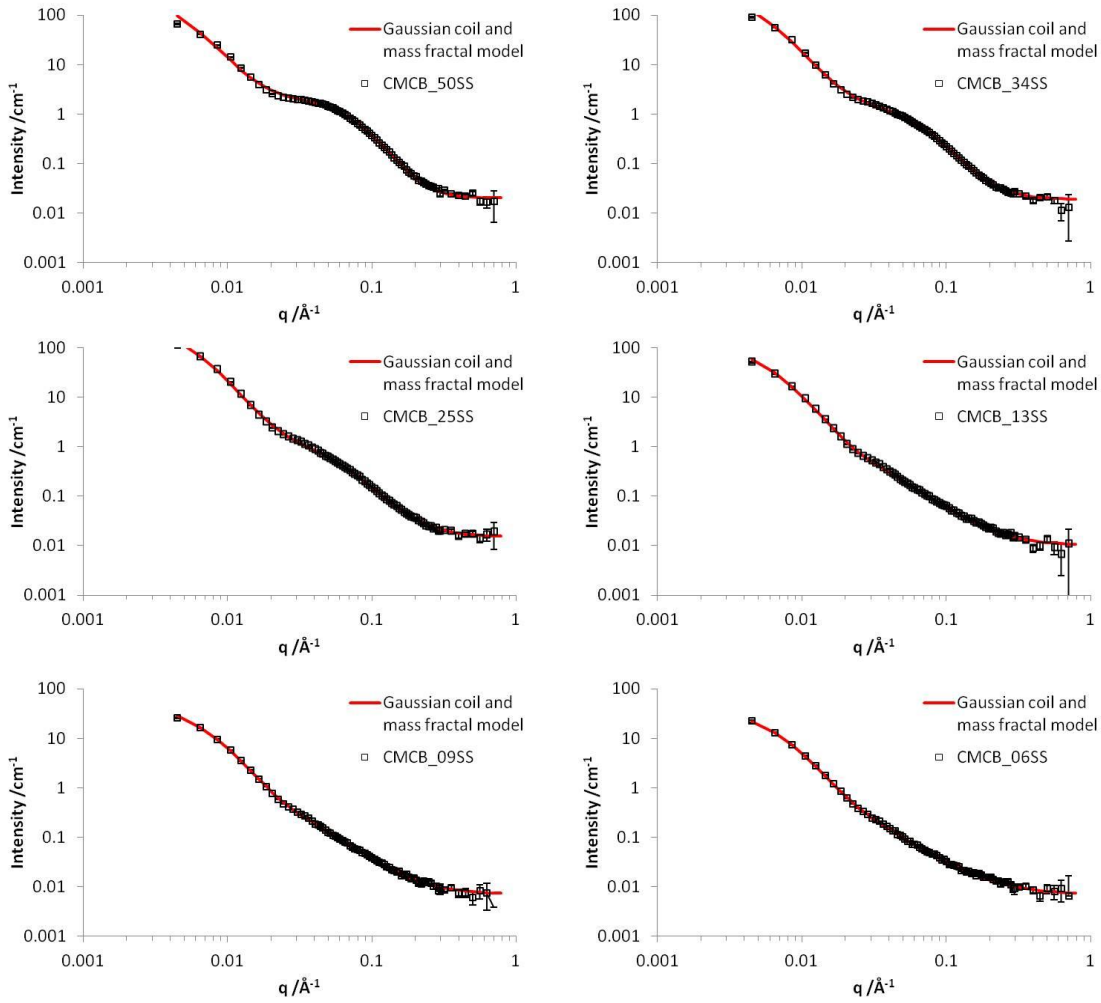

Figure 5.11. *SANS log intensity versus log q plots for six carbon black and p(MAA$_{39}$-ran-BzMA$_{61}$) dispersions whereby the concentration of p(MAA$_{39}$-ran-BzMA$_{61}$) has been varied to give 6, 9, 13, 25, 34 and 50 wt % loading on carbon black. Carbon black is 5 wt % in all six samples and has been contrast-matched in 100 % D$_2$O so only p(MAA$_{39}$-ran-BzMA$_{61}$) is visible by SANS. A combined model of a Gaussian coil and mass fractal model has been fitted. The data retrieved from the models is compiled in Table 5.9.*

Name	Gaussian chain model			Mass Fractal model			Background
	R_g /Å	nu	I_0 /cm^{-1}	R_0 /Å	x_i /Å	D	C_0 /cm^{-1}
CMCB_50SS	26	0.24	0.11	71	207	2.99	0.02
CMCB_34SS	31	0.30	0.097	58	197	2.99	0.015
CMCB_25SS	35	0.35	0.087	50	186	2.99	0.015
CMCB_13SS	46	0.46	0.059	48	161	2.99	0.010
CMCB_09SS	44	0.45	0.045	47	140	2.99	0.007
CMCB_06SS	54	0.51	0.044	51	137	2.99	0.007

Table 5.9. *Data from the combined model fitting of a Gaussian chain and mass fractal model to the plots shown in Figure 5.11. Symbols in the Table represent the following: R_g = radius of gyration, nu = Flory exponent where a collapsed coil is 1/3, a coil in a theta solvent is 1/2 and a swollen coil is 3/5, I_0 = forward scattering, R_0 = characteristic dimension of individual scatterers, x_i = size of fractal aggregate, D_m = fractal dimension, which was fixed at 2.99.*

In order to fit the combined model, the mass fractal dimension, D_m, had to be between 1 and 3 so D_m was fixed at 2.99 to generate a good fit. If D_m wasn't fixed then an implausible value above 3 would be obtained. If D_m was fixed to any value below 2.99, then the fit of the combined model became progressively worse.

It can be seen from Table 5.9 that, with decreasing p(MAA_{39}-ran-$BzMA_{61}$) content, the Flory exponent (nu) increases from 0.24 to 0.51. A Flory exponent of 1/3 indicates p(MAA_{39}-ran-$BzMA_{61}$) is in a collapsed conformation, whereas a value of 1/2 indicates a swollen coil in a theta solvent. In addition, with decreasing p(MAA_{39}-$BzMA_{61}$) concentration, R_g increased from 26 to 54 Å. It is speculated that R_g is larger at a lower p(MAA_{39}-ran-$BzMA_{61}$) concentration because the copolymer is able to adopt a flat conformation and adsorb a large fraction of its segments onto the carbon black surface. At high p(MAA_{39}-ran-$BzMA_{61}$) concentration, R_g is smaller due to adsorption sites on carbon black being occupied by other p(MAA_{39}-ran-$BzMA_{61}$) chains, leading to restricted unfolding of p(MAA_{39}-ran-$BzMA_{61}$). Because the p(MAA_{39}-ran-$BzMA_{61}$) chains are not able to unfold, more loops extending out into solution should be present. The presence of more loops is confirmed by examining $R_{0,}$ which is the characteristic dimension of the individual scatterers. Here the individual scatterers are presumed to be the copolymer-coated primary carbon black particles and they increase in size from 51 to 71 Å with

increasing p(MAA_{39}-ran-$BzMA_{61}$) concentration. For dispersions with loadings of 6, 9, 13 and 25 wt % p(MAA_{39}-ran-$BzMA_{61}$) on carbon black, R_0 stays almost constant at around 50 Å. This is confirmed by the TEM images of the carbon black dispersions, which show the primary particles to have a radius of approximately 50 Å (see Figure 5.12). At loadings of 34 and 50 wt % p(MAA_{39}-ran-$BzMA_{61}$) on carbon black, the SANS data shows R_0 increases to 58 Å and 71 Å respectively. This has been attributed to the presence of adsorbed copolymer forming loops, which leads to an increase in the radius of the copolymer-coated primary particles.

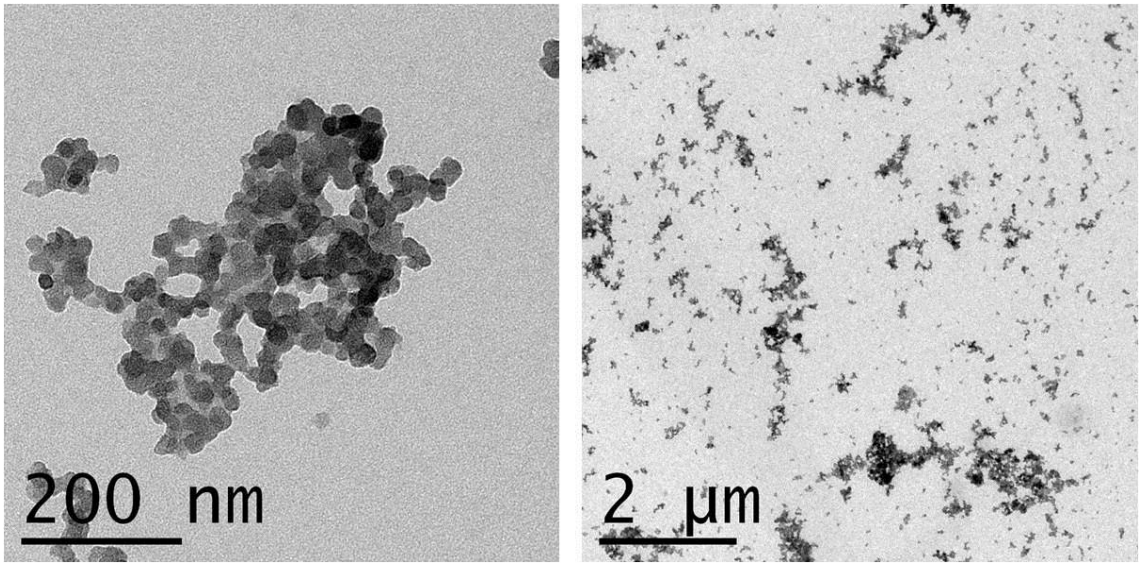

Figure 5.12. *TEM images of 13 wt % p(MAA_{39}-$BzMA_{61}$) loading on carbon black in 100 % D_2O at two different magnifications.*

The mass fractal model gives x_i which is the size of the fractal aggregate. This parameter increases from 137 Å to 207 Å with increasing p(MAA_{39}-ran-$BzMA_{61}$) concentration. It is speculated that this increasing size is the result of adsorbing polymer increasing the overall size measured by SANS. As the size continues to increase after monolayer coverage has been achieved, it is suggested that self-association of polymer at the adsorbed copolymer layer occurs. Self-association has been discussed in Chapter I and can occur when the adsorbing block in the copolymer is present in a non-solvent and at high concentration, which is the case here. Self-association between p(MAA_{39}-ran-$BzMA_{61}$) could occur through BzMA residues being attracted together (see Figure 5.13). The presence of a plateau in the adsorption isotherm for p(MAA_{39}-ran-$BzMA_{61}$) on carbon black indicates that self-association between the BzMA groups occurred via a

weak interaction and could be broken apart during centrifugation. Figure 5.14 summarises the data extracted from Table 5.9 in a schematic for samples CMCB_06SS and CMCB_50SS. For sample CMCB_06SS, the carbon black particles aggregate together forming agglomerates; this is due to an insufficient amount of p(MAA_{39}-ran-$BzMA_{61}$) adsorbing onto the carbon black leading to re-aggregation. These large agglomerates are not detected by SANS because the q-range available to the SANS instruments could only detect structures ranging from 1396 Å to 8 Å. The SANS data for CMCB_50SS indicates that the carbon black has been broken down to smaller aggregates and stabilised by adsorbed p(MAA_{39}-ran-$BzMA_{61}$) to give an average aggregate diameter of approximately 207 Å. It is probable that larger aggregates are also present in the CMCB_50SS dispersion, but these lie outside the q range that the SANS instrument could measure. It can be seen from the TEM image in Figure 5.12 that the carbon black agglomerates have been broken down to aggregates of approximately 200 in diameter. It is speculated that smaller aggregates are present in the dispersion, but these are not seen on the TEM micrographs because when the samples are drying on the TEM grid during preparation the carbon black particles cluster together.

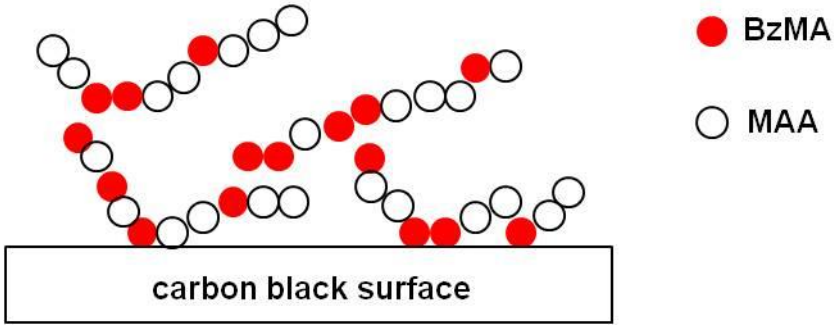

Figure 5.13. *Schematic representation of the self-association of p(MAA_{39}-ran-$BzMA_{61}$) at the carbon black surface.*

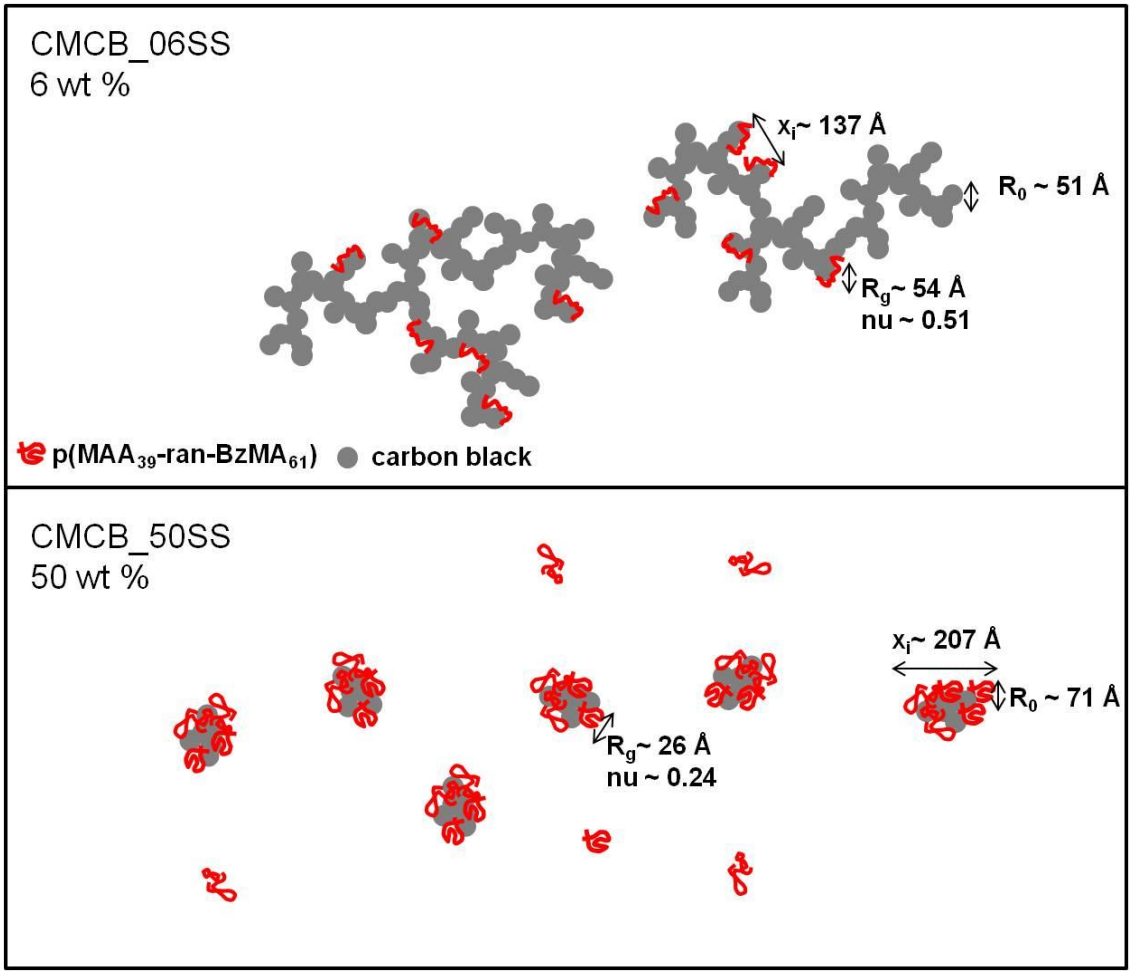

Figure 5.14. *Schematic representation of the possible conformation of p(MAA$_{39}$-ran-BzMA$_{61}$) on carbon black at loadings of 6 and 50 wt % that relate to the values extracted from SANS curves using a combined model fit (see Table 5.9). R_g is the radius of gyration of p(MAA$_{39}$-ran-BzMA$_{61}$), R_0 is the characteristic dimension of the copolymer-coated carbon black primary particles and x_i is the size of the fractal aggregates.*

5.2.5 Exploring the effect of using different milling techniques when preparing carbon black dispersions.

Milling of polymeric dispersant, pigment and water is an important step when creating stable ink-jet inks. Milling reduces the pigment size to give an ink of suitable viscosity that does not clog up the jets in printers. During the manufacture of inks, three milling techniques are commonly used: shear, sonic and bead milling. SANS was used to measure three contrast-matched carbon black dispersions prepared at 6, 13 and 50 wt % loadings of p(MAA$_{39}$-ran-BzMA$_{61}$) on carbon black in 100 % D_2O milled using three different techniques: a paint shaker, a bead mill and a sonic mill. The paint shaker used was a Red Devil paint shaker, the same model available in DIY stores. This breaks down large aggregates in dispersions before they are subjected to either bead or sonic milling.

Without the paint shaking step, large aggregates would clog up the bead and sonic mills. The sonic and bead mill is used for fine milling to break down the aggregates further. The sonic mill has the advantage of not requiring media (glass or ceramic beads) to aid milling. As well as being difficult to remove from the milled dispersion, beads can be expensive and need replacing due to wear over time. The energy transfer in a sonic mill is higher than a bead mill, but an ice bath is needed to prevent overheating of the sample. The carbon black dispersions prepared using the three different milling techniques are listed in Table 5.10 and the corresponding SANS plots are presented in Figure 5.15.

Name	Carbon black wt %	Wt % Polymer on pigment	Milling technique	Solvent	pH
CBCM_6RD	5	6	Red-devil	100 % D_2O	9.6
CBCM_6BM	5	6	Blackley Mill	100 % D_2O	8.0
CBCM_6SM	5	6	Sonic Mill	100 % D_2O	9.1
CBCM_13RD	5	13	Red-devil	100 % D_2O	9.8
CBCM_13BM	5	13	Blackley Mill	100 % D_2O	8.1
CBCM_13SM	5	13	Sonic Mill	100 % D_2O	9.8
CBCM_50RD	5	50	Red-devil	100 % D_2O	10.5
CBCM_50BM	5	50	Blackley Mill	100 % D_2O	8.8
CBCM_50SM	5	50	Sonic Mill	100 % D_2O	10.1

Table 5.10. *Summary of carbon black dispersions prepared at three different loadings of p(MAA_{39}-ran-$BzMA_{61}$) on pigment (6, 13 and 50 wt %). The overall wt % of carbon black in the dispersions was kept constant at 5 wt %. Each dispersion was prepared using three different mills: red-devil paint shaker (RD), Blackley mill (BM) and sonic mill (SM). Dispersions milled by the Blackley mill and sonic mill were also initially mixed on the red-devil paint shaker.*

The intensity (I) at q=0, depicted in Figure 5.15, can be used to compare the size of fractal aggregates mixed using either shear (RD), bead (BM) or sonic (SM) milling. The higher the intensity at q=0, the larger the fractal aggregate, which is indicative of the milling technique not being effective at breaking down the carbon black agglomerates. The SANS results obtained for dispersions prepared at 6 wt % loading of p(MAA_{39}-ran-$BzMA_{61}$) on carbon black reveal that the Red Devil paint shaker is the least effective technique for breaking down the aggregates and the higher energy sonic mill is most effective. The SANS plots for 13 and 50 wt % loading of p(MAA_{39}-ran-$BzMA_{61}$) in Figure 5.15 show that the Red Devil paint shaker is an adequate milling technique to break down the carbon black and shows the high energy Blackley mill and sonic mill are not necessary when a monolayer of p(MAA_{39}-ran-$BzMA_{61}$) is present.

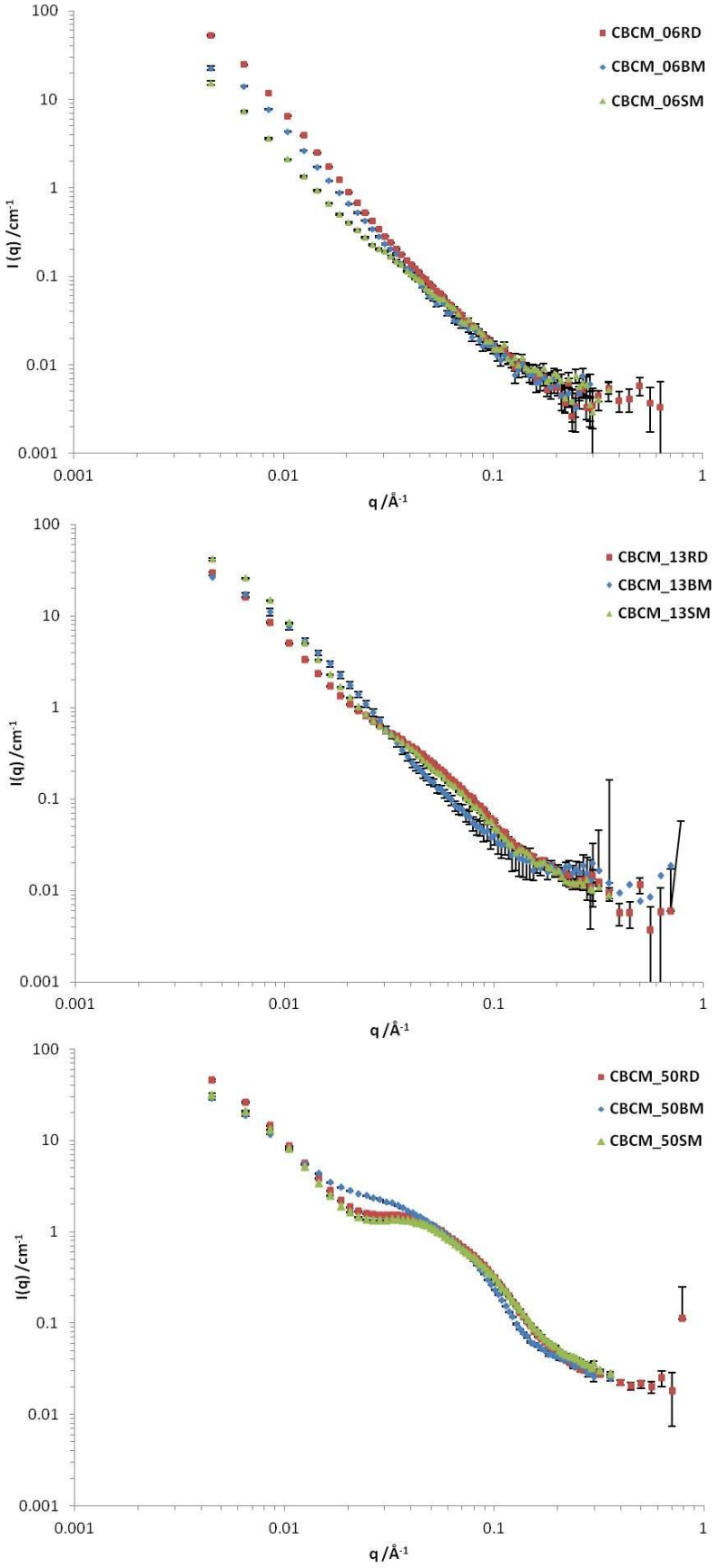

Figure 5.15. *Log I(q) vs. log q SANS plots for 6 wt % (top) 13 wt % (middle) and 50 wt % (bottom) p(MAA$_{39}$-ran-BzMA$_{61}$) on carbon black in 100 % D_2O using either a Blackley Mill (BM), a Red Devil paint shaker (RD) or a sonic mill (SM) to mix the dispersion.*

5.2.6 Effects of temperature on p(MAA_{39}-$BzMA_{61}$)-stabilised carbon black dispersions

SANS was used to measure contrast-matched carbon black dispersions stabilised by 6, 13 or 50 wt % p(MAA_{39}-ran-$BzMA_{61}$) loadings at either 5, 20 or 40°C. These dispersions are summarised in Table 5.11 and the corresponding SANS plots are presented in Figure 5.16.

Name	Wt % Carbon black	Wt % Polymer on pigment	Temperature /°C	Solvent
CBCM_6SS_5°C	5	6	5	100 % D_2O
CBCM_6 SS_20°C	5	6	20	100 % D_2O
CBCM_6 SS_40°C	5	6	40	100 % D_2O
CBCM_13 SS_5°C	5	13	5	100 % D_2O
CBCM_13 SS_20°C	5	13	20	100 % D_2O
CBCM_13 SS_40°C	5	13	40	100 % D_2O
CBCM_50 SS_5°C	5	50	5	100 % D_2O
CBCM_50 SS_20°C	5	50	20	100 % D_2O
CBCM_50 SS_40°C	5	50	40	100 % D_2O

Table 5.11. *Summary of carbon black dispersions prepared at loadings of 6, 13 and 50 wt % p(MAA_{39}-ran-$BzMA_{61}$) on carbon black and then measured by SANS at either 5°C, 20°C or 40°C. The overall wt % of carbon black in the dispersions was kept constant at 5 wt % and each dispersion was mixed by sonication at the University of Sheffield (SS). The SANS plots of the corresponding dispersions are presented in Figure 5.16.*

It can be seen from Figure 5.16 that at all three temperatures the neutron scattering from the dispersions prepared at loadings of 6, 13 and 50 wt % p(MAA_{39}-ran-$BzMA_{61}$) on carbon black produce the same scattering patterns confirming that the conformation of p(MAA_{39}-ran-$BzMA_{61}$) is unaffected between 5-40°C. It was expected that, at higher temperatures, the R_g of p(MAA_{39}-ran-$BzMA_{61}$) would increase due to being more solvated.

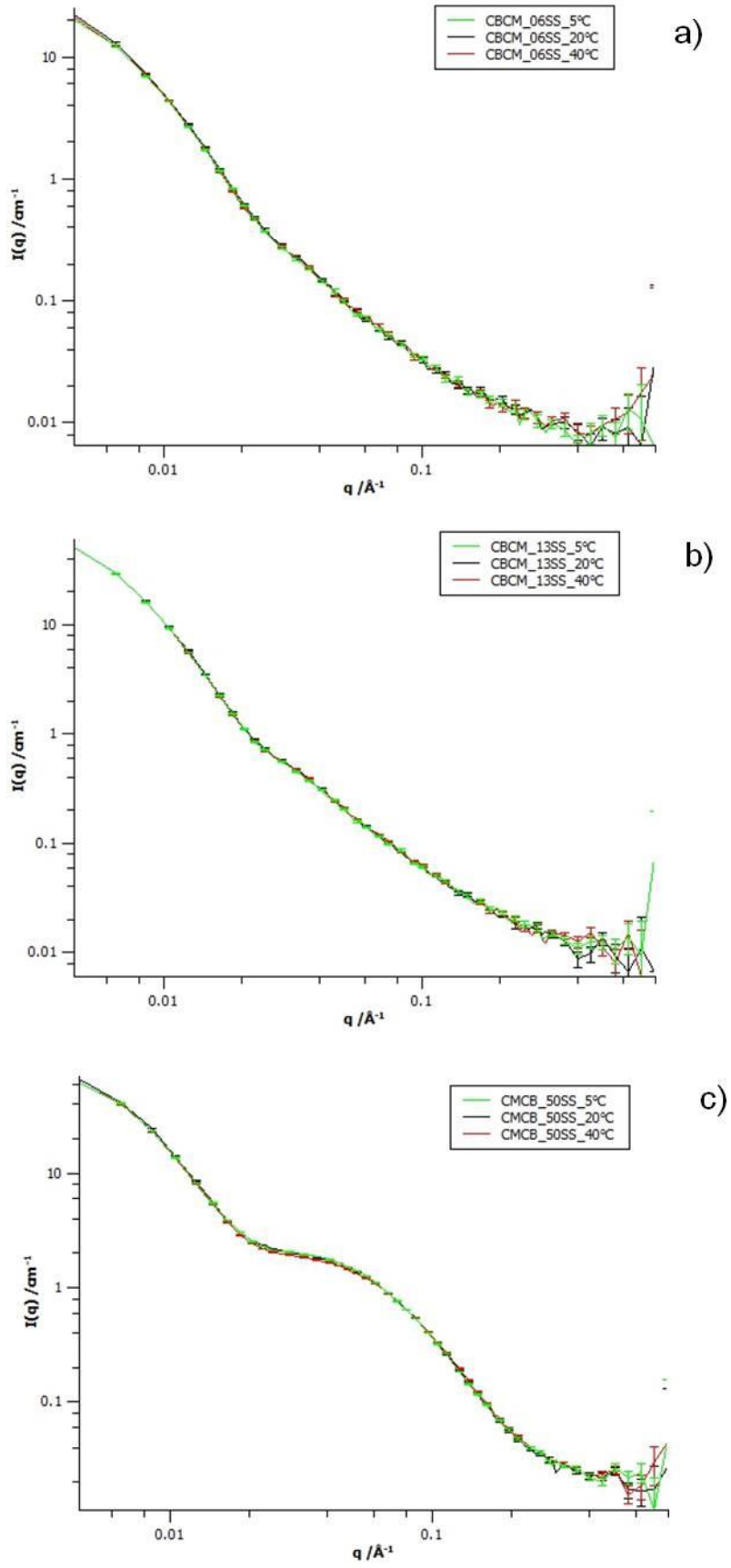

Figure 5.16. *Log I(q) vs log q SANS plots for a) 6, b) 13 and c) 50 wt % p(MAA$_{39}$-ran-BzMA$_{61}$) on carbon black dispersions mixed by sonication at the University of Sheffield (SS) at 5°C, 20°C and 40°C. Dispersions were prepared in 100 % D_2O so carbon black was contrast-matched.*

5.3 Summary

The adsorption of p(MAA_{39}-ran-$BzMA_{61}$) onto carbon black was investigated using SANS and SAXS. SANS measurements of a 1 wt % solution of p(MAA_{39}-ran-$BzMA_{61}$) in D_2O that had been neutralised with NaOD revealed the radius of gyration (R_g) to be 21 Å. In addition the R_g of several other p(MAA-ran-BzMA) copolymers with MAA mol % varying from 39 to 79 were examined using SANS. It was found that above 54 mol % MAA, scattering was minimal and was attributed to the MAA residues expanding the copolymer such that it fell outside the range for Guinier analysis. Viscosity measurements confirm that an increased MAA content in the p(MAA-BzMA) copolymers resulted in an increased viscosity. This supported the hypothesis that the polymers expand with increasing MAA content.

SANS was used to study carbon black dispersions stabilised with p(MAA_{39}-ran-$BzMA_{61}$) by either contrast-matching carbon black in 100 % D_2O or p(MAA_{39}-ran-$BzMA_{61}$) in 27:73: volume % D_2O:H_2O. SANS measurements on the contrast-matched p(MAA_{39}-ran-$BzMA_{61}$) dispersions displayed two power law regimes in the scattering curve. The power law exponent at low q gave a fractal dimension for the carbon black aggregates of 1.7, which is typical for an open, low density structure formed by primary particles clustering together through random motion. The exponent extracted at high q gave a Porod exponent of -4, indicating that the carbon black particles had a smooth surface with a sharp interface. The SAXS data were consistent with the SANS data, with both techniques producing the same power law exponent of -4 at high q.

SANS data were collected for contrast-matched carbon black dispersions with loadings of 6, 9, 13, 25, 34 and 50 wt % p(MAA_{39}-ran-$BzMA_{61}$) on carbon black. These loadings were used to target different points on the isotherm for p(MAA_{39}-ran-$BzMA_{61}$) adsorbed on carbon black. SANS plots revealed that when more than 13 wt % of p(MAA_{39}-ran-$BzMA_{61}$) was added to the dispersion, a broad peak appeared at around 0.08 $Å^{-1}$. SANS data of contrast-matched carbon black dispersions was fitted with a combined model of a Gaussian coil (for the polymer in solution) and mass fractal model (for the polymer bound to the carbon black). The results from the combined model indicated that with decreasing wt % of p(MAA_{39}-ran-$BzMA_{61}$), the R_g of p(MAA_{39}-ran-$BzMA_{61}$) and the Flory exponent both increase, suggesting that p(MAA_{39}-ran-$BzMA_{61}$) had become more swollen. It is speculated that the increase in R_g was a result of more carbon black surface area becoming available, allowing p(MAA_{39}-ran-$BzMA_{61}$) to uncoil and adsorb at multiple points on the carbon black. The mass fractal model revealed the radius of the

carbon black primary particles to be approximately 50 Å, which was in good agreement with TEM results. The mass fractal model also revealed that the size of the fractal aggregate increased from 137 Å to 207 Å with increasing p(MAA_{39}-ran-$BzMA_{61}$) concentration. The increasing size was attributed to the adsorbing polymer forming loops on the carbon black surface and self-association of p(MAA_{39}-ran-$BzMA_{61}$) between adsorbed and un-adsorbed copolymer.

The effect of the 6, 13 and 50 wt % loading of p(MAA_{39}-ran-$BzMA_{61}$) on carbon black dispersions, where carbon black was contrast-matched, was studied further by SANS by exploring the effect of milling during dispersion preparation. The effect of using different milling techniques shows that, above the knee in the Langmuir isotherm (13 wt % loading or above), the polymer is an effective dispersant and the extra time and effort in using the Blackley mill is not required; the Red Devil shaker gives comparable performance. At a concentration of 6 wt %, the copolymer is not sufficient to stabilise the carbon black without the input of considerable energy to break up the aggregates.

The effect of temperature on the carbon black dispersions was also investigated. The results indicated that there is no difference in scattering from p(MAA_{39}-ran-$BzMA_{61}$) at 5°C, 20°C and 40°C, suggesting that the conformation of p(MAA_{39}-ran-$BzMA_{61}$) remained the same at each temperature.

5.4 References

1. Donnet, J.; Bansal, R.; Wang, M., *Carbon Black*. 2nd ed.; Marcel Dekker: New York, 1993, 1-66.
2. Salman, M.; Ghadiri. M. J., *Handbook of Powder Technology*, Volume 12, Hounslow, Elsevier, **2007.**
3. Aschaffenburg, A. S.; Grosskrotzenburg, K. K.; Frankfurt, J. L.; Grundau, A. K., *Aqueous Carbon Black Dispersions*, 2001, US patent 6171382B1.
4. Sorensen, C. M.; *Aerosol Science and Technology*, **2001**, *35*, 648-687.
5. Medalia, A. I., *Journal of Colloid and Interface Science*, **1970**, *32*, 115-131.
6. Rieker, T. P.; Hindermann-Bischoff, M.; Ehrburger-Dolle, F., *Langmuir*, **2000**, *16*, 5588-5592.
7. Barrie, C. L.; Griffiths, P. C.; Abbott, R. J.; Grillo, I.; Kudryashov, E.; Smith, C., *Journal of Colloid and Interface Science*, **2004**, *272*, 210-217.
8. Lin, Y.; Smith, T. W.; Alexandridis, P., *Langmuir*, **2002**, *18*, 6147-6158.
9. Manelbrot, B.; Freeman, W. H., *The Fractal Geometry of Nature*, Freeman: San Francisco, 1982.
10. Witten, T. A.; Sander, L. M., *Phys. Rev. Lett*, **1981**, 47, 1400-1403.
11. Sorensen, C. M., *Aerosol Science and Technology*, **2001**, *35*, 648-687.
12. Medalia, A. I.; Heckman, F. A., *Carbon*, **1969**, 7, 567-569.
13. Medalia, A. I., *Journal of Colloid and Interface Science*, **1970**, *32*, 115-131.
14. Rieker, T. P.; Misono, S.; Ehrburger-Dolle, F., *Langmuir*, **1999**, *15*, 914-917.
15. Shar, J. A.; Cosgrove, T.; Obey, T. M.; Warne, M. R., *Langmuir*, **1999**, *15*, 7688-7694.
16. Lin, Y.; Alexandridis, *P., J. Phys. Chem.* B, **2002**, *106*, 10834-10844.
17. Nsib, F.; Ayed, N.; Chevalier, Y., *Progress in Organic Coatings*, **2006**, *55*, 303-310.
18. Ma, C.; Xia, Y., *Colloids and Surfaces*, **1992**, *66*, 215-221.
19. Bele, M.; Kodre, A.; Arcon, I.; Grdadolnik, J.; Pejovnik, S.; Besenhard, J. O., *Carbon*, **1998**, *36*, 1207-1212.
20. Hiemenz, P. C.; Lodge, T. P., *Polymer Chemistry*. 2nd Edition, CRC Press: Boca Raton, 2007, pg 230.
21. Cowie, J. M. G., *Polymers: Chemistry and Physics of Modern Materials*. 2nd edition, Chapman and Hall: London, 1991, pg 215.
22. Briber, R. M.; Bauer, B. J.; Hammouda, B., *Journal of Chemical Physics*, **1994**,

101, 2592-2599.

23. Ghazy, R., *American Journal of Applied Sciences*, **2011**, *6*, 603-609.
24. Ortiz, C.; Hadziioannou, G., *Macromolecules*, **1999**, *32*, 780-787.
25. Beaucage, G.; Schaefer, D. W., *Journal of Non-Crystalline Solids*, **1994**, *172*, 797-805.
26. Beaucage, G.; Rane, S.; Schaefer, D. W.; Long, G.; Fischer, D., *Journal of Polymer Science: Part B: Polymer Physics*, **1999**, *37*, 1105-1119.

6.0 Conclusions

To understand the role of p(MAA-co-BzMA) copolymers as polymeric dispersants for pigment particles, they were characterised using a variety of experimental techniques. The first part of this thesis describes the synthesis and characterisation by Raman spectroscopy and ^{13}C NMR of p(MAA-co-BzMA). Copolymers were synthesised with a target content of 36 mol % MAA by free-radical polymerisation in DPG at 70ºC under both batch and semi-batch conditions. Utilisation of the batch method resulted in a higher amount of MAA (43 mol %) being incorporated into the copolymer; it was speculated that this was caused by the differing reactivity ratios of MAA (r_1) and BzMA (r_2). Using the linear analysis methods of Kelen-Tudos and Finemann and Ross, the reactivity ratios of MAA and BzMA were calculated to be r_1=1.03 r_2=0.66 and r_1=0.93 r_2=0.72 respectively. These reactivity ratios indicate that the batch-produced p(MAA-co-BzMA) copolymers were mostly random, but also contained some longer sequences of MAA. The kinetics of the batch polymerisation of p(MAA-co-BzMA) (target 36 mol % MAA) was followed using Raman spectroscopy. When monitoring the change in C=C band intensity at 1640 cm^{-1}, it was observed that the copolymerisation reached 88 % conversion after 68 minutes. The peak at 1717 cm^{-1}, which corresponds to the C=O bond on BzMA, was monitored to determine the conversion rate of BzMA during the batch copolymerisation; it was found that 75 % conversion was achieved after 5 h.

Fluorescence spectroscopy was used to further analyse the copolymers, this was achieved by attaching the ACE fluorophore to the copolymer backbone. Particular focus was on semi-batch-prepared p(MAA_{39}-co-$BzMA_{61}$) since this macromolecule was used as the dispersant for pigment particles which are the focus of the work detailed in Chapters four and five. TRAMS allowed the conformation of p(MAA_{39}-co-$BzMA_{61}$) in water to be examined as a function of pH by monitoring the change in τ_c. It was observed that, in the pH range 5.6-6.7, τ_c varied from 51 to 40 ns and above pH 7 τ_c decreased to approximately 20 ns, which is indicative of the p(MAA_{39}-co-$BzMA_{61}$) undergoing a conformation transition from a coiled to more open chain structure. It was observed that, between pH 8 and pH 11, increasing the mol % of MAA to 45 and 64 resulted in the copolymer expanding more, as indicated by a lowering of τ_c to approximately 10 ns.

The results reported in Chapter three showed that ACE-labelled p(MAA_{143}-b-$BzMA_n$)

diblocks could be synthesised by alcoholic dispersion RAFT polymerisation in ethanol at 70ºC with n = 50, 100, 143, 200, 300. The ACE label was incorporated into the $PMAA_{143}$ macro-CTA, which was obtained with a PDI of 1.9. The unusually high PDI of the macro-CTA was attributed to the presence of ACE. Investigation of the system in the absence of ACE resulted in a lower PDI of 1.3 being observed. Analysis of the polymer by SEM revealed that the diblocks existed as micelles, with BzMA acting as the core and MAA as the corona. TRAMS measurements of the micelles in water at pH 4.5 and pH 12 showed T_c to be lower at pH 12, indicating that the PMAA corona was stretching out due to the COO^- groups.

Once the diblock and random copolymers had been characterised, aqueous pigment dispersions stabilised with either the random copolymer p(MAA_{39}-co-$BzMA_{61}$) or the block copolymer p(MAA_{143}-b-BzMAn) were prepared and investigated. An adsorption isotherm for the adsorption of p(MAA_{39}-co-$BzMA_{61}$) on carbon black was obtained using both indirect (centrifugation) and direct (TGA) methods. The results obtained via both methods were consistent with monolayer coverage being achieved at 13 wt % loading of p(MAA_{39}-co-$BzMA_{61}$) on pigment. The point of monolayer coverage was found to coincide with a reduction in mean diameter of the dispersion from 1400 to 220 nm. This was demonstrated by DLS and indicated the formation of a stable dispersion that did not re-aggregate. IR spectroscopy was used to confirm the presence of p(MAA_{39}-co-$BzMA_{61}$) on the surface of carbon black and a shift of the C=O peak located on carbon black from 1734 cm^{-1} to 1701 cm^{-1} indicated that p(MAA_{39}-co-$BzMA_{61}$) interacted with the surface via hydrogen bonding. Rheology of the dispersions showed that, after monolayer coverage was achieved, a lower viscosity of 2 mPa.s was attained, suggesting the breakdown of large carbon black aggregates. Because the yellow, cyan and magenta pigments have lower densities than carbon black, centrifugation was not a suitable method for constructing an isotherm for the adsorption of p(MAA_{39}-co-$BzMA_{61}$) onto the pigments. Analytical centrifugation was employed to compare the random copolymer p(MAA_{39}-co-$BzMA_{61}$) and diblock p(MAA_{143}-b-$BzMA_{300}$) as a dispersant for carbon black in water. It was found that the random copolymer was a more effective dispersant than the diblock; this was demonstrated by the transmission plots, which depicted how far the carbon black dispersion moved down the sample tube as a function of time when being centrifuged at 2000 rpm. The carbon black dispersions stabilised with more than 13 wt % loading of p(MAA_{39}-co-$BzMA_{61}$) did not move down the tube during centrifugation, whereas carbon black dispersions in the presence of 27 wt % loading of

p(MAA_{143}-b-$BzMA_{300}$) did move down the sample tube. It is speculated that the diblock was a less effective dispersant than the random copolymer because the former exists as micelles. The adsorption of the diblocks onto carbon black was assumed to be occurring via two different methods: as whole micelles or as unimers which are in equilibrium with the micelles.

In order to analyse the conformation of the random copolymer p(MAA_{39}-co-$BzMA_{61}$) when adsorbed onto carbon black pigment particles and to investigate the R_g of the random copolymer alone in solution SANS and SAXS was employed. The results of the SANS and SAXS studies are detailed in Chapter 5. Guinier analysis and SANS measurements on p(MAA_{39}-co-$BzMA_{61}$) alone in water revealed that the copolymer had a R_g of 21 Å. Increasing the content of MAA from 39 to 79 mol % caused neutralised copolymers to swell outside of the range required for Guinier analysis, as such an accurate value of R_g could not be obtained. SANS measurements on carbon black dispersions stabilised with p(MAA_{39}-co-$BzMA_{61}$) were conducted, these results were used in conjunction with contrast matching to either match carbon black in 100 % D_2O or p(MAA_{39}-co-$BzMA_{61}$) in 27/73 volume % D_2O/H_2O. Contrast-matched p(MAA_{39}-co-$BzMA_{61}$) dispersions were found to exhibit two power law regimes in the scattering curves, showing the mass fractal dimension at low q and the surface fractal dimension at high q. The mass fractal was found to be 1.7 and the surface fractal was found to be 2, indicating that the carbon black existed as an open structure with a sharp interface. SAXS data supported the SANS results with the same power law at high q being obtained. SANS data collected for contrast-matched carbon black dispersions was adequately modelled using a combined Gaussian coil and fractal model. This combined model showed that the R_g of p(MAA_{39}-co-$BzMA_{61}$) decreased from 54 to 26 Å with an increasing loading of p(MAA_{39}-co-$BzMA_{61}$). This was attributed to a smaller surface area on carbon black being available causing p(MAA_{39}-co-$BzMA_{61}$) to coil up more and form more loops at the carbon black surface. The hypothesis of the presence of more loops was supported by $R_{0,}$ which is the characteristic dimension of the individual scatterers; R_0 increased from 51 to 71 Å with increasing p(MAA_{39}-co-$BzMA_{61}$) concentration. The effect of using different milling techniques was explored by SANS and revealed that bead and sonic milling are more effective than using a paint shaker. This conclusion was drawn from the scattering curve, which showed the presence of a larger number of aggregates. SANS was also used to demonstrate that changing the temperature to 6, 13 and 50ºC did not affect the conformation of p(MAA_{39}-co-$BzMA_{61}$) at the carbon black/liquid interface. This is

indicated by identical SANS curves being obtained at each temperature.